A Report from the University of Vermont Transportation Research Center

Light-Duty Gasoline Hybrid-Electric and Conventional Vehicle Tailpipe Emissions Under Real-World Operating Conditions

TRC Report 14-007 | Holmen, Robinson, Conger, Sentoff | June 2014

DISCLAIMER

Light-Duty Gasoline Hybrid-Electric and Conventional Vehicle Tailpipe Emissions Under Real-World Operating Conditions

University of Vermont Transportation Research Center

June 30, 2014

Prepared by:
Britt A. Holmén, Professor, Civil & Environmental Engineering
Mitchell Robinson, Graduate Research Assistant
Matthew Conger, Graduate Research Assistant
Karen Sentoff, Research Specialist

Transportation Research Center
Farrell Hall
210 Colchester Avenue
Burlington, VT 05405

Phone: (802) 656-1312
Website: www.uvm.edu/trc

Acknowledgements

The Project Team would like to acknowledge the efforts of all members of the UVM Transportation Air Quality (TAQ) Laboratory who assisted in collection of emissions data upon which the results of this report are based. U.S. DOT support under Project #025668 via the UVM TRC is gratefully acknowledged.

Disclaimer

Table of Contents

List of Tables

List of Figures

1. Introduction

1.0 Overview and Introduction

This report summarizes the development of an on-board tailpipe emissions measurement system developed to compare the emissions and performance of two Toyota Camry model year 2010 gasoline-powered light-duty vehicles during real-world driving in Chittenden County, Vermont over multiple seasons. One vehicle, denoted as the "conventional vehicle" or CV, had a regular transmission and drivetrain powered solely the by a 4-stroke gasoline internal combustion engine (ICE). The second Camry vehicle, denoted at "hybrid-electric vehicle" or HEV, was powered by the traditional ICE in addition to the Toyota Synergy DriveR hybrid platform.

To our knowledge the study is the first to compare the emissions and performance of a HEV to its conventional counterpart of the same manufacturer and model design. Thus, the emissions and performance results of this study are important to evaluating the real world, in-use benefits of this HEV technology. Gas-phase and particle number emissions as well as fuel economy performance results are presented here by vehicle specific power (VSP) and MOVES operating model classification schemes to enable comparison to other studies.

1.1 Background on Emissions from Conventional and Hybrid-Electric Light-duty Vehicles

The internal combustion engine (ICE) propelled nearly all of the 190 million on-road, light-duty vehicles in the U.S. fleet in 2010,[1] with less than 60,000 vehicles utilizing solely electric motors as the only other prevalent alternative.[2] In response to fuel economy standards and in anticipation of stricter emissions regulation, automobile manufacturers, starting in 1999, introduced vehicles that employ conventional ICE systems in combination with various hybrid-electric vehicle (HEV) configurations (series, parallel, and series-parallel). The intended results of HEV technology are fuel savings and emissions reductions, addressing concerns of meeting regulations, energy independence, climate change, and local and regional air quality. Production share of HEVs have increased to over 5% in the first decade of the 21st century (**Figure 1-1**) and are expected to continue to increase.[3] Annual sales of HEVs have increased almost 40 times since their introduction and the number of models available has also grown dramatically (**Figure 1-1**).[4]

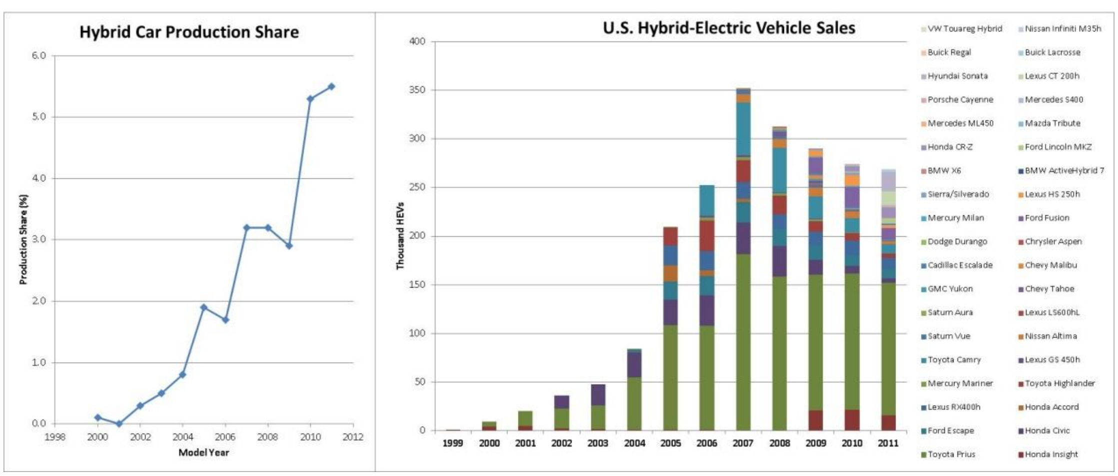

Figure 1-1. Hybrid production share increases[5] and hybrid make and model sales[4].

The transportation sector, specifically light-duty passenger vehicle use, significantly affects the air quality and energy consumption profiles of the United States. In 2011, the transportation sector accounted for 1,877 million metric tons CO_2 equivalent, which totaled 28% of US GHG emissions.[6] Increasingly stringent regulations help to limit fuel use and curb emissions from this increasing utilized transportation mode. The hybridization of the fleet will potentially help to meet long-term fuel consumption and tailpipe emission goals, but little is known on how late-model year hybrid-electric vehicles compare with their modern, relatively low emission conventional vehicle counterparts during real-world operation.

1.2 Hybrid-Electric Vehicle Technology

1.2.1 HEV Configuration and Function

Basic operating principles of the HEV include the combination of an ICE with an electric motor to propel the vehicle. In addition, an electric storage device, typically a battery pack, is used to store electric energy produced by the ICE or via regenerative braking. Configurations vary with HEV make and model, but typical designs for most of today's HEVs are categorized as series, parallel or combination series-parallel (**Figure 1-2**). *Series* hybrid designs utilize the electric motor as the mechanical power connection to the drivetrain, illustrated in Frame **A** of **Figure 1-2** by a red arrow, with the ICE either assisting in propulsion or regenerating the batteries during vehicle braking. *Parallel* hybrid drivetrains are connected to both the ICE and electric motor to allow propulsion of the vehicle by contributions of both systems simultaneously, indicated by two red mechanical linkages in Frame **B** of **Figure 1-2**. *Series-parallel* designs (Frame **C**) are a combination of the two, optimizing the advantages of higher speed, highway conditions in parallel mode and stop-and-go, city conditions in series mode. As a result, the series-parallel design generally has an all-electric mode in which it operates and optimizes during operation at low speeds with stop, go, and idle sequences.

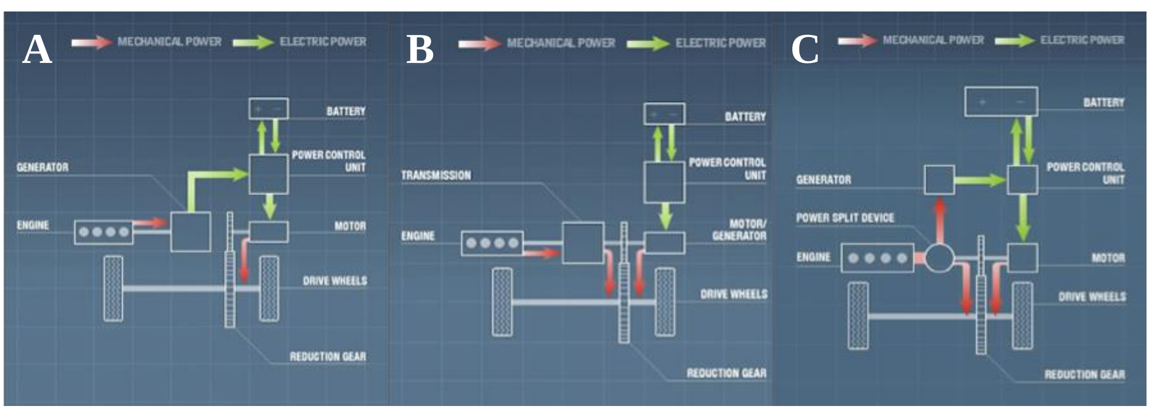

Figure 1-2. Common (A) series, (B) parallel, and (C) series-parallel HEV frameworks (adapted from Toyota[7]).

1.2.2 Ambient Temperature and HEVs

Designers of HEVs recognize that divergence from optimal operating ambient temperature conditions affects the ability of the HEV battery to maintain its target state-of-charge (SOC) via charging and discharging.[8] This consideration is critically important to realizing the potential benefits of HEVs while operating in cold climates, outside the range of optimal temperatures. Decreased capacity of the battery system to maintain SOC during operation outside of the optimal temperature ranges would be expected to affect the reliance of the electrical system to assist the ICE or independently propel the vehicle.

1.3 Tailpipe Emissions Data Collection Practices

Aggregate emissions data, historically collected using laboratory dynamometer tests, may be sufficient for developing local, regional, or national inventories across the fleet of in-use vehicles. However, evaluating the influence of vehicle technology, operating modes, traffic characteristics, or environmental (ambient temperature (T) and relative humidity (RH)) and road features (grade, curvature) on tailpipe emissions requires data collection at high temporal and/or spatial resolution, such as that available with more sophisticated PEMS. A disaggregate emissions data collection approach better informs modal and micro-scale models and is important to understand the impact of specific in-vehicle technologies, driver behavior,[9, 10] roadway geometry,[11, 12] driver-traffic interactions,[13] innovative traffic management approaches,[14, 15] or other potential real-world factors.

Portable emission measurement systems (PEMS) have the ability to quantify tailpipe emissions during real-world vehicle use. Most commercially available PEMS have generally been limited to quantifying a selection of gases (NOx, CO, THC, and carbon dioxide (CO_2)) and particle *mass* during real-world operation of a single vehicle[16, 17] without additional consideration of potential human health or environmentally harmful constituents such as mobile source air toxics or ultrafine particles. Tailpipe emissions analysis with Fourier Transform Infrared (FTIR) spectrometry during real-world driving allows for more comprehensive real-world data collection by measurement of speciated exhaust constituents at high temporal resolution.[18-22] Particle number emissions data collected by the Engine Exhaust Particle Sizer (EEPS) and the Condensation Particle Counter (CPC) allows for analysis at 1-Hz resolution of both total number (CPC) and size-resolved particle number to obtain second-by-second particle (number) size distributions (EEPS).[23]

1.3.1 Scantool Measurement of Vehicle Operating Parameters

Every vehicle manufactured since 1996 is equipped with an on-board diagnostics (OBD) connection, enabling communication with the vehicle computer. Through this OBD connection, specific vehicle parameters can be selected and recorded to a computer on a second-by-second basis. It is possible to record dozens of different parameters, but some of the most important in relation to vehicle emissions include; engine RPM, engine load, vehicle speed and mass air flow (MAF). Recording these parameters simultaneously with emissions data allows relationships to be quantified between emissions and engine operating parameters. Furthermore, when testing emissions from HEVs, the SOC of the batteries, electric motor and generator parameters, and energy flow throughout the vehicle must also be monitored. Ideally, when collecting emissions data, the SOC before and after every run would be identical. This would represent a net energy change(NEC) of 0%. Under laboratory emissions testing protocols for HEVs, if NEC is not less than 1%, a data correction should be applied to avoid artificially skewing the data, as is recommended by the California Air Resources Board[24] and SAE J2711.[25] The correction is necessary to enable comparisons between tests. As mentioned in other studies however, it is not always possible to apply the recommended correction.[26] This is the case with real-world studies, where the objective is to analyze multiple runs conducted under realistic driving conditions.

1.3.2 Vehicle Specific Power

Vehicle Specific Power (VSP) is a measure of the power required of a vehicle to overcome internal and external resistance to propel forward at a given speed and acceleration, normalized by vehicle mass. The kilowatt per ton (kW/ton) computation allows for the power exerted by a vehicle to be summarized into a single parameter. Jimenez (1999)[27] first presented the VSP concept and evaluated the feasibility of VSP as an independent vehicle operating parameter for use in modeling emissions. The convention was adopted by the EPA for use as the foundation of the Motor Vehicle Emissions Simulator (MOVES), the regulatory model for mobile source emissions estimation.[28] **Figure 1-3** illustrates the principle forces enumerated in the VSP measure, with kinetic, potential, aerodynamic and rolling components all acting on the body in motion.

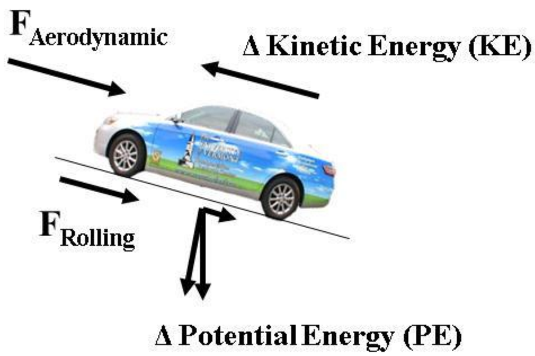

Figure 1-3. The basic forces acting on a vehicle in motion, adapted from Jimenez (1999).[27]

In the governing equation of VSP (Equation 1), the instantaneous power produced from the engine and/or electric motor of a vehicle is balanced with forces of aerodynamic drag and rolling resistance, multiplied by the velocity of the vehicle, and changes to the potential and kinetic energy of the body in motion.

$$VSP = \frac{\frac{d}{dt}(KE + PE) + F_{Rolling} * v + F_{Aerodynamic} * v}{m} \qquad 1$$

where: VSP = vehicle specific power (kW/ton)
KE = kinetic energy
PE = potential energy
$F_{Rolling}$ = rolling resistance force
$F_{Aerodynamic}$ = aerodynamic drag force
v = vehicle speed
m = vehicle mass

1.3.3 Factors Affecting Particle- and Gas-Phase Tailpipe Emissions

Evolution of the gasoline vehicle to increase fuel efficiency and optimize power through improvements in engine design and emission control devices has subsequently decreased the average hot stabilized trip emissions from passenger cars considerably. These low emitting vehicles, however, can attribute most of a trip's cumulative emissions to short-duration, high magnitude bursts of unburned fuel, combustion products, and catalysis by-products in the tailpipe.

It's been confirmed that short duration, HEEs contribute substantially to average emissions.[29] The mechanisms of tailpipe pollutant formation dictate which pollutants will be present in these HEEs. **Table 1-1** lists the factors influencing gaseous and particulate emissions from light-duty vehicles based on the last 15 years of research. Note that various MSAT's are affected by the parameters differently. **Table 1-1** indicates effects observed by one or more of the gas-phase emissions.

Table1-1. Parameters influencing emissions from internal combustion engines.

Parameter	Gaseous	Reference	Particulate	Reference
Air/Fuel Ratio	✓	[18, 21]	✓	[30-34]
Ambient Temperature	✓	[35]	✓	[26, 36, 37]
Vehicle Specific Power	✓	[27]	✓	[27]
Fuel Composition	✓		✓	[30]
Oil Type			✓	[33, 38]

1.4 Gas-phase Vehicle Emissions

Motor vehicle tailpipe emissions contribute significantly to increasing anthropogenic influence on the environment and public health. Although some mobile source, gas-phase pollutants detrimental to human health and/or the environment are regulated under the National Ambient Air Quality Standards (NAAQS), similar health and environmental welfare concerns exist for many other *unregulated* pollutants emitted by the transportation fleet. The regulated criteria gas-phase pollutants attributed to mobile sources include carbon monoxide (CO), oxides of nitrogen (NO_x), and total hydrocarbons (THC). Increasing awareness of the climate change potential of greenhouse gases (GHG), the carcinogenic nature of mobile source air toxics (MSATs), and formation of secondary organic aerosol (SOA) due to precursor pollutants has put new emphasis on the *unregulated* emissions from mobile sources. The on-road vehicle fleet was estimated to be responsible for approximately 42% of CO, 29% of THC, 40% of NO_x, 16% of volatile organic compounds (VOCs), 1% of sulfur dioxide (SO_2), and 3% of ammonia (NH_3) emissions emitted into the atmosphere in 2010.[39] Additionally, the proportion of GHG emissions attributed to transportation activity is estimated to be about 30 percent of the overall GHG budget, with passenger vehicles and light-duty trucks making up about 60 percent of the transportation-related emissions.[40]

1.4.1 Gas-Phase Emissions from HEVs

Few studies have examined emissions from hybrid vehicles. Most work to date on characterizing HEVs has been limited primarily to investigation of fuel consumption, criteria pollutant emission rates, and CO_2 emissions during simulated driving cycles on a chassis dynamometer.[41, 42] A more thorough gas-phase characterization of a single HEV (2000 Toyota Prius) emissions output was conducted on a dynamometer, with Tedlar bag sample evaluation for regulated and unregulated gas constituents.[43] Studies focused on extremely low-emitting vehicles (those vehicles meeting strict regulations including ULEV, SULEV, and PZEV) have collected more comprehensive tailpipe emissions data on dynamometer, real-world and test track driving for 2003 Honda Civic hybrid vehicles, but limited reporting to criteria pollutants averaged over 20 and 24 low-emitting vehicles in each study.[18, 19] The most comprehensive study to report on hybrid vehicle emissions involved dynamometer driving cycle tests conducted on a Toyota Prius and analysis of tailpipe emissions by FTIR.[44] The authors reported speciated GHG emissions (CO_2, CH_4, and N_2O) and seven other gas-phase constituents (ammonia (NH_3), methanol (CH_3OH), sulfur dioxide (SO_2), formaldehyde (H_2CO), CO, NMHC, and NO) for the single hybrid vehicle in laboratory conditions. Of significance was the authors' identification of the need to collect on-board emissions profiles during real-world operation of these vehicles together with spatial information.[44]

Results of research on HEV emissions to date find occasional high THC emission events from two models of HEVs (2004 Toyota Prius; 2005 Ford Escape), which was attributed to possible cooling of the catalyst during engine-off operation.[41] According to Reyes (2006)[44] steadily optimal catalysis temperature ranges may not be attainable for HEVs where the ICE turns off. Because the three-way catalysts (TWC) systems were designed for more stable conditions produced during conventional vehicle (CV) operation, turning the ICE on and off in the HEV may lead to catalyst inefficiencies, and cause relatively high emission events.[44]

Of the gas-phase pollutants studied by Christenson (2007)[41], it was observed that high power demand correlated with elevated CO_2 emission rates and the engine-off function of the HEV was associated with low, background concentrations of CO_2. These engine-off events were longer in duration for the Prius and Escape models, as they operate in engine-off at low speeds. At lower ambient temperature, the time in engine-off mode for these two vehicles decreased significantly for urban drive cycles including UDDS (also referred to as LA4), the Unified Cycle Driving Schedule (UCDS also referred to as LA92), and NYCC.[41] The temperature dependence of HEV engine cycling behavior is related to the manufacturer's hybrid architecture logic, information that is proprietary.

Elevated cold start emissions (CO, HC, and CO_2) and fuel consumption were demonstrated at low temperatures for five European HEV models, with decreasing emission trends as ambient temperatures increased.[45] Investigations of NO_x start emissions had no observable relationship with temperature, unlike the other quantified emissions.[45] Of particular interest was the relationship between CO_2 and three sample temperatures (-7, 8, and 23°C) across the hot, stabilized portion of the laboratory sampling: decreasing trends of CO_2 emissions were observed with increased temperature.[45] This relationship was not corroborated by investigation of the HEV system battery, which did not demonstrate a significant relationship of electric drive operation to temperature.[45]

Our previous analyses demonstrated that operation of the HEV in this study was (a) statistically different across seasonal temperatures in terms of battery state-of-charge; and (b) electric drive only propulsion (engine-off operation) in cold/cool temperatures was statistically different than warm/hot temperature operation.[46] In addition, emissions models developed for carbon dioxide prediction from the test vehicles indicated that temperature was a significant factor for the CV (11 mg/s decrease in CO_2 for every 1°C increase in temperature) and for the HEV during operation with the ICE on (i.e., excluding electric drive only data, 4 mg/s decrease in CO_2 for every 1°C increase in temperature).[46] It is important to note that these temperature effects were over an order of magnitude less important than the road grade effects on CO_2 emissions (CV/HEV increased by 633/535 mg/s CO_2 for every 1% increase in road grade).[46]

1.5 Particle-Phase Emissions

Airborne particulate matter (PM) – one of the 6 criteria pollutants under the Clean Air Act's NAAQS – has been correlated with many pulmonary and cardiovascular diseases. As a result, the Environmental Protection Agency regulates ambient PM concentrations through two different PM air quality standards; PM_{10} and $PM_{2.5}$. Both PM_{10} and $PM_{2.5}$ are regulated on the basis of the *mass* of particles per unit volume of air. PM_{10} is associated with particles less than 10 micrometers in median aerodynamic diameter and has a maximum allowable 24-hour mean concentration of 150 $\mu g/m^3$.[47] The $PM_{2.5}$ standard regulates particles less than 2.5 micrometers in median aerodynamic diameter and sets a maximum allowable annual mean ambient air concentration of 15 $\mu g/m^3$ and a 24-hour mean concentration maximum of 35 $\mu g/m^3$.[47]

Particulate matter exhibits complicated behavior (nucleation, condensation, coagulation, and adsorption), making it difficult to measure and regulate. This is largely why particulate air pollution is regulated based on mass concentration and under the broad size ranges of 10 microns and 2.5 microns.[48] However, little correlation exists between particle *number* and particle *mass* in vehicle exhaust. While particles in the nuclei mode make up 90% or more of the total particle number, they may account for only 1-20% of the total particle mass.[49] Figure 1-4 displays the number-weighted versus mass-weighted particle distributions for particles in vehicle exhaust.

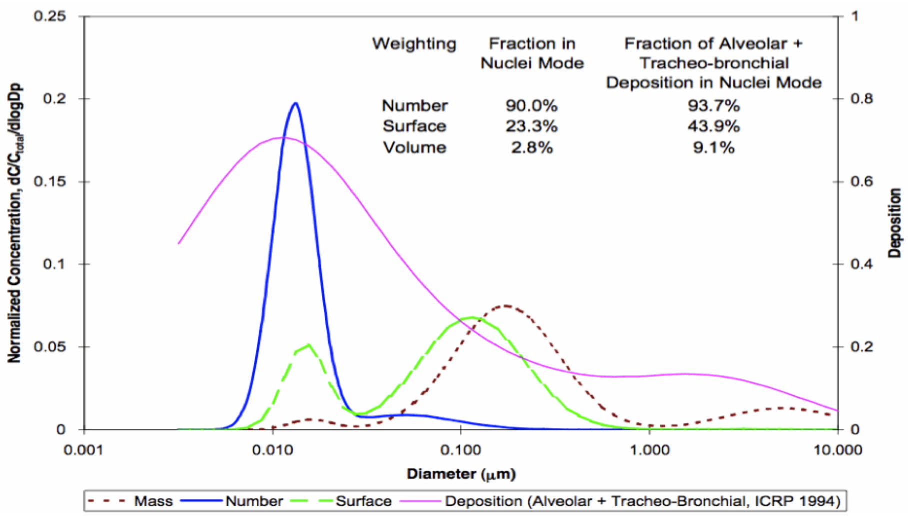

Figure 1-4. Particle distributions weighted towards: mass (red dashed line), number (blue line) and surface area (dashed green line). The pink line represents the deposition fraction of particles in the alveolar and tracheo-bronchial regions of the human respiratory system (adapted from Kittelson [50]).

Figure 1-4 clearly shows that while most particle number in vehicle exhaust is less than 50 nm in diameter, most of the particle mass is between 50 and 1000 nm. Furthermore, particle numbers from combustion make up the majority of airborne particulate matter under the $PM_{2.5}$ regulation[48] and most of these particles are less than 100 nanometers (nm) in diameter. The particles falling under the $PM_{2.5}$ regulation are of greatest concern, specifically particles in the ultrafine (< 100 nm) and nanoparticle (< 50 nm) ranges.[51-55] This is because smaller particles have a higher total surface area to volume ratio, facilitating adsorption and potentially increasing their toxicological effects.[56, 57]

1.5.1 Vehicle Particle Emissions from On-Road Sources

Diesel vehicles have traditionally been seen as the principal emitters of particulate air pollution, resulting in the focus of early particle emissions research on diesel vehicles. Due to recent advances in technology such as diesel particulate filters and ultra-low sulfur fuels, PM emissions from diesel vehicles have been drastically reduced.[32] Also, of the 201.6 million on-road vehicles in the U.S. in 1997, 136.1 million (68%) were passenger cars, 56.8 (26%) million were light-duty trucks and only 8.7 million (6%) were heavy-duty diesel vehicles.[58] Based on fuel consumption, approximately 65% of fuel used by mobile sources is gasoline, while 20% is diesel.[58] These factors have caused a shift in recent years towards research on particle emissions from spark-ignition vehicles, and in particular, light-duty passenger cars. Particle emissions data from real-world, on-board tailpipe measurement and for newer technologies such as HEVs are limited.[31] Furthermore, data on exhaust particle size distributions in relation to real-world, vehicle operating conditions are still poorly understood. This is because the majority of particle emissions studies on light-duty vehicles to date collected data on a dynamometer in idealized lab conditions[30, 34, 59-62], by the roadside[63, 64] or using chase vehicles.[31] There have been on-board studies conducted[65, 66] where a vehicle is instrumented, driven on the road network, and exhaust is sampled directly from the tailpipe or in the exhaust plume behind the vehicle, but these studies lacked either particle number measurements altogether[65] or high temporal resolution of the particle number distribution.[66] Although these studies do allow for significant insight into particle emission levels, they fail to capture how a vehicle is operating – and what the vehicle is subsequently emitting – under real-world conditions at key points in time.

1.5.2 Particle Size Distributions from Spark-Ignition Engines

Many previous studies have looked at particle size distributions from SI engines. Most of these studies either lack high temporal resolution or bin particles based on broad sizing classifications due to limitations in the available instrumentation. Quantifying these real-world particle distributions with high temporal resolution is essential. Particle number distributions may change under different operating parameters. Cold ambient temperatures have been found to increase the number of particles in the nuclei mode[36, 37] while having little effect on solid particles.[37] These increases due to temperature have often been sufficiently small, however, to make a direct correlation to ambient temperature difficult,[37] necessitating further study. Roadside measurements have found particle diameter modes to be between 60 and 100 nm during high concentration events (> 10^6 particles/cc) and less than 60 nm during lower concentration events (< 50,000 particles/cc), which accounted for 80% of the cases studied.[64] The smaller sizes during lower concentrations was attributed to few particle interaction effects, such as coagulation and adsorption, whereas higher concentrations encourage particle growth.[26, 64] Urban ambient traffic measurements were shown to have a primary particle diameter mode between 10 and 20 nm with a second smaller mode around 80 nm.[66] Particle numbers were shown to increase under freeway speeds (150 km/h) for diameters between 7 and 200 nm with the greatest increase in concentrations between 10 and 60 nm.[66]

1.5.3 Particle Number Emissions from Light-Duty Hybrid-Electric Vehicles

Few studies of particle number emissions from hybrid gasoline-electric light-duty vehicles exist. One laboratory study compared emissions and fuel economy from four different models of light-duty hybrids (two series-parallel hybrids and two parallel hybrids). Reported particle number emission rate patterns were similar to those documented for conventional vehicles: emission rates increased during acceleration events, transient operating events and with increasing vehicle speed.[26] Two of the four hybrid vehicles studied by Christenson et al. (2007) had the capability to shut down the ICE for electric-only low power, low speed operation (Toyota Prius and Ford Escape).[26] The observed emission patterns differed between CV and HEV because particle emission rates were at ambient background levels during periods of electric-drive-only operation for the HEV.[26] Furthermore, the frequency of occurrence of electric-only HEV operating events varied with ambient temperature, as discussed above. Lower ambient temperature (-18˚C) resulted in fewer electric-drive-only operating periods. For example, the Toyota Prius and Ford Explorer ICE operated in electric-only mode during the NYC cycle 66% and 55% of the time, respectively, at 20˚C, compared to 20% and 18% at an ambient temperature of -18˚C.[67] An unexpected result of this study was the magnitude of the HEV particle number emission rate when the engine restarted after the periods of electric-drive-only operation. These emissions could be several orders of magnitude higher than for the one CV studied (SmartCar) and lasted for several seconds.[26] Furthermore, HEV particle number emission rates were not higher at lower ambient temperatures, as expected, but the number distributions shifted to larger diameters under the colder test conditions (-18˚C). These larger particles were attributed to increased particle growth via adsorption and condensation at lower ambient temperature.[26]

The restarting of the hybrid vehicle's ICE, described as ICE restart, has been shown to cause HEEs. These HEEs typically last between 3-5 seconds,[26, 68] with peak emission rates reaching at least 3.5 x10^{10} particles/second.[68] This ICE restart behavior has also been shown to increase particle number emissions, relative to comparable conventional vehicles, in city environments where a high number of ICE restarts occur.[68, 69] Furthermore, hybrid ICE restarts shift the number distributions to larger particles. A 10 nm mode is lacking for the hybrid vehicle when ICE restart data are separated from stabilized ICE data.[69]

1.5.4 Particle Number Emissions from HEVs: Lessons from The Literature

Previous HEV study results (from both light-duty and heavy-duty vehicles) highlight that percent reductions in exhaust emissions depend strongly on the make and model year of the baseline CV used for comparison. Furthermore, when sampling emissions from HEVs that allow for electric-only propulsion, it is important to use sampling techniques that will accurately quantify the elevated particle emissions associated with each ICE restart.[26] These high emission events are not surprising given that typical light-duty vehicle engine cold starts involve fuel-rich operating conditions that result in an increase in emitted unburned fuel, higher particle number emissions[32] and the formation of nanoparticles between 30 and 50 nanometers.[31] These nanoparticles decrease in number concentration quickly with increased distance from the roadway due to volatilization, coagulation and condensation,[70] but in city environments, pedestrians will be exposed to these particles almost immediately after they are emitted. Thus, it is important to collect temporally-and spatially-resolved data on exhaust particle number emissions from HEVs, preferably under real-world driving conditions, and compare these emissions to conventional vehicles of the same manufacturer and model. Only then can the actual real-world benefits of the hybrid-electric technology be quantified.

2. Research Methodology

2.1 TOTEMS and Real-World Measurement Study Design

2.1.1 Study Vehicles

Real-world tailpipe emissions data were collected with the Total On-Board Tailpipe Emissions Measurement System (TOTEMS) on two model year 2010 vehicles: Toyota Camry XLE (Conventional) and Toyota Camry Hybrid (**Figure 2-1**). The Toyota Camry vehicles were comparable in most aspects with identical frames, bodies, model years, emission control devices, and climate control systems. Some aspects of the vehicles differed slightly, like the drag coefficients, overall weight, suggested tire pressure, and fuel capacity. The largest discrepancies between the two test vehicles were the drive train and transmission systems. The Toyota Camry Hybrid employed a Toyota Hybrid Synergy Drive (HSD) system. Toyota's hybrid design included a series of batteries, two electric motors/generators, and a continuously variable transmission. Specifications for each vehicle were compiled in **Table 2-1** and emissions specifications are in Appendix I.

Figure 2-1. The Toyota Camry 2010 model year test vehicles with the XLE (left) and hybrid (right) packages.

For propulsion of the vehicles, the conventional vehicle employed a 2.5-liter Otto cycle engine[8] with a six speed automatic transmission rated at 22/32 (city/highway) or 26 combined mile per gallon fuel economy. The Camry hybrid was rated at 33/34 (city/highway) or 34 combined fuel economy with a slightly smaller engine at 2.4-liters and, dissimilar to the conventional cycle, ran on the Atkinson cycle[8] Phase II emission ratings were applied to the 2010 vehicles, with the conventional designated an Ultra-Low Emission Vehicle II (ULEV II) rating and the hybrid assigned an Advanced Technology Partial Zero Emission Vehicle (AT-PZEV) rating.[71, 72] The AT-PZEV rating complies with Super Ultra Low Emission Vehicle II (SULEV II) emission standards with the additional benefits of a PZEV for employing technologies eliminating evaporative emissions and AT- for electric motor propulsion.

Table 1-1. Toyota Camry Specifications (Toyota, 2010)

Specification	CV	HEV
Make/Model	Toyota Camry	Toyota Camry
Trim	XLE	Hybrid
Year	2010	2010
Engine	2.5-Liter 4-Cylinder	2.4-Liter 4-Cylinder
Transmission	6-speed Automatic	Continuously Variable
Horsepower (hp@rpm)	169 @ 6000	187 @ 6000
Torque (lb-ft@rpm)	167 @ 4100	138 @ 4400
Electric Motor		Permanent Magnet AC Synchronous Motor
Batteries		Sealed Nickel-Metal Hydride (Ni-MH) 40 hp 244.8V
Fuel Economy		
Combined [MPG (L/100km)]	26 (9.0)	34 (6.9)
City [MPG (L/100km)]	22 (10.7)	33 (7.1)
Highway [MPG (L/100km)]	32 (7.4)	34 (6.9)
Fuel Capacity [gal (L)]	18.5 (70.0)	17.2 (65.1)
Emission Rating	ULEV II	AT-PZEV
Brakes	Power-assisted ventilated front/solid rear discs	Power-assisted ventilated front/solid rear discs with integrated regenerative braking
Tires	All-Season P215/60R16	All-Season P215/60R16
Climate Control	Dual zone CFC-free	Dual zone CFC-free
Curb Weight [lbs (kg)]	3373 (1533)	3680 (1673)
Actual Weight **m** [lbs (kg)]	4397 (1996)	4704 (2136)
Coefficient of Drag C_D	0.28	0.27
Frontal Area A [m^2]	2.48	2.45
Odometer Start of Study [miles (km)]	3074 (4947)	4242 (6827)
Odometer End of Study [miles (km)]	6164 (9920)	8215 (13221)

The Camry vehicles operated new, identical emission control devices including three-way catalysts and heated oxygen and air-to-fuel sensors. Though many newer MY vehicles employ electrically heated catalysts, the Toyota vehicles instead invest energy to precise stoichiometric control through heated oxygen and air-to-fuel sensors.[73] Toyota specified electric heating at 100% heater duty ratio during cold start, 0% to 100% during driving, 0% during high speed driving, and 40% to 50% during idle.[74] Advances in Variable Valve Timing-intelligent (VVT-i) provided highly precise control of combustion stoichiometry in both vehicles. The technology controls timing of the intake and exhaust valves, fine tuning the engine out air-to-fuel ratio with feedback from the sensitive oxygen and air-to-fuel sensors. An optimal exhaust mix reaches the catalyst for further oxidation of carbon monoxide and hydrocarbons and reduction of oxides of nitrogen.

2.1.2 Sampling Runs and Data Collection Phases

Data were collected on a single vehicle over a number of replicates and then switched to the other vehicle, targeting the same season for each of the vehicles. This resulted in 75 sampling runs attempted, 32 in the conventional vehicle and 43 in the hybrid vehicle, identified by run numbers 5 through 79. Sampling techniques and equipment employed in this body of work were previously used on a Toyota Sienna minivan, responsible for sampling run identifiers 1 through 4, as part of a proof-of-concept study conducted before the Camry test vehicles were acquired (see [75] for more information). A single sampling run constituted nine phases of data collection as outlined in **Table 2-2**.

Table 2-2. Sampling Run Data Collection Phases

Phase Number	Shorthand	Phase Identification	Description
1	IB_1	Pre-Run Instrument Blank	Pre-sampling emissions instrumentation zero
2	TB_1	Pre-Run Tunnel Blank	Pre-sampling ambient background measurement with vehicle off
3	WARM	Warm-Up Driving	Journey to gas station and engine warm-up
4	OUT	Outbound Phase	Stabilized data collection: Burlington city loop to Richmond via I-89
5	PARK	Park-and-Ride	Idle at Richmond Park-and-Ride for at least one minute
6	IN	Inbound Phase	Stabilized data collection: Richmond to Burlington via state and local roads
7	POST	Post Route Travel	Votey Hall to gas station and back
8	TB_1	Post-Run Tunnel Blank	Post-sampling ambient background measurement with vehicle off
9	IB_1	Post-Run Instrument Blank	Post-sampling emissions instrumentation zero

The *instrument* and *tunnel* blank phases both before and after a sampling run fulfilled quality assurance and quality control measures for all sampling events, discussed in further detail in **Section 2.4** of this document. The *warm-up* phase of data collection included the cold start of the vehicle, the journey to the gas station to fill the gasoline tank, and driving a short, 2.5-mile loop to allow the vehicle's engine to sufficiently warm-up and reach stabilized operation. Data collection was initiated on all instruments before or during the *warm-up* phase, as to have everything running continuously when the vehicle passed the run starting location of Votey Hall on the University of Vermont campus. The *outbound* phase of data collection was conducted from Votey Hall, through downtown Burlington (*city*), and out to Richmond via Interstate 89 (*highway*). An idle event lasting at least one minute took place at the *park-and-ride* facility in Richmond. Stabilized data collection was continued on an *inbound* route back to Burlington through Richmond and Williston via state and local roads (*arterial*). A short *post-run* trip to and from the gas station followed the sample route completion at Votey Hall and allowed for data collection to cease and instrument data to be saved.

2.1.3 Driving Route

A fixed 32-mile route in Chittenden County (**Figure 2-2**) included various facility types (urban arterial, rural arterial, interstate highway, state highway), traffic conditions, and terrain (road grade shown by color indication). The route depicted in **Figure 2-2** encompasses the hot-stabilized emissions data collection during *outbound* and *inbound* run phases, described above. The primary goal of the route selection was to reflect real-world driving over a variety of facility types with hilly terrain. The turn-by-turn directions for the route are included in **Appendix C**.

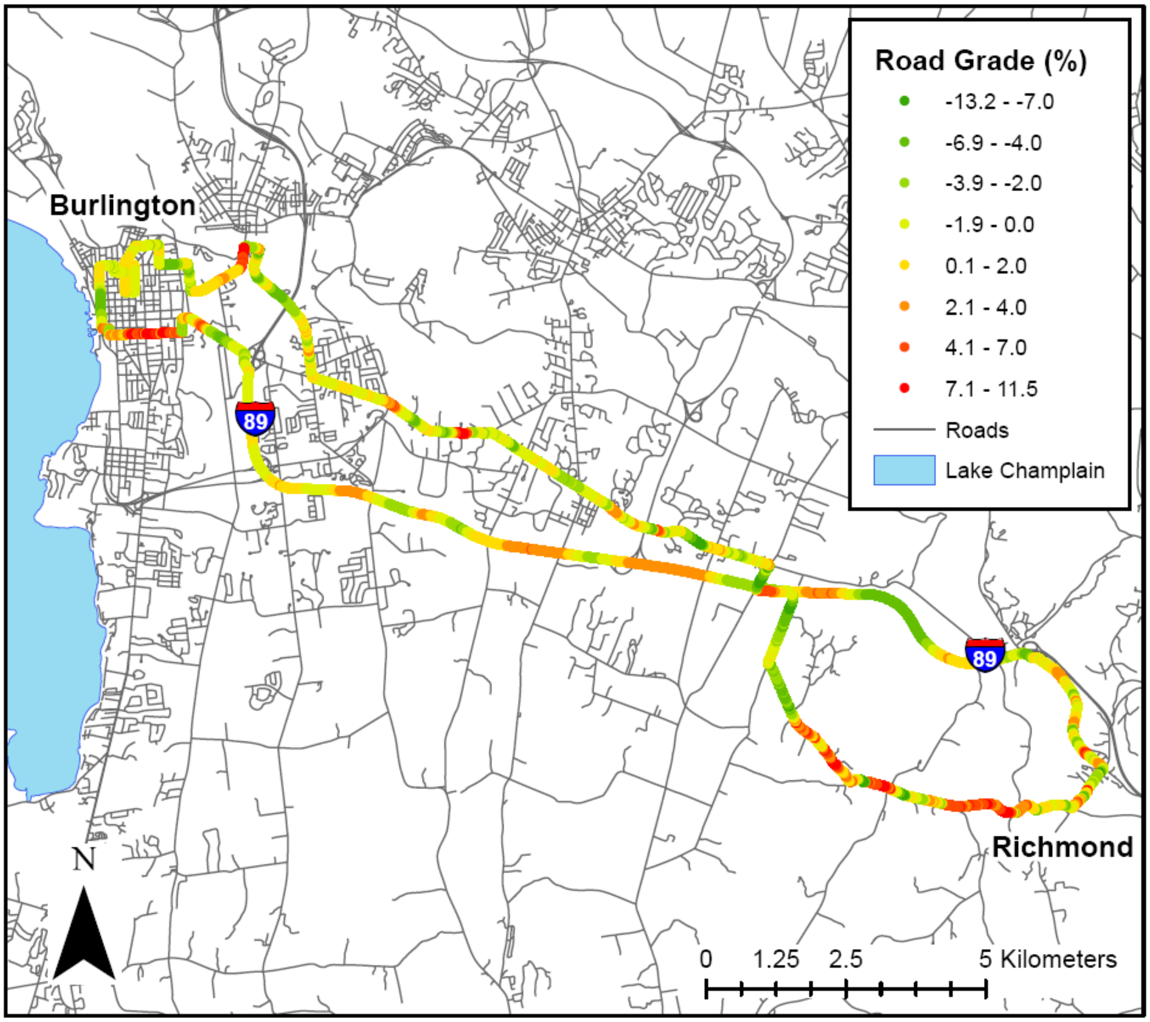

Figure 2-2. Thirty-two mile driving route including facilities outbound through downtown Burlington, VT and southbound Interstate 89 to Richmond, VT, and facilities inbound over rural and suburban arterials and collectors. Varying terrain represented by broad range of road grades (color indicated) along different facility types.

2.1.4 Sampling Schedule

To collect comparable data between the two vehicles over a broad range of temperatures and humidity, sampling continued from February 2010 to September 2011. Average run temperatures ranged from -13°C to 40°C with relative humidity ranging from 19% to 90%, with comparable ranges for each vehicle type illustrated in **Figure 2-3**. Seasonal temperature classes were defined by the quartiles of the temperature distribution for all runs: cold (< 5°C), cool (5 ≤ T < 22°C), warm (22 ≤ T < 29°C), and hot (T ≤ 29°C). All data for a test run were binned to one of four temperature classes based on the mean run ambient air temperature for later analysis by season. A complete tabulated summary of all sampling runs is included in **Appendix A**.

Sampling was conducted at varying times of day to capture the different traffic congestion levels and traffic patterns during peak and off-peak times throughout the daylight hours. Sample time of day (**Figure 2-4**) ranged from 8:00 AM to 8:00 PM with sufficient data across the range to account for variability due to traffic fluctuations. TOTEMS was only deployed in the vehicles with dry road conditions as a safety precaution for both researchers and instrumentation.

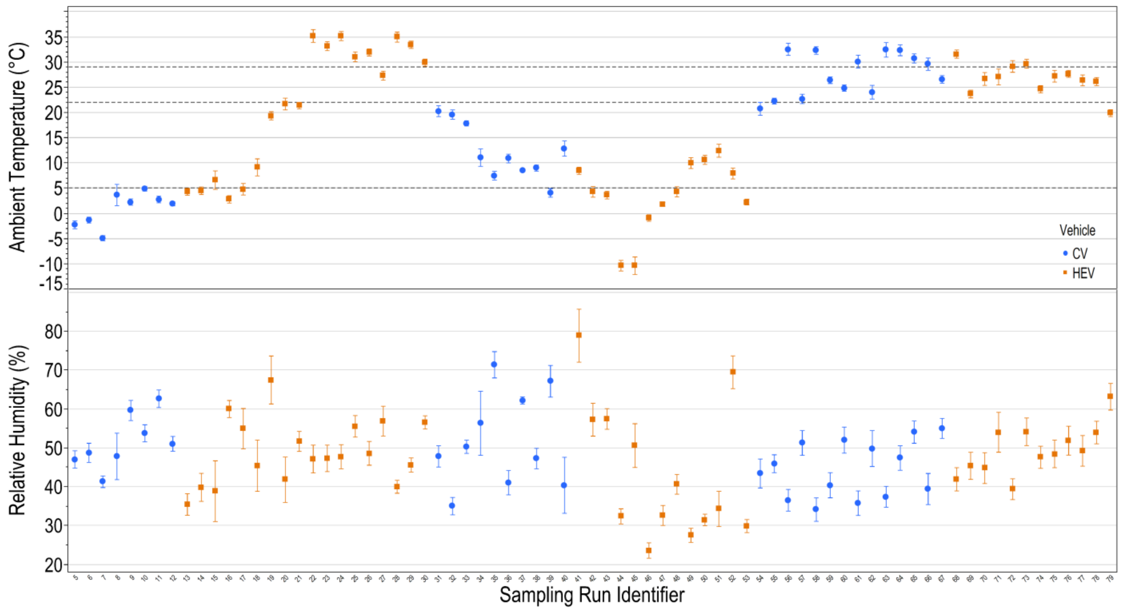

Figure 2-3. Ambient temperature and relative humidity for all sampling runs from the 18-month study with sampling run number identifiers. Orange squares indicate mean HEV ambient conditions and blue circles indicate mean CV ambient conditions, with error bars representing the standard deviation during the sampling run. Dashed horizontal lines indicate the temperature bin delineations for each season.

2.1.5 Total On-Board Tailpipe Emissions Measurement System (TOTEMS)

TOTEMS, a suite of 30 on-board components, collected real-time, second-by-second parameters characterizing the vehicle's gas-phase and particle number emissions, exhaust characteristics (flow rate and temperature), vehicle operation, spatial location, ambient conditions, road network features, and traffic environment during real-world driving. An exhaustive list of TOTEMS components in **Table 2-3**, an associated diagram of sample and data transfer through the system (**Figure 2-5**), and a series of photographs depicting the actual implementation in the equipped vehicles in **Figure 2-6** illustrate the setup of TOTEMS for sampling.

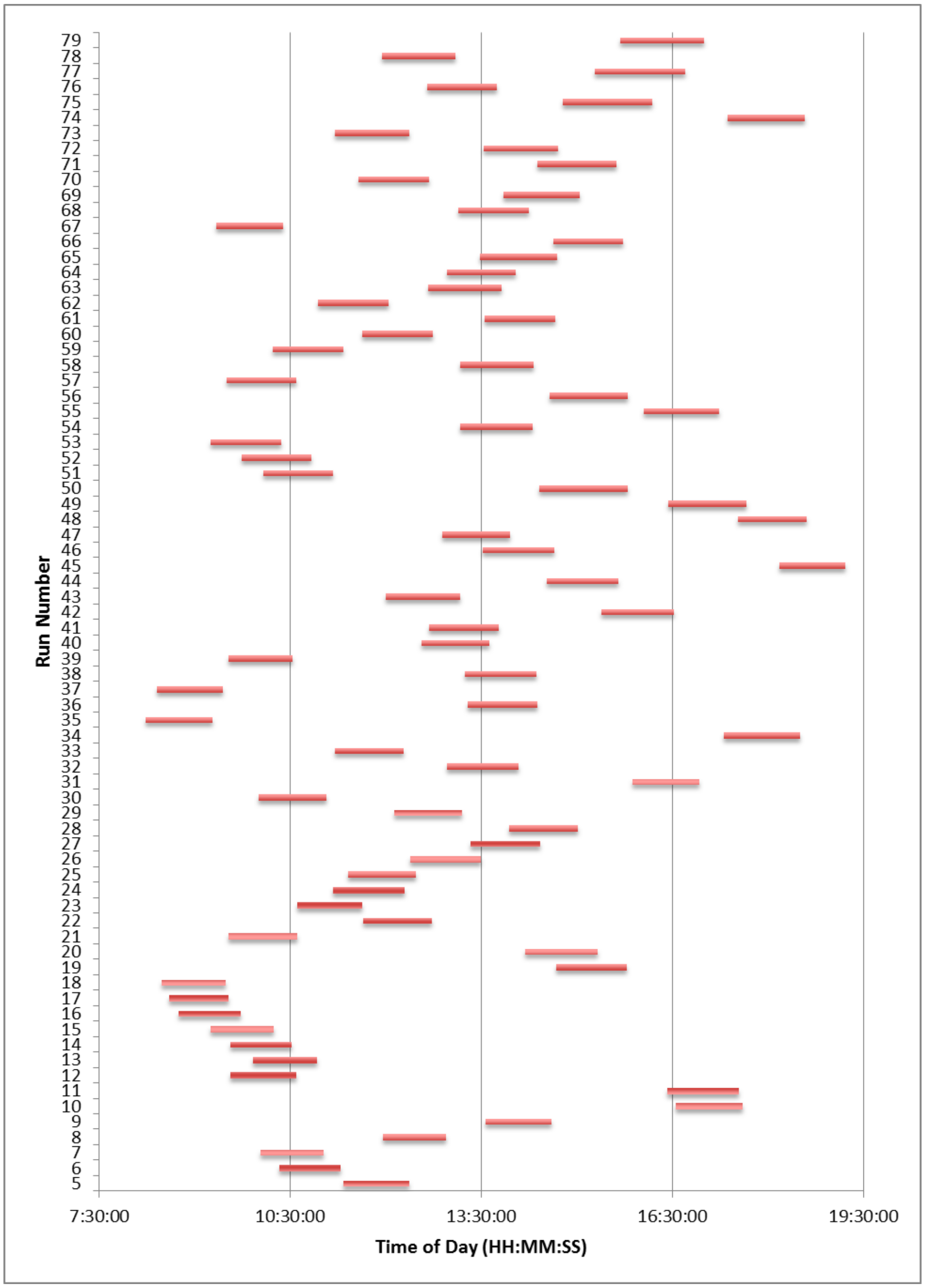

Figure 2-4. Data collection time of day for the full sampling campaign across 75 sampling runs.

TOTEMS Power Supply

TOTEMS utilized two Lifeline GPL-8DA absorbent glass mat lead-acid batteries, with 12-volt and 255 Amp-hour ratings, as the power supply separate from the vehicle batteries. The configuration prevented artificial loading of the engine during sampling. Power delivered by the two batteries was passed through the Vector 2500-watt power inverter. A GoPower automatic transfer switch (ATS) allowed for an uninterrupted transition from grid power to

on-board power, conserving batteries for use only while the vehicle was driving the route. Additionally, a small 12-volt Optima battery powered the differential pressure transducers and their DAQCard connector block directly.

Table 2-3. Total Onboard Tailpipe Emission Measurement System Components

Instrument	Acronym	Model	Purpose	Label No.
		Emissions Analysis		
Fourier Transform Infrared Spectrometer	FTIR	MKS MultiGas2030HS	Gas-Phase Emissions Analysis at 1-hertz	1
Personal Sampling Pump	SKC	SKC Leland Legacy	Draw Exhaust Sample through FTIR	2
Engine Exhaust Particle Sizer	EEPS	TSI 3090	Particle Size Distribution (D_p = 5.6 - 560 nm)	3
Ultrafine Condensation Particle Counter	UCPC	TSI 3025A	Total Particle Number (D_p = 3 - 3000 nm)	4
Rotating Disk Diluter	MD19-2E	Matter Engineering 379020	1st Stage Particle Sample Dilution	5
Air Supply Evaporation Tube	ASET	TSI 379030	2nd Stage Particle Sample Dilution	6
		Exhaust Parameters & Sample Transport		
Tailpipe Adapter	TA	Custom Built	Extends Tailpipe to Provide Sampling Ports and House Pitot Tube	7
Thermocouple Type T	T1	Omega GTMQSS-125E-2	Exhaust Sample Temperature at end of Heated Line	8
Thermocouple Type J	T2	Omega GTMQSS-125E-3	Exhaust Temperature in Tailpipe Adapter	9
Thermocouple Type T	T3	Omega GTMQSS-125E-2	Exhaust Sample Temperature at Inlet of FTIR	10
Thermocouple Type T	T4	Omega GTMQSS-125E-2	Exhaust Sample Temperature at Inlet EEPS/UCPC	11
Differential Pressure Transducers (4)	DiffP#	Omega PX-277	Exhaust Flow Rate	12
Static Pressure Sensor		Omega PX181-030G5V	Exhaust Flow Rate	-
Heated Line	HL	Atmoseal IGH-120-S-6/X-G13	Transport of Exhaust Sample from Tailpipe to FTIR, CPC, and EEPS	13
		Vehicle Operation, Spatial Location & Environment		
Scan Tool	SCN	Toyota Techstream	Records Vehicle Operation Parameters from Vehicle's ECU(s)	14
Garmin GPS Receiver	GAR	Garmin GPS16-HVS	Spatial Position of Vehicle	15
Geologger	GEO	Geostats DL-04 V2.4	Spatial Position of Vehicle	-
Accelerometer	ACC	Crossbow CXLO2LF3	Acceleration in X, Y, and Z Directions	-
Temperature and Relative Humidity Loggers (2)	RHT	Onset HOBO U23-001	Ambient and Interior Conditions	16
Video Camera	VID	Canon Optura 30	Driver Perspective of Roadway	17
		Power Supply		
Automatic Transfer Switch	ATS	GoPower Electric GP-ATS-30	Uninterrupted Transfer from Grid to On-board Power Supply	18
Absorbent Glass Mat Lead-Acid Batteries (2)		Lifeline GPL-8DA	On-board power supply	-
Deep Cycle Battery Charger		Xantrex TrueCharge 40	Three Stage Battery Charger to Large AGM Marine Batteries	19
Optima Yellow Top Battery		Optima D31A	Pressure transducer DC power supply	20
Power Inverter		Vector VEC56D	Conversion from DC to AC power	-
		Data Acquisition		
On-Board Emissions PC		Dell Optiplex GX620	Records data from instruments	21
FTIR Laptop		Dell Latitude D630	Records data from FTIR	22
Labview Device 1	L1	Labivew DAQCard-6024E	National Instruments SCB-68 Connector Block and DAQCard for Data Acquisition from Crossbow, Static Pressure, and Thermocouples	23
Labview Device 2	L2	Labview DAQCard-6024E	Connector Block and DAQCard for Data Acquisition from Differential Pressure Transducers and Dilution System	24

TOTEMS Power Supply

TOTEMS utilized two Lifeline GPL-8DA absorbent glass mat lead-acid batteries, with 12-volt and 255 Amp-hour ratings, as the power supply separate from the vehicle batteries. The configuration prevented artificial loading of the engine during sampling. Power delivered by the two batteries was passed through the Vector 2500-watt power inverter. A GoPower automatic transfer switch (ATS) allowed for an uninterrupted transition from grid power to on-board power, conserving batteries for use only while the vehicle was driving the route. Additionally, a small 12-volt Optima battery powered the differential pressure transducers and their DAQCard connector block directly.

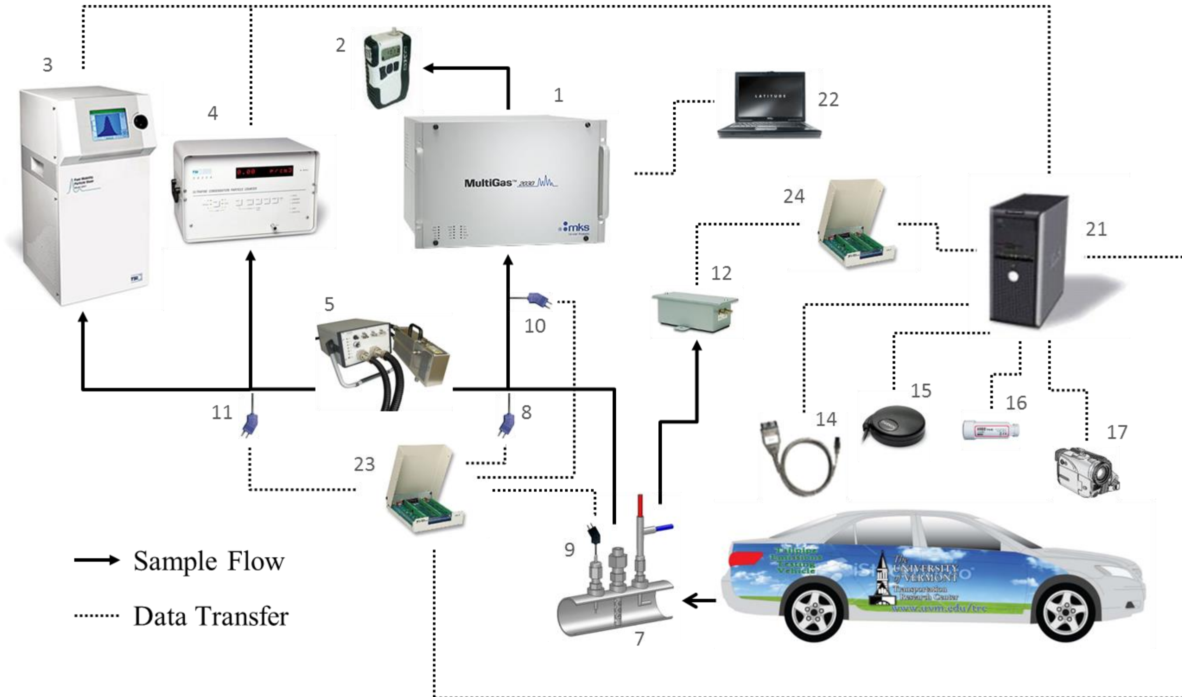

Figure 2-5. Diagram of TOTEMS instrumentation during onboard data collection numbered according to Table 2-3. Note the power supply system is not shown here.
Photo credits in numerical order include: http://www.mksinst.com/, http://www.skcinc.com/pumps.asp, http://www.tsi.com/, Scott Quinn (UVM URA), http://www.omega.com/, https://techinfo.toyota.com/, http://www.garmin.com/, http://www.onsetcomp.com/, http://www.usa.canon.com/, http://www.dell.com/, http://www.ni.com/.

Figure 2-6. TOTEMS equipped vehicle with associated components numbered according to Table 2-3

2.1.6 Exhaust Characteristics and Sample Transfer Lines

A custom-built tailpipe adapter, **Figure 2-7** with flow directed from right to left, extended the factory tailpipe of the testing vehicle to facilitate collection of emissions samples and characterization of exhaust temperature and flow rate in the tailpipe. Four ports on the tailpipe adapter accommodated (a) a pitot tube connected to four differential pressure transducers, (b) a line to the static pressure sensor, (c) a thermocouple, and (d) a sampling probe connected to a heated line for transfer of continuous samples from the tailpipe adapter to the emission analyzers.

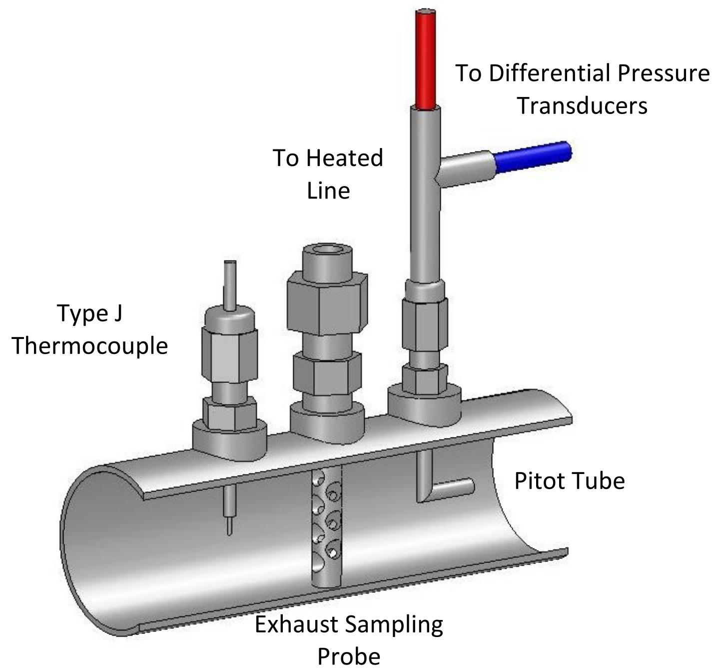

Figure 2-7. Tailpipe adapter with three of the four sampling ports shown (static pressure port located on the near side of the tailpipe adapter 90° from the thermocouple port; missing here to facilitate the cutaway view). **Drawing Credit: Scott Quinn.**

The pitot tube and series of four differential pressure transducers were used to derive exhaust flow rate. Each of the four Omega PX-277 differential pressure transducers were adjusted to account for a specific range of the flow regime experienced at the tailpipe of these light-duty vehicles. The differential pressure voltage signals were recorded using the secondary Labview connector block (L2) and data acquisition card (DAQCard-6024E). Calibrations of the pitot tube were conducted each time TOTEMS was transferred to a different vehicle to account for any changes in configuration of the pitot tube. Calibration assays are presented in more detail in **Section 2.6** of this document and in **Appendix D**.

A static pressure sensor verified that samples were collected from the tailpipe near ambient pressures. The port for the static pressure was positioned 90° from the thermocouple connector. A line from the tailpipe port was connected to an Omega PX181-030G5V static pressure transducer. The signal voltage was collected by the primary Labview connector block (L1) and interpreted using a DAQCard-6024E.

An Omega Type J thermocouple measured exhaust temperature at the end of the tailpipe. The voltage signal from the thermocouple was collected and recorded with the primary connector block (L1) and data acquisition card, as with the static pressure sensor. For occurrences of the tailpipe thermocouple malfunctioning, an estimated exhaust temperature was computed as outlined in **Section 2.6** of this document.

The sampling probe was a 3/8" outer diameter perforated stainless steel tube that spanned the 1-13/16" inner diameter of the tailpipe adapter perpendicular to flow. To continuously transport a heated exhaust sample to the emissions analyzer instruments inside the vehicle, the sampling probe was connected to a 3/8"-diameter flexible, smooth, thin-walled, stainless steel heated line. The custom manufactured heated line (Atmoseal Model: IGH-120-S-6/X-G13) was strung through a hole in the bottom of the spare wheel well in the trunk of the testing vehicle. The 10-foot length of the stainless steel insulated line was heated with a control box at 191°C to deliver the sample at constant conditions to the emissions instrumentation.

2.1.7 Recording Vehicle Operating Parameters

Toyota Techstream® software in combination with a Drew Technologies Mongoose scantool communicated with the vehicle engine control unit (ECU) to measure engine and vehicle operating parameters. Parameter selection was based on information explaining the state of the vehicle's operation at a given second, with focus on the parameters with known or proposed causality to emission output. General operating parameters were selected for both vehicle systems where available, including the parameters displayed in non-italicized text in Table 2-4. Parameters specific to either the HEV or the CV are tabulated as italicized text in Table 2-4. Fuel injection volume, air-to-fuel (A/F) ratio, and mass air flow (MAF) were selected for the conventional vehicle, due to known relationships between air and fuel composition in the engine and resulting emissions. Catalyst temperature was selected for the conventional vehicle as a pertinent factor in efficiency of the emission control devices and resulting emissions. Need for a comprehensive measure of the hybrid system operation led to the selection of the additional hybrid parameters (italicized in Table 2-4) to compute the hybrid system contribution to the ICE during operation. Limitations in the Techstream software prevented simultaneous collection of engine operating parameters from the ECU (i.e., catalyst temperature and air-to-fuel ratio) and HEV control parameters (battery SOC and regenerative braking).

Spatial Location

Two Global Positioning System (GPS) receivers collected spatial data on the latitudinal and longitudinal position of the vehicle along the driving route. Roof-mounted Garmin GPS16-HVS and Geostats Geologger DL04 V2.4 antennas were linked to Fugawi software and a Geologger data acquisition unit, respectively. Each unit collected second-by-second latitude, longitude, and speed.

Acceleration

Instantaneous accelerations along three axes were collected with a Crossbow CXLO2LF3 accelerometer. The accelerometer provided an independent measure of acceleration experienced in the vehicle, as opposed to derived accelerations from scantool and GPS measured velocities. The primary Labview (L1) connector block and data acquisition card recorded raw Crossbow acceleration signals, along with the thermocouple temperatures and static pressure.

Ambient Conditions

Onset HOBO U23-001 loggers positioned on the roof of the vehicle and inside the cabin of the vehicle measured temperature and relative humidity. The purpose of the exterior logger was to collect ambient conditions over the driving route. TOTEMS instrumentation performance may be influenced by temperature; therefore, the interior logger monitored the temperature and relative humidity that TOTEMS instruments experienced within the vehicle.

Table 2-4. Conventional and Hybrid Electric Operation Parameters from Scantool

Conventional Vehicle		Hybrid Vehicle	
Parameter	**Unit**	**Parameter**	**Unit**
Sample Time	MM:SS.mmm	Sample Time	MM:SS.mmm
Vehicle Speed	km/h	Vehicle Speed	km/h
Engine Speed	rpm	Engine Revolutions	rpm
Calculated Load	%	Calculated Load	%
Coolant Temperature	°C	Engine Coolant Temperature	°C
Ambient Temperature	°C	Ambient Temperature	°C
Run Distance	km	Run Distance	km
Mass Air Flow	gm/s	*Motor Revolution*	rpm
Fuel Injection Volume	ml	*Motor Torque*	Nm
Air to Fuel Ratio Lambda	Dimensionless	*Generator Revolutions*	rpm
Catalyst Temperature Sensor 1	°C	*Generator Torque*	Nm
Catalyst Temperature Sensor 2	°C	*Regenerative Brake Torque*	Nm
		State of Charge (All Batteries)	%
		Acceleration Sensor	%
		Maximum Chargeable Power to HV Battery	W
		Maximum Chargeable Power Out of HV Battery	W

2.1.8 Road Grade

Road grade was a significant road network feature to be considered in this analysis. Grade was collected for the driving route by the Vermont Agency of Transportation using an Automatic Road Analyzer (ARAN) vehicle in the Fall of 2009. The vehicle collected grade and GPS location every 10 meters to provide a spatially resolved road grade data set. The ARAN vehicle employed integrated gyroscopes measuring attitude of the vehicle in space, sonar based sensors measuring vehicle orientation in reference to the road surface, GPS units measuring spatial location, and a camera collecting pictures at each measurement location to derive pitch, roll, heading, cross-fall, grade, latitude, longitude, and graphic route chronology. The ARAN data were joined to the 1-hertz TOTEMS data via the nearest GPS position.

2.2 Particle Number Emissions Measurement

2.2.1 Particle Number Instrumentation Operating Principles.

Two particle measurement instruments were used in the study because of limitations associated with each. Particle Number Distributions were counted (± 20% accuracy in concentration) and sized (± 10% accuracy in particle diameter) with the TSI, Inc. (Shoreview, Minnesota) Model 3090 Engine Exhaust Particle Sizer Spectrometer (EEPS). A 1 micrometer cut cyclone is placed on the inlet of the EEPS to remove large particles above the detectable range of 5.6 to 562 nanometers. The EEPS operates to separate particles in a polydisperse aerosol using the theory of electrical mobility (TSI, 2006). As particles flow into the instrument, they pass through a positively charged ion cloud which applies a positive charge to the particles to (a) remove any excessive negative charge on the particles, and (b) reduce the potential for overcharging by the subsequent negative charger. The particles then flow through a negatively charged electron cloud – which applies a predictable charge based on particle size – and then enter the electrometer column. In this column, there are 24 electrometer rings, 22 of which actively detect particles while the upper two act as spacers at the top of the column. A reverse differential mobility analyzer (DMA) is placed as a central rod in the column. The DMA deflects the particles outward towards the 22 active rings. The active rings measure the discharged current (in fempto amps) across 32 different particle diameter channels (channel widths are provided in Table F.1 in Appendix F and are equally spaced on a log scale). The diameter midpoint of each channel is the reported particle size. The EEPS can record particle number distribution data at a rate of 10 Hertz, but values were recorded here at a 1 Hertz rate. The 1 Hertz measurements represent discrete average of the ten measurements within a given second[76]. The EEPS samples at 10 lpm with 8 lpm traveling through the electrometer column. Two liters per minute are removed at the top-center of the electrometer column as extraction flow because the charging is less uniform here.

A TSI, Inc. (Shoreview, Minnesota) Model 3025A Ultrafine Condensation Particle Counter (UCPC) was used in parallel with the EEPS to count the total particles in vehicle exhaust every second. The UCPC was used partly because of accuracy limitations of the EEPS, but also to validate the EEPS concentration and to compare results to previous on-board studies. The UCPC samples at a flowrate of 1.5 Lpm and counts all the particles in the diameter range of 3 to 3000 nanometers at a 1 Hz rate.

The UCPC counts particles by first sending the aerosol through a 37°C saturator filled with butanol-laden air. The butanol condenses at 10°C onto the particles in the condenser chamber, growing them to a light-scattering detectable size. After the aerosol passes through the condenser chamber, it passes through an optical laser detector, using light scattering to count the particles.

The limitations of the EEPS necessitated the addition of the UCPC to the TOTEMS system. The EEPS has limited accuracy (± 20%), which further deteriorates at low concentrations, but the EEPS is capable of sizing particles (± 10%) at a 1 Hz rate. Additionally, the EEPS has very high maximum reported detection limits (RDL), making it ideal for sampling particle number emissions from vehicles. The EEPS RDLs are variable, depending on the particle size and averaging time selected. The selected time averaging interval (0.1 Hz, 1 Hz or 10 Hz) affects the RDLs for minimum concentrations, but the maximum concentration RDLs remain constant for each channel regardless of averaging interval. Specific detection limits are not provided by TSI, but are instead plotted for reference in the **Appendix F** [76]. The minimum and maximum channel limits form a linear line on a log-log axis plot and are equally spaced. The maximum concentration limits are 10^7 #/cc at channel 1 (channel midpoint: 6.04 nm) and 10^5 #/cc for channel 32 (channel midpoint: 523 nm). At the 1 Hz averaging rate, the minimum detection limits are approximately 130 #/cc for channel 1 and 30 #/cc in channel 32. The EEPS is also sensitive to road vibrations, further limiting its accuracy for low concentrations. The UCPC has no minimum detection limit, but does have a maximum limit of 99,900 #/cc. Even with dilution, this is often exceeded while sampling vehicle emissions. Furthermore, the UCPC only provides total particle counts and does not perform particle sizing. It does however, provide much greater accuracy (detection efficiency of 90% at and above 5 nanometers) and is not sensitive to road vibrations. Because the EEPS and UCPC total particle number concentrations track well together[23], UCPC data at the maximum limit can be extrapolated to the higher concentrations based on EEPS data (more detail is provided in the Appendix F).

2.2.2 Particle Sample Transfer and Dilution

The raw exhaust sample transported by the heated line into the vehicles was split between the gas- and particle-phase instrumentation. Prior to introduction into the particle emissions instrumentation, the raw sample was diluted with a two-stage dilution system. The first-stage dilution is performed by a Matter Engineering MD19-2E Rotating Disk Mini-Diluter. The MD19-2E included a peristaltic pump that draws raw exhaust through the heated line at 1 lpm. The raw exhaust was diluted using a 10-cavity disk, and the potentiometer – which controls the rotation rate of the disk – was set to 100% (minimum dilution). The dilution air heating element was set to 80˚C to prevent condensation during dilution. A first-stage dilution factor (total volume/exhaust volume) of 15.23 was therefore used, and was determined using the following equation[77]:

$$DF = \frac{X * CF}{pot\%} \qquad (2)$$

where: X = instrument specific calibration factor (1523 for 10-cavity disk)[78]
CF = temperature correction factor (1.00 for a setting of 80˚C)
pot% = the MD19-2E potentiometer setting (100 was used)

The Air Supply Evaporation Tube (ASET 15-1) – specifically designed to work alongside the MD19-2E to supply first-stage and second-stage dilution in one self-contained device – provided second-stage dilution for the vehicle exhaust. The ASET, which is necessary to overcome the maximum flow rate output limit of 5 lpm for the MD19-2E, draws first-stage diluted exhaust from the MD19-2E at 1.5 lpm into the evaporation tube set to 50˚C (to minimize thermophoretic losses). At the end of the evaporation tube is a cell where the second-stage dilution occurs. The potentiometer on the ASET was set to 7.1, meaning the second-stage dilution ratio was 1:7.1 (it's a one-to-one correlation between potentiometer setting and dilution factor). The second-stage dilution ratio of 1:7.1 was determined by the flow rates required by the instruments connected to the dilution system. Therefore, the total dilution ratio for the raw exhaust was 15.23 (first stage) times 7.1 (second stage), for the total of 1:108 (1 part raw exhaust to 108 parts dilution air).

From the outlet of the ASET, the diluted exhaust traveled through a 76 centimeter long section of 0.64 centimeter silicone conductive tubing (TSI, Inc.), which connected to a stainless steel Swagelok fitting. From this Swagelok fitting, the exhaust was split, first to the EEPS at 10.0 lpm, then to the UCPC at 1.5 lpm. The length of silicone conductive tubing (134 centimeters from Swagelok fitting to instrument) carrying the exhaust to the EEPS and UCPC was the same length to minimize artifacts from diffusive losses.

2.2.3 Particle Data Recording

The Dell Optiplex GX620 with a Pentium D central processing unit was used to record all particle-related emissions data used in the analysis. The EEPS data was recorded to the computer using TSI EEPS version 3.1.0 software, and the UCPC data was recorded to the PC using TSI AIM version 5.2.0 software.

2.2.4 Particle Instrumentation Vibration Mounts

Anti-vibration platforms were constructed for both the EEPS and UCPC to minimize inaccuracy and instrument error resulting from vibration while driving. The instrument platform for the UCPC uses 6 natural rubber mounts, and because the UCPC is influenced little by vibrations, these mounts serve to help minimize instrument malfunctions that could result from being jostled. The EEPS is mounted on 10 silicone gel mounts, which reduced electrometer noise caused by driving by 64%. The noise reduction was quantified by driving the route with the HEPA filter on the inlet of the EEPS over multiple runs (meaning electrometer noise was the result of electrometer particle counts). Two runs were performed without the platform and two runs were performed with the platform. The percent reduction was then quantified using Equation 3 on the total particle counts.

$$\%\ Reduction = \left[\frac{no\_platform - platform}{no\_platform}\right] * 100 \qquad 3$$

2.3 Gas-Phase Emissions

A commercially available Fourier transform infrared spectrometer analyzed tailpipe samples for gas-phase pollutants from the test vehicles. The MKS MultiGas 2030 high-speed analyzer, designed for fuel combustion applications, specifically for diesel and gasoline engines, was used for both qualitative and quantitative gas-phase emissions data collection.

2.3.1 FTIR Operating Principles

Growing applications for quantitative methods with IR spectroscopy have developed recently with the desire to differentiate and quantify constituents in atmospheric or more complex samples.[79] In infrared spectroscopy, compounds have a distinctive set of absorption features in the infrared portion of the electromagnetic spectrum resulting from the vibrational or rotational frequency of the molecule. As molecules become more complex, their vibrations depend on the interactions of many charge center which limits the ability to identify the unique absorption of the molecule and estimate its concentration.[79] Further complexity occurs in a mixture of compounds such as vehicle exhaust, where analytes may be identified, but difficult to quantify because the absorption at a given wavelength may be attributed to multiple constituents.[79]

In Fourier transform infrared spectroscopy (FTIR), the principles of infrared spectroscopy are applied to a unique method in which all of the frequencies across a range of IR are simultaneously detected. The advantages of FTIR over other infrared devices include improved throughput, known as the Jacquinot advantage, and multiplex design, known as the Fellgett advantage.[80] In traditional dispersive instruments, a narrow wavenumber range interacts with the sample, effectively limiting the light intensity reaching the detector. Although some of these instruments scan through a wide range of wavenumbers, the temporal resolution is limited, as single observations for a given wavenumber only exist for a small portion of the full sampling time.[80]

In FTIR, an infrared source produces radiation directed into an interferometer, where the beam is split, reflected, and recombined. Splitting the beam allows approximately half of the signal to be reflected on a fixed mirror and half on a moving mirror. The position of the moving mirror is known precisely, and as it translates produces a signal that has a varying phase pattern. The signal reflected on the moving mirror is then recombined with the signal reflected from the fixed mirror, producing a modulated signal with peaks and troughs altered based on the interference of the two beams. In-phase signals constructively interfere, increasing the magnitude of peaks and troughs, whereas out-of-phase signals destructively interfere, canceling the recombined signals out. The interferometer produces a modulated signal ranging from completely constructive to completely destructive interferences between the two signals, referred to as an interferogram. It is this signal that is passed through a gas sample. A detector captures the resulting range of infrared frequencies simultaneously. The signal reaching the detector is encoded with the absorption of compounds in the sample across the wide range of frequencies in the modulated signal. The Fourier transform is used to decode the summation of signals, which contains all of the intensity information across the wavenumber range of interest. The transform produces a single beam spectrum, indicating transmittance across the wavenumber region.

The signal passed through the gas cell is compared to a reference signal with nitrogen (N_2 and other homonuclear molecules non-detectable in the IR spectrum) in the gas cell. The comparison allows for conversion to absorbance of the particular gas compound of interest. Gas concentrations are quantified by comparison of the absorbance fingerprint to internal calibration curves of individual gas absorbance and concentration. Spectral regions used to quantify gases are selected to avoid interferences between gases with similar spectral identities.

2.3.2 MultiGas 2030 HS Gas Analyzer

A commercially available FTIR, the MKS MultiGas 2030 High-Speed Gas Analyzer, was used to collect near second-by-second spectral data from the tailpipe samples and quantify a large selection of gas-phase pollutants. The MKS unit operates with an infrared source of silicon carbide at 1200°C passed into the 200-milliliter (mL) volume gas cell through potassium bromide (KBr) windows and along the 5.11-meter path length reflected on gold-plated mirrors. A liquid nitrogen cooled mercury cadmium telluride detector interprets the signal after it has passed through the gas mixture.

In this application, the MKS MultiGas simultaneously quantified 30 gas-phase constituents, (31 data columns with CO reported in both parts-per-million and percent measures, see **Table 2-5**). Calibration curves internal to the MultiGas 2000 software (and reported in **Appendix E**) were referenced to convert the Fourier transformed absorbance of each compound in the IR spectra to a volumetric concentration by the Beer-Lambert Law

Classical Least Squares (CLS) method. The resulting compound quantification was reported at near one-second (0.98 seconds) temporal resolution.

Table 2-5. Gas-phase Constituents Analyzed by FTIR Method with Associated Structures

Pollutants		Formula	Structure	Pollutants		Formula	Structure
Greenhouse Gases	**Methane**	CH_4	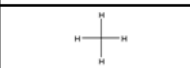	Alkanes	**Ethane**	C_2H_6	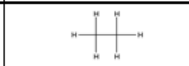
	Carbon Dioxide	CO_2	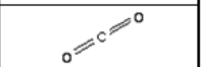		**Propane**	C_3H_8	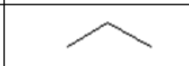
	Nitrous Oxide	N_2O	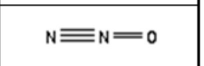		**Octane**	C_8H_{18}	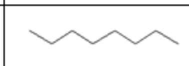
National Ambient Air Quality Standards	**Carbon Monoxide**	CO	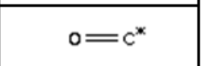		**IsoOctane**	C_8H_{18}	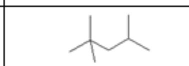
	Nitric Oxide	NO	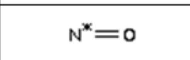	Alkenes	**Ethylene**	C_2H_4	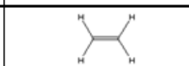
	Nitrogen Dioxide	NO_2	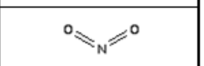		**Propylene**	C_3H_6	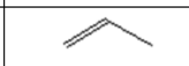
	Sulfur Dioxide	SO_2	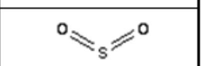		**2-Methylpropene**	C_4H_8	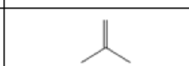
Mobile Source Air Toxics	**Formaldehyde**	CH_2O	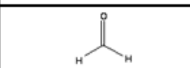	Allene	**1,2-Propadiene**	C_3H_4	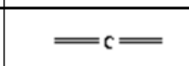
	Acetaldehyde	C_2H_4O	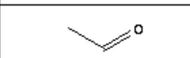	Alkynes	**Acetylene**	C_2H_2	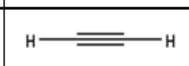
	Acrolein	C_3H_4O	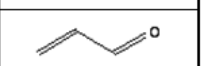		**Propyne**	C_3H_4	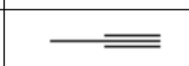
	1,3-Butadiene	C_4H_6	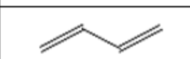	Aromatics	**Toluene**	C_7H_8	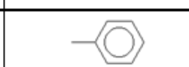
	Benzene	C_6H_6			**m-Xylene**	C_8H_{10}	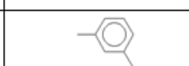
Alcohols	**Methanol**	CH_4O	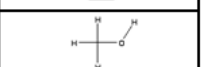		**1,2,4-Trimethylbenzene**	C_9H_{12}	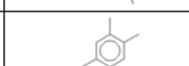
	Ethanol	C_2H_6O	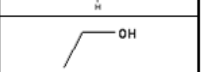		**1,3,5-Trimethylbenzene**	C_9H_{12}	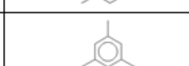
Misc	**Water**	H_2O	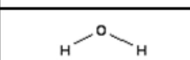		**Ammonia**	NH_3	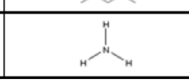

2.3.3 Gas-Phase Sample Handling

Condensed water and particulate present in the gas cell would interfere significantly with FTIR analysis. Maintaining high temperature samples (analyzed at 191°C) prevents water vapor from condensing in the gas cell, protecting the KBr windows from pitting and other damage. Particles could interfere with the signal passing through the gas cell either by remaining suspended and interfering with the signal as it passes through the sample cell or by accumulating on the sensitive sample cell mirrors and disrupting the reflection of the signal. To remove particles of concern from raw exhaust samples, a 2.0-micron particulate filter (Fiberfilm Pall Teflo Filters, United Filtration Systems T60A20-47) in-line with a 0.1-micron cartridge filter (Disposable Filter Elements, United Filtration Systems 12-57-50S21-R) was positioned at the inlet of the FTIR. The stainless steel filter housings were insulated with high heat insulation foam to ensure minimal heat loss as the filtered sample was transferred into the instrument from a heated line, delivering continuous exhaust samples from the tailpipe of the vehicle. The filters were exchanged for new filters each time TOTEMS was transferred to a different vehicle.

A personal sampling pump, the SKC Leland Legacy, drew tailpipe emission samples through the FTIR instrument at an adjustable 5 to 15 liters per minute on a self-contained battery pack. A set rate of 13-liters per minute, with considerations of tubing and filter resistances, achieved a flow rate of 12-liters per minute through the FTIR. Flow through the instrument was independently verified with a TSI digital flow meter. The sample had a one-second cell residence time as a result of the chosen flow rate and the known sample cell volume of 200 mL. A series of two water condensate traps, Nalgene bottles wrapped in ice packs, were positioned at the pump inlet to cool and condense the analyzed exhaust sample, preventing water damage to the pump.

2.3.4 Gas Species Quantification

The MKS MultiGas instrument quantification method was determined by the manufacturer according to spectra data collected in the Signature Project 2 Proof of Concept with the 1999 Toyota Sienna minivan and checked against preliminary data from the 2010 Toyota Camry conventional vehicle. The selected 31 gases provided a robust method of compounds expected in the exhaust sample. Quantification regions were assigned to each compound in the infrared spectra where there are features resulting from the absorbance of that species, commonly referred to as an IR fingerprint. Interferences between compounds in a selected quantification region were rectified by selection of narrower analysis bands, a process known as picket-fencing. Most of the compounds in the method were cross-checked for interference with H_2O and CO_2, as they are broad absorbers and notorious interferences in infrared analysis. The final analysis bands selected for each gas are represented in **Figure 2-8** with lower and upper bounds of each analysis band plotted. Additionally, algorithms used to analyze the spectra accounted for compounds absorbing in overlapping ranges, or "crosstalk" between compounds. It was important that the analysis bands were verified and that crosstalk, which can be quantified as residual in the MG2000 software, was minimized for each compound. It is reasonable to have residuals less than 0.005 absorbance units.

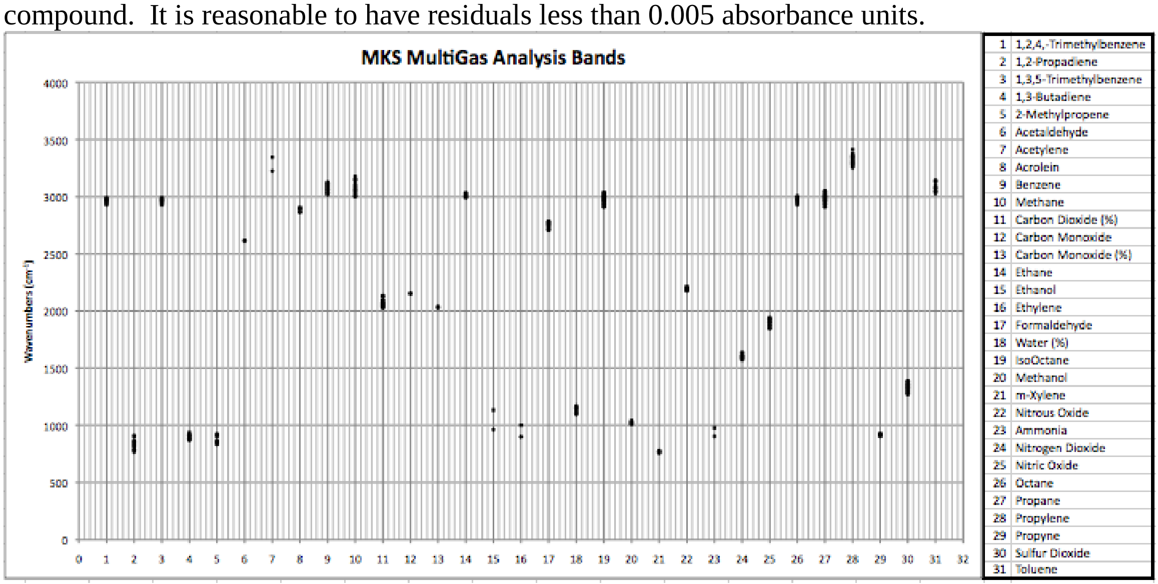

Figure 2-8. MKS MultiGas lower and upper wavenumbers for analysis bands selected from the quantification regions.

The analysis bands were selected from regions depicted in the calibration files of each of the analytes in the quantification method and reported in **Appendix E**.

Specifications of the FTIR were checked before and after each sampling run to make certain of consistent instrument behavior over the course of the study. Before the background was commenced for each run, the instrument monitor, peak analysis, and signal-to-noise functions verified instrument specifications. The instrument monitor assured a dry sample cell void of any contaminant signal and the health of the interferogram. Peak analysis data were tabulated as a check of the laser frequency and a water peak with a trace amount of water in the sample cell (full-width half-height (FWHH), frequency, peak absorbance units). Additionally, the signal-to-noise analyzer measured the noise of the signal over a selection of wavenumber ranges across the pertinent spectra (1000 to 1100 cm^{-1}, 2100 to 2200 cm^{-1}, and 2900 to 3000 cm^{-1}). The specifications checks were conducted in reverse order following a run to account for any drift that may have occurred during the run. Potential for damage to the sensitive components in the FTIR was highest during sampling, making post-run specification checks a means of documenting any potential compromise to the instrument while sampling exhaust. The specification check data for each run are tabulated and included in the **Appendix E**.

2.4 TOTEMS Quality Assurance and Quality Control (QA/QC) Procedures

2.4.1 Instrument and Tunnel Blanks

QA/QC procedures ensured that the TOTEMS instrumentation was consistently and accurately measuring parameters from day-to-day, both before and after each of the sampling runs. Additionally, the procedures established background measures on the instruments to ensure analysis was only of contributions by the vehicle. The QA/QC measures included acquisition of:

> (1) A *background*, or zero quantity for all gas- and particle-phase constituents. For the FTIR, this required the sample cell and inlet/outlet to be void of detectable constituents (nitrogen). This background series of spectra were referenced throughout the data collection period. For the EEPS, this required a zeroing of the electrometer rings while on clean air (HEPA) to ensure any residual particulate or charges were accounted for in any new measurements. Zeroing the electrometers reduced noise and artificial particle counts caused by electrical noise and mechanical vibrations. During the 45 second zeroing period, particle counts were assumed to be only instrument noise. From the data collected during the zeroing period, the EEPS calculated offsets independently for each electrometer and applies the offsets to every data point when sampling.
>
> (2) A ten-minute *instrument blank* data collection period with the FTIR sample cell and inlet/outlet void of detectable constituents (nitrogen) and the EEPS and CPC on inlet HEPA air to assess the noise of each of the instruments.
>
> (3) A ten-minute *tunnel blank* data collection period with the emissions instrumentation plumbed into the TOTEMS system, drawing samples through the tailpipe adapter but with the vehicle off, to quantify an ambient background measure of any trace contaminants in the system and assess the noise of the instruments with sample flow. This required the FTIR and SKC pump to running draw sample through the gas-phase system and the EEPS and CPC running in conjunction with the dilution system (MD-19/ASET) set at the proper settings.

These procedures were conducted in reverse order following each run.

2.4.2 Detection Limits and Blank Correction

A detection limit for each of the particle number size bins, total particle number measurements, and gas constituents accounted for the noise of the tailpipe sample measurements. Detection limits (DL) were calculated as a background measurement by the average of the tunnel blank data (pre- and post- run for the gas-phase measurements; pre-tunnel only for the particle measurements) plus three times the standard deviation of the tunnel blank data for a given sampling run as outlined in Equation 4.

$$DL_i = \overline{TB_i} + 3 * \sigma_{TB_i} \tag{4}$$

where: $\overline{TB}_i$ = mean of pre- or pre- and post-run tunnel blank data for given run i

σ_{TB_i} = standard deviation of tunnel blank data for given run i

Subtracting the detection limit from the gas- or particle-phase measured concentrations accounted for the noise in the measurement and any ambient background presence of a pollutant, effectively excluding instrument noise and background measures from any further analysis. This blank correction was applied to all raw emissions concentrations before calculating emission rates (outlined in Section 2.6).

Given that the EEPS channels each have a different acceptable electrometer noise level, blank correction was applied on a channel-by-channel basis. **Error! Reference source not found. Figure 2-9** shows an example of the noise that was subtracted from the particle number concentrations from one run as a function of particle diameter.

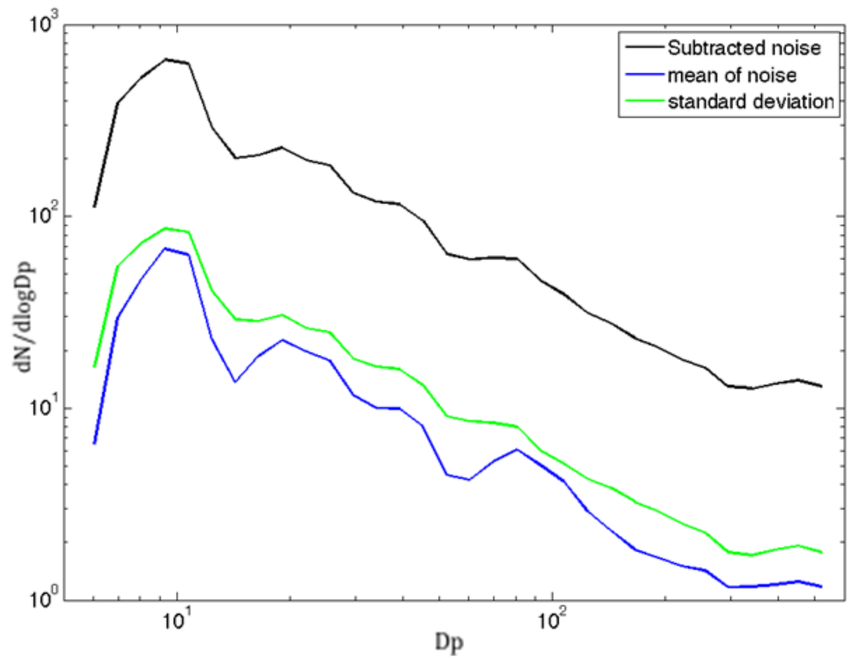

Figure 2-9. Run 7 EEPS noise correction showing the mean tunnel blank plus 3σ from each run subtracted off the EEPS raw data. “Mean of noise” is the calculated mean of the Run 7 tunnel blank (μ), “standard deviation” is the standard deviation of the tunnel blank (σ), and “subtracted noise” is μ + 3σ, which is subtracted from the 1 Hz EEPS run data.

2.5 TOTEMS Data Compilation and Post-Processing Methods

2.5.1 Time Alignment of Sub-Second Data

Alignment of data according to the time stamp was the first step in preparation for analysis. Data from the scantool and FTIR were recorded with sub-second time stamps, requiring adjustment to match the one-hertz data from all of the other TOTEMS instruments. The FTIR data were generated at a 0.98 second interval and reported to millisecond precision. To align the gas-phase data with the other instrument parameters, each record was rounded to the closest whole second and multiple records for a single time stamp were discretely averaged. Scantool parameters were recorded at inconsistent time intervals, ranging typically from 3 to 60 Hz intervals. These data were handled in the same fashion, rounded to the closest whole second with multiple records for a common time stamp discretely averaged. Aggregated scantool and FTIR data were then time-stamp aligned with all other data recorded with second-by-second resolution.

2.5.2 Lag Adjustment

Time-resolved vehicle emissions data posed a unique challenge in terms of aligning instantaneous vehicle operation parameters with associated emission events. Although data from each of the instruments was compiled by the second-by-second time stamp associated with each recorded measurement, additional consideration of the lag associated with a given parameter due to sample transfer or signal processing must be accounted for to make associations between parameters. For instance, a simple time stamp alignment would inaccurately associate engine functions (i.e. fuel injection or engine speed) with gas-phase tailpipe exhaust analysis. Lag adjustments were necessary due to two general considerations: (1) physical lag due to flow of a sample volume from the engine through the vehicle's exhaust system (engine to tailpipe) and from the tailpipe to each of the analysis instruments (tailpipe to instrument); and (2) computational or instrument response lag to account for the delay between an event and the time stamp assigned to the event within a data file.

Though lag adjustments existed in two forms, alignment for each instrument was treated as a single lag adjustment value for a given run phase (inbound and outbound). Lags were applied sequentially to different data subsets as **Table 2-6** identifies the stationary instrument (*Instrument A*) and the lag-adjusted instrument (*Instrument B*) with the corresponding parameters used for each step of lag adjustment. Pearson's correlations were calculated between Parameters A and B while varying the lag adjustments (i.e. t+1, t+2, etc.) on Parameter B in Matlab 7.10.0. The optimal Pearson's correlation coefficient between each set of *Parameters A* and *B* by run phase determined the corresponding lag adjustment ultimately assigned to *Instrument B*.

Table 2-6. Lag Adjustments by Pearson's Correlation (* indicates parameters that are defined in Section 2.6)

Instrument A	Parameter A	Instrument B	Parameter B
GPS	Vehicle Speed	Scantool	Vehicle Speed
Scantool	Acceleration*	Accelerometer	Acceleration*
Scantool	Engine Speed (RPM)	Differential Pressure Sensors, Thermocouples, Static Pressure Transducer	Flow Rate*
Scantool	Engine Speed (RPM)	FTIR	CO_2 ($\%_{vol}$)
EEPS	Total Particle Number	UCPC	Total Particle Number
Scantool	Engine Speed (RPM)	EEPS	Total Particle Number

Additional considerations of lag adjustment for the GPS units were determined through observation. Time stamp alignment of the Garmin and Geologger GPS units resulted in latitude and longitude locations typically less than 5 meters of one another, but speed from the two units consistently demonstrated Geologger speed preceding the Garmin by one second, likely due to the method of speed calculation by each unit. The Garmin speed was therefore lag-adjusted for the entire data set by one second ahead. Adjusted speed data from both GPS units was aligned with the Scantool speed, as outlined in **Table 2-6**, with the final lag adjustment determined by the GPS device speed with the best correlation coefficient.

The relative humidity and temperature sensors were joined to the primary Labview (L1) device based on their assigned time stamp before Labview was adjusted to other instruments. These units were launched via the onboard computer prior to logging run data and were assumed to have consistent readings during sampling, not requiring a fast response rate to rapid changes.

Lag adjustments actually applied to the raw data for each instrument combination, run, and phase were tabulated and are found in their entirety in **Appendix G**.

2.5.3 Grade Join

The spatially resolved ARAN data were spline fit to 1-meter resolution and used to develop a distance traveled value for the whole data collection route (not including warm-up or post-run driving). Temporally-resolved GPS data were assigned a distance traveled value based on the location, and filled for missing location gaps of up to 15 second duration using a speed-based interpolation. GPS data were filtered by a 25-meter buffer surrounding the route to ensure that the GPS information used in the join was actually on the driving course, using ArcGIS. Distance along the route assignments were the means by which ARAN road grade was joined to the temporally resolved data set, with priority for distance traveled from measured locations for each GPS unit over distance along the route at interpolated locations. Recommended grade from the 1-meter resolution data set was assigned for over 95% of the data set. Data that were collected off route due to detours or before or after the designated sampling run locations were not assigned a distance along the route or a recommended grade.

2.5.4 Valid Data for Analysis

A subset of the acquired data set was suitable for analysis. Data were omitted from analysis if there were known errors in the data collected (e.g. the FTIR pump failed or the heated line was turned off). Data were also omitted if more than 15% of a parameter was missing from the data set for a given outbound or inbound run phase. Results of this data validation procedure are enumerated in **Section 3.1** and further detailed in **Appendix A**.

2.6 Calculated Parameters

2.6.1 Exhaust Flow Rate

As TOTEMS sampled a small portion of the total tailpipe emissions output, it was critical to have a measure of the total flow rate at the tailpipe to calculate the total contribution of the vehicle's tailpipe pollutants to the atmosphere. Sampled compound concentrations (in percent or parts per million) measured by the FTIR were converted into an emission rate (grams per second) primarily by multiplying by the measured exhaust flow rate (liters per minute) for a given second of sampling, along with a few other conversion factors discussed in the next section. The pitot tube and four differential pressure sensors were calibrated in the laboratory each time TOTEMS was transferred from one vehicle to the other.

An apparatus for pitot tube calibration purposes was assembled of a large blower, lengths of mock tailpipe (steel and PVC), and a Sierra 620S flow meter. The tailpipe adapter was placed in line with the blower and the Sierra flow meter was connected to the tailpipe adapter with the pitot tube, pressure transducers, thermocouple, and sampling probe, with the exception of the heated line connection, which was capped during the calibration. The primary Labview (L1) connector block and data acquisition card assembly collected the Sierra flow meter raw voltage signal that was subsequently converted to flow in units of liters per minute (lpm) based on the factory calibration.

In the calibration setup, a combination of the blower potentiometer and the overflow valve were adjusted starting from a low flow setting through the tailpipe adapter and increased incrementally every sixty seconds to cover flow rates between zero and 4000 lpm (the upper bound of the Sierra as calibrated). An example raw signal from April 21, 2011 with increasing flow rate steps is shown in **Figure 2-10**.

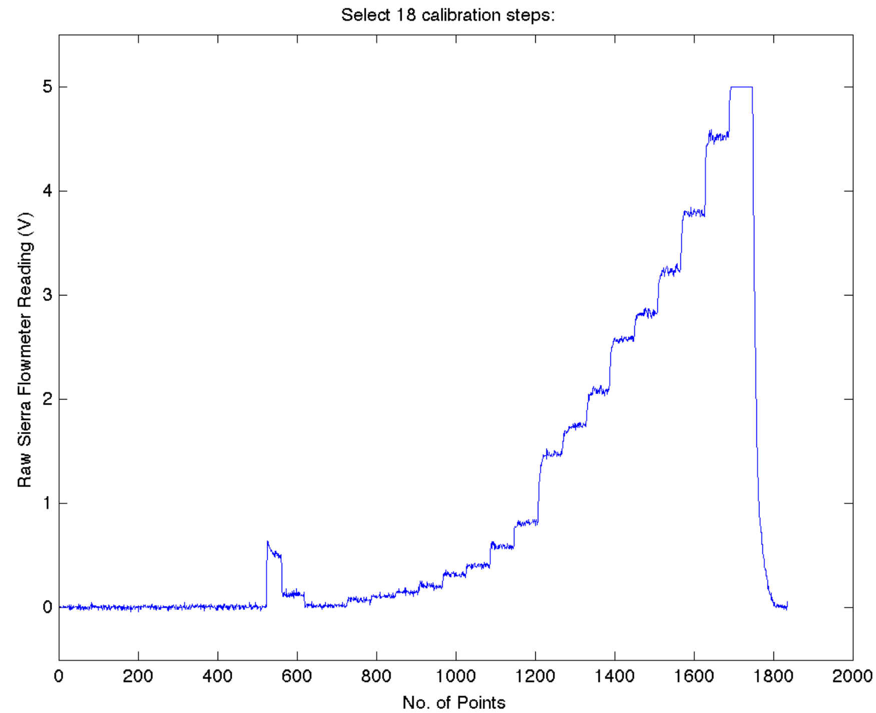

Figure 2-10. Typical pitot tube calibration sequence with raw voltage signal from the Sierra flow meter as the blower was adjusted to change flow through the mock tailpipe and TOTEMS tailpipe adapter during a calibration procedure on April 21, 2011.

Data compiled for all eight of the calibrations included flow rate plateau data, but excluded data transitions between flow rate settings over the study period to remove the influence of the Sierra flow meter response time. The raw Sierra signal was converted to a flow rate by a regression of the calibration included originally with the instrument.

Flow rate measures for each calibration step were regressed over the corresponding differential pressure signals measured from the pitot tube transducers using a square fit and forcing through zero intercept. Four calibration curves resulted (see **Appendix D** for detail) and were applied across all sampling runs, with additional conditions to select the sensor of appropriate flow range. Each of the pressure transducers was tuned to a specific range of the flow regime, with the fourth sensor the most sensitive and the first sensor the least sensitive. If the most sensitive sensor signal was reported within its usage range, it was selected for calculation of the exhaust flow rate; otherwise the next most sensitive was checked, and so on, until one of the four signals was selected. Final regressions, associated voltage usage ranges, and R-squared values were combined in the exhaust flow rate ($Q_{Exhaust}$) equation presented in Equation 5 and the complete analysis is included in **Appendix D**.

$$QExhaust = \begin{cases} \sqrt{83609.257 * (DiffP4 - 5)} & if\ 0.4 \le (DiffP4 - 5) < 4.6 \quad (R^2 = 0.87) \\ \sqrt{394516.8 * DiffP3} & if\ 0.4 \le DiffP3 < 9.6 \quad (R^2 = 0.98) \\ \sqrt{2129720.5 * DiffP2} & if\ 0.4 \le DiffP2 < 9.6 \quad (R^2 = 0.94) \\ \sqrt{14499240 * DiffP1} & if\ 0.4 \le DiffP1 < 9.6 \quad (R^2 = 0.70) \end{cases} \qquad 5$$

where: DiffP1 = Omega Differential Pressure Sensor 1 Raw Voltage Signal
DiffP2 = Omega Differential Pressure Sensor 2 Raw Voltage Signal
DiffP3 = Omega Differential Pressure Sensor 3 Raw Voltage Signal
DiffP4 = Omega Differential Pressure Sensor 4 Raw Voltage Signal

For a selection of sampling runs, the differential pressure sensors became unreliable. This was due to a low voltage on the battery providing power to the Labview device. The exhaust flow rate data for these runs (19, 23, 24, 25, 26, and 27) were estimated using an empirical relationship developed between engine speed (rpm) and exhaust flow rate. This equation was also applied to one run where the differential pressure sensors were not functional for the outbound section of data collection (run 74 phase 4). Equation 6 was used to calculate the estimated chosen flow for these instances as opposed to calculating the chosen flow rate from one of the differential pressure sensors (as in Equation 5).

$$Estimated\ Q_{Exhaust}[lpm] = -219.2309 + 0.7634308 * \mathrm{RPM} + 0.0003573 * (\mathrm{RPM} - 947.284)^2 \qquad 6$$

where: Estimated $Q_{Exhaust}$ = estimated chosen exhaust flow rate based on empirical RPM relationship

RPM = Scantool measured engine speed (rpm)

Exhaust flow rate was adjusted for temperature at the tailpipe adapter, as collected by the Type J Thermocouple. Erroneous signals from the tailpipe thermocouple affected about 12% of the sampling runs. Data became unreliable in part due to electrical interferences of the raw thermocouple signal, fixed by isolating the probe from the tailpipe adapter with a Teflon ferrule, and in part due to wear on the exposed tip thermocouple open to tailpipe exhaust and the environment, requiring more frequent replacement than originally anticipated. These erroneous data were recovered with an estimation of the exhaust temperature according to Equations 7 and 8 for the HEV and CV, respectively. These equations were derived based on scantool measurements and thermocouple data.

$$T_{Exhuast} = 0.02531 * RPM_{ICE} + 0.12429 * RPM_{\substack{Electric \\ Motor}} - 8.02726 * v - 0.06836 * Load_{ICE} + 100.7577 \qquad 7$$

where: RPM_{ICE} = internal combustion engine speed (rpm)
$RPM_{Electric\ Motor}$ = electric motor speed (rpm)
v = vehicle speed (kph)
$Load_{ICE}$ = internal combustion engine load (%)

$$T_{Exhaust} = 1.18298 * v + 0.02821 * RPM_{ICE} + 92.5954 \qquad 8$$

where: v = vehicle speed (kph)

RPM_{ICE} = engine speed (rpm)

Calculation of the temperature-compensated flow rate was necessary as the flow of a fluid through a pipe, in this case the exhaust system of the vehicle and the tailpipe adapter, is sensitive to temperature. Adjusting for temperature at the tailpipe was a function of the selected flow rate from $Q_{Exhaust}$ resulting from one of the four differential pressure sensors (or the estimated $Q_{Exhaust}$ for select runs from *6*) and the temperature either measured by the thermocouple or estimated by Equations 7 or 8. The flow rate to be used in further calculations was derived as shown in Equation 9.

$$Q_{TC} = Q_{Exhaust} * \left[\frac{T_{Exhaust} + 273.15}{298.15} \right] \qquad 9$$

where: Q_{TC} = temperature compensated tailpipe flow rate (lpm)
$Q_{Exhaust}$ = tailpipe flow rate chosen from the four differential pressure sensors (lpm)
$T_{Exhaust}$ = tailpipe exhaust temperature (°C)

2.6.2 Emission Rates

A method commonly used to report emissions from vehicles is by the emission rate of a specific pollutant or an aggregation of pollutants (i.e. grams per second of total hydrocarbons, THC). A rate of mass pollutant emitted from a vehicle over time or distance is a convenient metric to assess a vehicle's atmospheric pollutant contribution over a driving cycle or route.

Raw data from the FTIR were reported as volumetric concentrations in parts per million (ppm) or percent (%) for each individual gas. To account for the small volume sampled from the total tailpipe flow, concentration measures were converted to emission rates. Emission rates were reported on a mass per time basis as the data were collected on a second-by-second basis. The other typical convention is to report emission factors, mass of pollutant per unit distance. Additionally, emission rates or factors allow for ease of comparison with literature values. The general formula for calculating emission rates (Equation 10) was applied to all 1-hertz data after alignment of pitot data with scantool RPM (see **Table 2-6**).

$$ER_i\left[{}^{g}/_{s}\right] = \frac{C_i[\%\ or\ ppm] * MW_i\left[{}^{g}/_{mol}\right] * Q_{TC}\left[{}^{L}/_{min}\right] * P_{FTIR}[atm]}{R\left[{}^{L \cdot atm}/_{mol \cdot K}\right] * (T_{FTIR}[°C] + 273.15)[K] * V[\%\ or\ ppm] * 60\left[{}^{sec}/_{min}\right]} \qquad 10$$

where: C_i = detection limit corrected volumetric concentration of gas i (% or ppm)
MW_i = molecular weight of compound i (g/mol)
Q_{TC} = temperature compensated exhaust flow rate measured at the tailpipe (lpm)
P_{FTIR} = exhaust sample pressure at sampling point reported by FTIR (atm)
R = universal gas constant = 0.0821 (L.atm/mol.K)
T_{FTIR} = exhaust sample temperature at sampling point reported by FTIR (°C)
V = volumetric conversion constant (10^2 (%) and 10^6 (ppm) for equivalent liters)

Raw data from the EEPS and UCPC were converted from particle number concentrations to emission rates in a similar manner to the gas-phase pollutants. Relative to the recorded particle number concentrations (#/cc), emission rates (#/second) account for exhaust flow rate to provide the total particle number emissions on a second-by-second basis. Equation 11 was used to calculate the emission rate for every second of data.

$$ER_i\left[\#/_{\sec}\right] = C_i\left[\#/_{cc}\right] * Q_{TC}\left[L/_{\min}\right] * \left[\frac{1000cc}{1L}\right] * \left[\frac{1\min}{60\sec}\right] * DF \qquad 11$$

where: ER_i = emission rate in #/second for channel i (or total particle number)
C_i = UCPC concentration
Q_{TC} = temperature-corrected exhaust flow rate in lpm
DF = exhaust dilution factor of 108

2.6.3 Vehicle Specific Power

A measure of power exerted by a vehicle to overcome aerodynamic and rolling resistances and increase kinetic and potential energy, normalized by the mass of the vehicle, was computed as vehicle specific power (VSP). As previously discussed, the MOVES model uses VSP and speed to bin data according to operating modes, but utilizes a simplified version of the VSP equation due to limits in the data available to build a robust EPA modeling tool, primarily lacking sample sets with road grade terms. Jimenez (1999)[27] defined VSP and presented typical values for many of the vehicle parameters, including coefficients for internal resistances and rolling resistance, which are reflected in the equations used for this analysis. With vehicle specific information and road grade information in this comprehensive data set, a detailed approach may be used to calculate VSP, with the general and derived calculations presented in Equations 12 and 13, respectively.

$$VSP = VSP_{Kinetic} + VSP_{Potential} + VSP_{Rolling\mathrm{Resistance}} + VSP_{Drag} \qquad 12$$

$$VSP = 1.1(v * a) + g\left(\frac{grade}{100} * v\right) + 0.13244 * v + \frac{1}{2}\rho_a \frac{C_D * A}{m}\left(v^3\right) \qquad 13$$

where: VSP = vehicle specific power (kW/ton)
v = vehicle speed (m/s)
a = vehicle acceleration (m/s^2) (from Crossbow or Scantool)
grade = road grade (%)
ρ_a = air density (kg/m^3)
C_D = coefficient of drag (unitless)
A = vehicle cross-sectional area (m^2)
m = vehicle mass (kg)

Most of the VSP inputs were measured directly or referenced specific vehicle parameters provided by the manufacturer, with the exception of estimated vehicle mass and derivations for acceleration and air density. Two acceleration derivations were explored; one used acceleration from the x-axis of the Crossbow accelerometer (Equation 14), the other a derivation of speed as measured by the Scantool (Equation 15). Scantool derived acceleration was used for the purposes presented here.

$$accel_{Crossbow} = acc_x - 1.5 \tag{14}$$

where: $accel_{Crossbow}$ = acceleration (m/s^2)
acc_x = raw acceleration signal in the x-axis (V)

$$accel_{Scantool} = \frac{v(t+1) - v(t)}{\Delta t} \tag{15}$$

where: $accel_{Scantool}$ = acceleration (m/s^2)
v = vehicle speed (m/s)
t = time

The measure of air density included in the calculation of VSP was considered temperature dependent and calculated based upon measures from the relative humidity and temperature logger on the exterior of the vehicle. Air density was calculated according to Equation 16 on a second-by-second basis due to slight temperature fluctuations during the course of a sampling run.

$$\rho_a = \frac{P_a}{R_a * T_a} = \frac{352.977}{T_{Exterior} + 273.15} \tag{16}$$

where: ρ_a = Air density (kg/m^3)
P_a = Atmospheric pressure (1.01325*10^5 N/m^2)
R_a = Gas constant for air (287.058 N.m/kg.K)
T_a = Ambient air temperature (K)
$T_{Exterior}$ = Temperature collected by Onset logger (°C) with conversion to K

Actual vehicle mass was also needed to compute VSP. Although TOTEMS did not artificially load the engine for supply of power, TOTEMS loaded the vehicle with additional mass of the equipment and personnel in the vehicle. The added mass on the system resulting from driver, passenger, and instrumentation added to the curb weight of the vehicle provided by Toyota specifications. Distribution of the additional weight included front seat passengers, equipment in the back seat, and a full trunk load, as detailed in **Table 2-7**. Here, "phase" refers to two phases of data collection, each with a different passenger, for sampling runs 5 through 21 (Phase A) and 22 through 79 (Phase B). It was assumed that the average of the passenger weights from each phase could be used in the calculation of the totals for TOTEMS+personnel+ vehicle curb weight, tabulated **Table 2-8**, because the personnel weight represented less than 10% of the total calculated mass of the vehicle. The total average mass for each of the vehicles was used in calculation of VSP.

Table 2-7. Distribution of Weight in Vehicles due to TOTEMS Equipment and Personnel

Weight Distribution		
Component	**Weight (kg)**	**Weight (lbs)**
Front Seats		
K. Sentoff	62.1	138
M.Robinson (Phase A)	71.6	159
M. Conger (Phase B)	85.5	190
Total Phase A (Runs 5-21)	*133.7*	*297.0*
Total Phase B (Runs 22-79)	*147.6*	*328.0*
Back Seats		
EEPS	32	70
CPC	11	25
PC (on-board)	21.8	48
FTIR laptop	2.72	6
EEPS vibration mount	5.0	11.2
CPC vibration mount	1.5	3.4
2 Lifeline Batteries	143	316
Inverter	5.45	12
Yellow Top Battery	27.18	59.8
Total	*249.7*	*551.4*
Trunk		
FTIR	50	110
Legacy Pump	1	2.2
ASET 15-1/MD 19-2E	17.5	38.6
Differential Pressure Box	1.8	4
Labview Box	0.9	2
Heated Line	1.4	3.1
Total	*72.6*	*159.9*

Table 2-8. Total Curb Weight, TOTEMS, and Personnel Mass for VSP Calculation

Total Weight of Vehicles		
	Weight (kg)	**Weight (lbs)**
Total TOTEMS	322	711
Vehicle CV	*1533*	*3373*
Vehicle HV	*1673*	*3680*
Phase A Data Collection (Runs 5-21)		
Total Personnel	134	297
Total Phase A CV	*1989*	*4381*
Total Phase A HV	*2129*	*4688*
Phase B Data Collection (Runs 22-79)		
Total Personnel	148	328
Total Phase B CV	*2003*	*4412*
Total Phase B HV	*2143*	*4719*
Campaign Averages		
CV	**1996**	**4397**
HV	**2136**	**4704**

2.6.4 HEV Electric Drive Only Designation and Fuel Consumption

Electric drive only (EDO) was identified by a binary value (engine on = 0; engine off = 1) where engine speed was less than 775 RPM, the threshold established as the transition between the two engine states. The engine-off, or EDO, state of the HEV was determined for every record of the data set. In order to calculate a percentage EDO, the data had to be binned into categories, such as % EDO by run, VSP bin, OpMode, etc.

Instantaneous fuel consumption rates and fuel economy were calculated by the carbon balance method using Equations 17 and 18. These methods of determining fuel consumption rates and fuel economy were adapted from the code of federal regulations.[81, 82]

$$Fuel\ Consumption\ \left(\tfrac{gal}{s}\right) = \frac{0.273 * ER_{CO_2} + 0.429 * ER_{CO} + 0.817 * ER_{C_3H_8}}{2421} \quad (17)$$

$$Fuel\ Economy(mpg) = \frac{2421 * v * \tfrac{1}{3600} * 0.621}{0.273 * ER_{CO_2} + 0.429 * ER_{CO} + 0.817 * ER_{C_3H_8}} \quad (18)$$

Where: ER_{CO2} = carbon dioxide emission rates (g/s)
ER_{CO} = carbon monoxide emission rates (g/s)
ER_{C3H8} = propane emission rates (g/s)
v = vehicle speed (kph)

2.6.5 Additional Gas-Phase Constituents

Aggregations of gas-phase emissions as measured by the FTIR were used to summarize the tailpipe emissions profile of each vehicle. Equations 19 through 25 enumerate these calculations.

$$Alkanes = \sum(Ethane + Propane + Octane + IsoOctane) \quad (19)$$

$$Alkenes = \sum(Ethylene + Propylene + 2-Methylpropene) \quad (20)$$

$$Alkynes = \sum(Acetylene + Propyne) \quad (21)$$

$$Dienes = \sum(1,2-Propadiene + 1,3-Butadiene) \quad (22)$$

$$Aromatics = \sum(Benzene + Toluene + m\text{-}Xylene + Trimethylbenzenes) \quad (23)$$

$$NMHC = \sum(Alkanes + Alkenes + Alkynes + Dienes) \quad (24)$$

$$NO_x = \sum(Nitric\ Oxide + Nitrogen\ Dioxide) \quad (25)$$

3. Results

3.1 TOTEMS Data Subset For Analysis

Results presented in the following sections are from a subset of the full 75 run dataset because not all data from all runs met the QA/QC criteria. Data were included in the data analysis subset if at least 85% of the instrument data (indicated by a check mark in **Table 3-1**) for the given run section (outbound and inbound data were treated separately for QA purposes) were available for: scantool vehicle operating parameters, gas-phase emission rates (exhaust temperatures, tailpipe flow rate, and gas-phase concentrations), particle number emission rates (EEPS particle number distributions and tailpipe flow rate), location (latitude, longitude, and associated road grade), and ambient temperature. Run section was selected as the natural break for treatment of the data because any outbound section data collection issues were addressed at the Phase 6 Park-and-Ride facility location between the outbound and inbound sections of the run. The outbound portion of the run included operation on *city* and *highway* facility types, where the inbound portion of sampling was comprised of rural and suburban *arterials*. Detailed information on data collection issues for each run can be found in **Appendix A.**

The total number of 1 Hz sample records for each of the sampling run sections (Outbound or Inbound) included in the data analysis subset are indicated in **Table 3-2** for each vehicle type. **Table 3-2** also shows that the average number of records by section for each sampling run for the CV and HEV vehicles was quite similar. The main difference in the dataset between the two vehicle types was the larger number of tests run with the HEV; there were 38% more records for the HEV compared to the CV due to the larger number of runs attempted. The breakdown of runs by ambient temperature "season" (Cold, Cool, Warm, Hot) shown in **Table 3-2** indicates that there were at least 3 replicate runs of each vehicle in each season. Although there were more sampling runs conducted with the HEV in total, vehicle activity across these runs was expected to be equivalent and the total number of 1Hz records should therefore not impact average run data interpretation by vehicle type.

In addition to omitting erroneous or missing data sections from analysis, the QA/QC data was evaluated to ensure that gas- and particle-phase emissions were detectable for analysis. It is important to note that tailpipe pollutant concentrations for these two new, low-emitting vehicles were often near or at the conservative detection limits set by the pre- and post-tunnel blank data. This was particularly true for the HEV in electric drive only (EDO) operation, where pollutant concentrations would drop to background (or tunnel blank) values. The instrument detection limits defined by the TB data are available in **Appendix B.**

3.2 Vehicle Activity Comparison of CV and HEV

Comparison of the emissions between the two vehicle types depends on ensuring that both vehicles experienced the same range and frequency of driving activity over the test program. Here, the CV and HEV vehicle operating data are compared in terms of temporal patterns and distributions of speed and acceleration, VSP, MOVES OpMode, and measured fuel economy. Data are compared for each of the three facility types along the driving route: City, Arterial and Highway (recall that ramps are included in Highway classification, in agreement with MOVES). Furthermore, for the HEV only, data are summarized for the frequency of electric drive only (EDO) operation by facility type. (EDO operation was defined in Section 2.6.4).

Table 3-1. Run Section Data Evaluation for Data Analysis Subset Delineation*

Run No	Vehicle Type	Outbound	Scantool	Gas-Phase	Particulate	Location	Temperature	Inbound	Scantool	Gas-Phase	Particulate	Location	Temperature
5	CV	~~O~~	✓			✓	✓	~~I~~	✓		✓	✓	✓
6	CV	~~O~~	✓	✓	✓		✓	I	✓	✓	✓	✓	✓
7	CV	~~O~~	✓			✓	✓	I	✓	✓	✓	✓	✓
8	CV	O	✓	✓	✓	✓	✓	~~I~~		✓	✓	✓	✓
9	CV	~~O~~		✓	✓	✓	✓	~~I~~		✓	✓	✓	✓
10	CV	~~O~~	✓		✓	✓	✓	~~I~~	✓		✓	✓	✓
11	CV	~~O~~	✓		✓	✓	✓	~~I~~	✓		✓	✓	✓
12	CV	O	✓	✓	✓	✓	✓	I	✓	✓	✓	✓	✓
13	HEV	~~O~~	✓	✓		✓	✓	I	✓	✓	✓	✓	✓
14	HEV	O	✓	✓	✓	✓	✓	I	✓	✓	✓	✓	✓
15	HEV	O	✓	✓	✓	✓	✓	~~I~~	✓			✓	✓
16	HEV	O	✓	✓	✓	✓	✓	I	✓	✓	✓	✓	✓
17	HEV	O	✓	✓	✓	✓	✓	I	✓	✓	✓	✓	✓
18	HEV	O	✓	✓	✓	✓	✓	I	✓	✓	✓	✓	✓
19	HEV	~~O~~	✓		✓	✓	✓	I	✓	✓	✓	✓	✓
20	HEV	O	✓	✓	✓	✓	✓	I	✓	✓	✓	✓	✓
21	HEV	O	✓	✓	✓	✓	✓	I	✓	✓	✓	✓	✓
22	HEV	~~O~~	✓	✓	✓		✓	~~I~~	✓	✓	✓		✓
23	HEV	O	✓	✓	✓	✓	✓	I	✓	✓	✓	✓	✓
24	HEV	~~O~~	✓	✓	✓		✓	~~I~~	✓	✓	✓		✓
25	HEV	O	✓	✓	✓	✓	✓	I	✓	✓	✓	✓	✓
26	HEV	O	✓	✓	✓	✓	✓	I	✓	✓	✓	✓	✓
27	HEV	O	✓	✓	✓	✓	✓	I	✓	✓	✓	✓	✓
28	HEV	~~O~~	✓		✓		✓	~~I~~	✓		✓	✓	✓
29	HEV	~~O~~	✓		✓	✓	✓	~~I~~	✓		✓	✓	✓
30	HEV	~~O~~	✓		✓	✓	✓	~~I~~	✓		✓	✓	✓
31	CV	~~O~~	✓			✓		~~I~~	✓		✓	✓	✓
32	CV	~~O~~	✓		✓	✓	✓	~~I~~	✓		✓	✓	✓
33	CV	~~O~~	✓		✓	✓	✓	~~I~~	✓		✓	✓	✓
34	CV	~~O~~	✓			✓	✓	I	✓	✓	✓	✓	✓
35	CV	O	✓	✓	✓	✓	✓	I	✓	✓	✓	✓	✓
36	CV	O	✓	✓	✓	✓	✓	I	✓	✓	✓	✓	✓
37	CV	O	✓	✓	✓	✓	✓	I	✓	✓	✓	✓	✓
38	CV	O	✓	✓	✓	✓	✓	I	✓	✓	✓	✓	✓
39	CV	O	✓	✓	✓	✓	✓	~~I~~					
40	CV	O	✓	✓	✓	✓	✓	I	✓	✓	✓	✓	✓
41	HEV	~~O~~	✓			✓	✓	~~I~~	✓			✓	✓
42	HEV	O	✓	✓	✓	✓	✓	I	✓	✓	✓	✓	✓
43	HEV	O	✓	✓	✓	✓	✓	I	✓	✓	✓	✓	✓
44	HEV	~~O~~	✓	✓		✓	✓	~~I~~	✓	✓		✓	✓
45	HEV	~~O~~		✓		✓	✓	~~I~~	✓	✓		✓	✓
46	HEV	~~O~~	✓	✓		✓	✓	~~I~~	✓	✓		✓	✓
47	HEV	~~O~~	✓	✓		✓	✓	~~I~~	✓	✓		✓	✓
48	HEV	O	✓	✓	✓	✓	✓	~~I~~				✓	✓
49	HEV	O	✓	✓	✓	✓	✓	~~I~~		✓	✓		✓
50	HEV	~~O~~		✓	✓		✓	I	✓	✓	✓	✓	✓
51	HEV	O	✓	✓	✓	✓	✓	I	✓	✓	✓	✓	✓
52	HEV	O	✓	✓	✓	✓	✓	~~I~~	✓	✓	✓		✓
53	HEV	O	✓	✓	✓	✓	✓	I	✓	✓	✓	✓	✓
54	CV	O	✓	✓	✓	✓	✓	~~I~~		✓	✓		✓
55	CV	O	✓	✓	✓	✓	✓	I	✓	✓	✓	✓	✓
56	CV	O	✓	✓	✓	✓	✓	I	✓	✓	✓	✓	✓
57	CV	O	✓	✓	✓	✓	✓	~~I~~	✓			✓	✓
58	CV	O	✓	✓	✓	✓	✓	I	✓	✓	✓	✓	✓
59	CV	O	✓	✓	✓	✓	✓	I	✓	✓	✓	✓	✓
60	CV	O	✓	✓	✓	✓	✓	I	✓	✓	✓	✓	✓
61	CV	O	✓	✓	✓	✓	✓	I	✓	✓	✓	✓	✓
62	CV	~~O~~	✓	✓	✓		✓	I	✓	✓	✓	✓	✓
63	CV	~~O~~		✓	✓	✓	✓	I	✓	✓	✓	✓	✓
64	CV	O	✓	✓	✓	✓	✓	I	✓	✓	✓	✓	✓
65	CV	O	✓	✓	✓	✓	✓	I	✓	✓	✓	✓	✓
66	CV	O	✓	✓	✓	✓	✓	I	✓	✓	✓	✓	✓
67	CV	X O	✓	✓	✓	✓	✓	X I	✓	✓	✓	✓	✓
68	HEV	O	✓	✓	✓	✓	✓	I	✓	✓	✓	✓	✓
69	HEV	O	✓	✓	✓	✓	✓	I	✓	✓	✓	✓	✓
70	HEV	O	✓	✓	✓	✓	✓	I	✓	✓	✓	✓	✓
71	HEV	O	✓	✓	✓	✓	✓	I	✓	✓	✓	✓	✓
72	HEV	O	✓	✓	✓	✓	✓	I	✓	✓	✓	✓	✓
73	HEV	O	✓	✓	✓	✓	✓	I	✓	✓	✓	✓	✓
74	HEV	O	✓	✓	✓	✓	✓	~~I~~	✓	✓	✓		✓
75	HEV	~~O~~			✓		✓	I	✓	✓	✓	✓	✓
76	HEV	O	✓	✓	✓	✓	✓	I	✓	✓	✓	✓	✓
77	HEV	O	✓	✓	✓	✓	✓	I	✓	✓	✓	✓	✓
78	HEV	~~O~~	✓			✓	✓	I	✓	✓	✓	✓	✓
79	HEV	X O	✓	✓	✓		✓	X I	✓	✓	✓	✓	✓

✓ data are valid ╲ run phase omitted X aggressive driving
I Inbound O Outbound

*** A slash indicates that either the outbound (O) or inbound (I) section data for that run were omitted from analysis for the reasons given in Appendix A. Runs 67 and 79 are marked with "X" to indicate that driver was instructed to drive more aggressively for these runs only.**

Table 3-2. Number of Records and Number of Runs in the Valid Data Analysis Subset by Vehicle Type

Phase	Temperature	Vehicle CV	Vehicle HEV
		Number of Records	
		74859	**103633**
		Number of Records	
Outbound		**35240**	**49864**
Inbound		**39619**	**53769**
		Number of Valid Runs	
Outbound		**19**	**27**
Inbound		**20**	**27**
		Records per Run (Mean ± Std Dev)	
Outbound		**1855 ± 132**	**1847 ± 190**
Inbound		**1981 ± 120**	**1991 ± 129**
		Number of Records	
Outbound	Cold (T < 5°C)	5464	10197
Inbound		5441	13697
Outbound	Cool (5°C ≤ T < 22°C)	10930	14478
Inbound		11696	12145
Outbound	Warm (22°C ≤ T < 29°C)	7252	14184
Inbound		8088	16045
Outbound	Hot (29°C ≤ T)	11594	11005
Inbound		14394	11882
		Number of Valid Runs	
Outbound	Cold (T < 5°C)	3	6
Inbound		3	7
Outbound	Cool (5°C ≤ T < 22°C)	6	8
Inbound		6	6
Outbound	Warm (22°C ≤ T < 29°C)	4	7
Inbound		4	8
Outbound	Hot (29°C ≤ T)	6	6
Inbound		7	6

Vehicle Activity Patterns

Overall, the speed, acceleration, road grade, and VSP activity was consistent between individual sampling runs across the route. Typical activity for two example runs, one for each vehicle type, are shown in **Figure 3-1**. The outbound section was characterized by lower mean speed, stop-and-go driving in the city initially, followed by ~65 mph travel on the highway. After a stop at the Park-and-Ride, the inbound section included transient driving at intermediate speeds on arterial roads with less frequent stops than the city (**Figure 3-1**). Road grade associated with distance along the route only varied by small margins between runs depending on the timing of the vehicle passing a particular location.

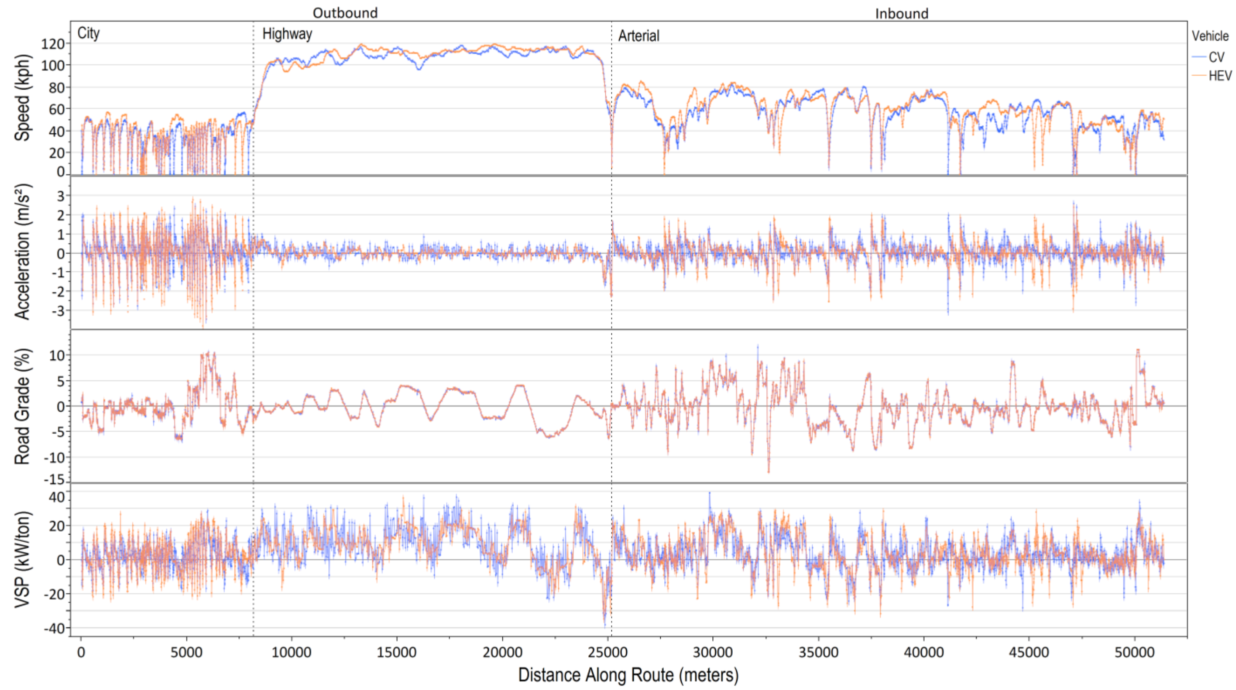

Figure 3-1. Second-by-second vehicle activity for example runs from each vehicle type (Runs 18 and 40) across the full route by distance travelled. The dashed vertical lines delineate between the city, highway, and arterial facility types along the sampling route.

Each of the three facility types along the route provided different ranges of vehicle operation, as demonstrated by the magnitude of mean vehicle speed, calculated load, engine speed, and VSP shown in **Table 3-3**. Mean vehicle speed and VSP were generally consistent between the two vehicles for a given facility type (**Figure 3-1** and **Table 3-3**, as expected for a single driver operating the two vehicles on a designated driving route. Small, if any, discrepancies between the vehicles for these parameters were due to real-world factors such as traffic, constrained driving due to car-following, pedestrian activity, signalization, etc. Differences between vehicles for engine parameters (load and RPM, **Table 3-3**) can be attributed to the performance of the hybrid platform, primarily enabling ICE-assist and electric drive only operation to varying degrees for each facility type. For example, the very low mean engine speed on city and arterial sections of the route reflects the relatively high percent of operating time in EDO operation under low load driving.

Table 3-3. Mean Vehicle Activity Parameters for CV and HEV across the Test Route's Three Facility Types (± Standard Deviation)

Parameter	Vehicle	City			Arterial			Highway		
Speed (kph)	CV	23.5	±	16.4	47.0	±	20.9	101.7	±	17.4
	HEV	22.7	±	17.2	46.1	±	21.3	99.2	±	20.1
Load (%)	CV	43.2	±	17.9	48.3	±	21.2	61.9	±	25.2
	HEV	30.2	±	35.2	39.8	±	36.2	65.8	±	23.7
Engine Speed (RPM)	CV	1301.7	±	489.9	1480.5	±	491.3	2093.0	±	396.3
	HEV	626.5	±	797.0	886.2	±	889.5	1832.3	±	802.2
VSP (kW/ton)	CV	1.4	±	6.7	2.6	±	8.3	8.3	±	11.7
	HEV	1.4	±	6.9	2.5	±	7.8	7.4	±	10.2

Characteristic vehicle activity by facility type is demonstrated by the box plots of speed, acceleration, and road grade by VSP encountered on the route (**Figure 3-2**). Low, moderate and high speed driving were characteristic of city, arterial, and highway facility types, respectively. Wider ranges of acceleration typical of stop-and-go operation were measured for city driving than for arterial or highway driving where more activity was likely occurring at target speeds set by speed limits of 45 and 65 mph, respectively. The range of road grade was largest for the arterial portion of the route.

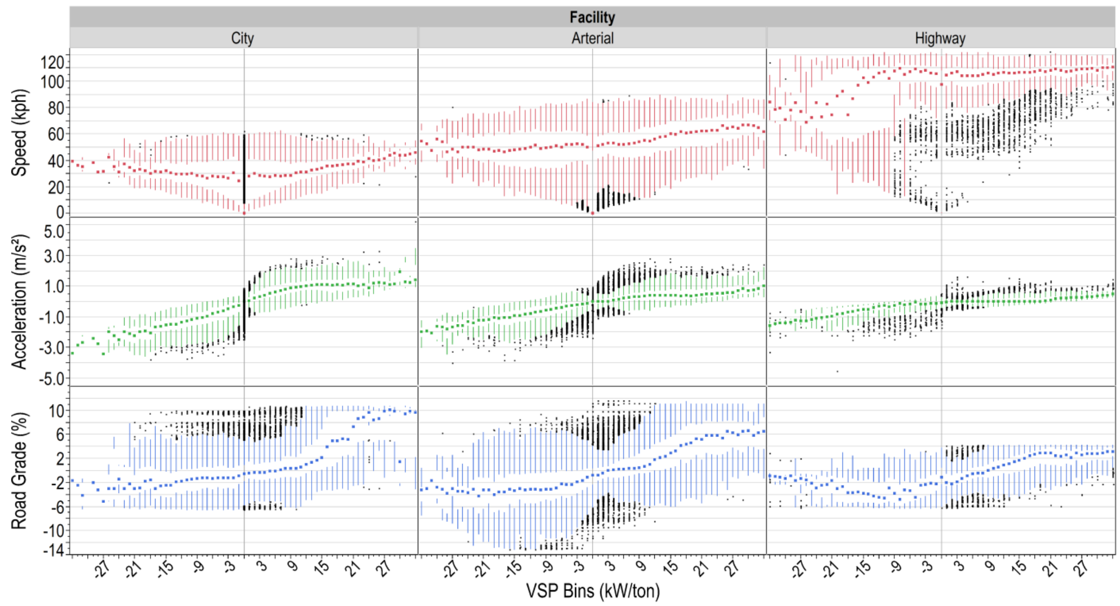

Figure 3-2. Speed, acceleration, and road grade across VSP bins, where the box represents the median, white space between whiskers is the interquartile range, and the whiskers represent 1.5 times the interquartile range.

Vehicle Specific Power and Operating Mode Comparison

Vehicle specific power not only increased on average across facility types (**Table 3-3**), but the distribution of data across the range of VSP experienced on the route changed by facility type (**Figure 3-3**). City and arterial driving show a near normal distribution centered at 0 kW/ton, characteristic of the stop-and-go, acceleration/deceleration, uphill/downhill nature of the driving on these facilities. Each had a significant amount of activity (>10%) at 0 kW/ton representing the higher frequency of idle operation on these two facilities compared to highway driving. Highway activity was chiefly at higher speeds, allowing the kinetic term of the VSP equation to dominate and skewing the VSP distribution to the right of 0 kW/ton. Although the distribution changed across facility types, the distributions were generally comparable (within 2% for each VSP class) between vehicle types (compare orange bars vs. blue line in **Figure 3-3**).

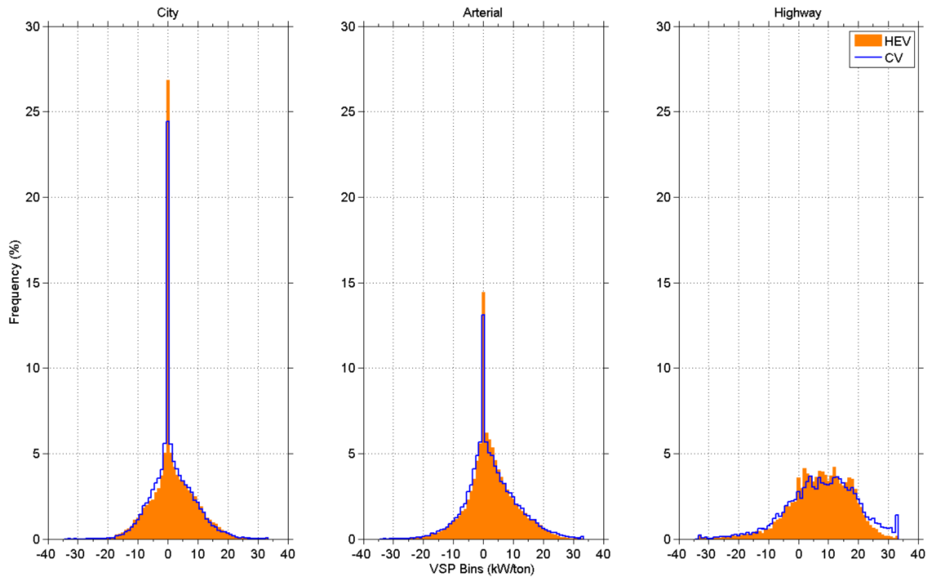

Figure 3-3. Histograms of VSP (±1 kW/ton increments) for each vehicle type, separated by facility type.

Because MOVES operating modes are defined by three vehicle speed categories as well as VSP, activity differences between the three facility types are more evident in the operating mode (OpMode) distributions (**Figure 3-4**). Again, on a given facility type, the OpMode distributions for the two vehicles were comparable (within 5% for any given OpMode), as expected for a single driver on a designated driving route. Variability in the OpMode distributions between vehicles was likely due to uncontrolled real-world driving factors outside of the control of the driver. These factors chiefly included signal timing and traffic congestion.

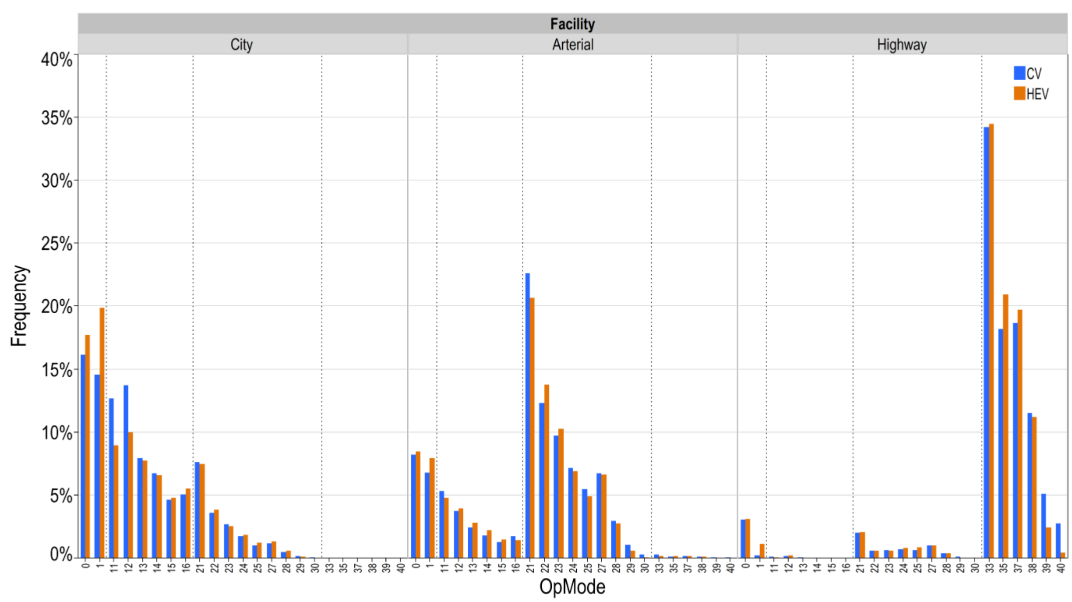

Figure 3-4. Frequency distribution of vehicle activity by MOVES OpMode across all three facility types for each vehicle type. Vertical dashed lines indicate the three MOVES speed categories.

HEV Electric Drive Only (EDO) Operation

Given that vehicle activity, defined either by VSP or OpMode distribution, was equivalent for the two test vehicles, differences in fuel consumption and emissions could be attributed to the functionality of the hybrid-electric vehicle platform. Electric drive only (EDO) operation was responsible for the most significant differences in engine operation between the two vehicle types. The frequency of EDO also changed with the facility type: greater reliance on EDO operation occurred for low speed city driving than for arterial or highway driving. The time spent in EDO operation on the arterial section of the route was surprisingly high, only about 15% less than the city (~60%). The measured 4-5% EDO operation for the HEV on the highway generally occurred on the on- and off-ramps of the route.

The HEV's mean time spent in EDO operation changed across facility types, but also changed across the range of VSP within each facility (**Figure 3-5**). At low VSP (< 0 kW/ton), the likelihood of EDO operation was higher for city and arterial driving than for highway, as expected. For the highway, ICE-off activity never surpassed 40% and most of the EDO activity was attributed to on/off ramp driving. For city and arterial driving, the HEV repeatedly operated on EDO propulsion over 50% of the time for all negative VSP operating points, consistent with downhill and deceleration driving modes. With increasing positive VSP, the frequency of ICE-off operation fell from greater than 90% to 0% between 0 kW/ton and 9-12 kW/ton, depending on facility type. Thus, when driving conditions demanded the HEV operate at VSP > 12 kW/ton, the load on the vehicle was too great for the Hybrid Synergy Drive® technology to allow the ICE to shutdown. This VSP maximum for EDO operation agrees with the Mode 7 (10 to 13 kW/ton) reported by Zhai and Frey (2011) for a model year 2001 Toyota Prius.[83] It should be noted that there were few data records in some of the high negative VSP classes (i.e., VSP < -25 kW/ton) and this contributed to the large error bars in **Figure 3-5**.

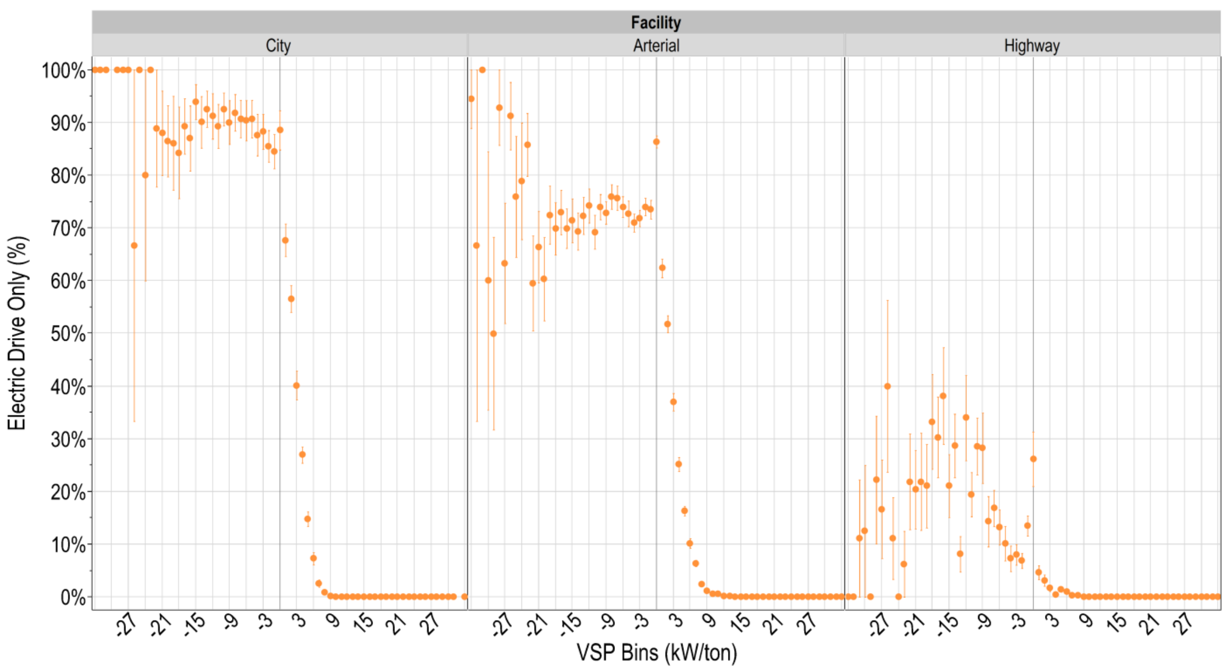

Figure 3-5. Percent time the HEV operated with the ICE off in EDO propulsion mode across the VSP bins for each facility type. Points and error bars represent the mean ± standard error across all valid run data.

Low speed (<25 mph) operation dominated the city driving, moderate speed (25 to 50 mph) the arterial driving, and high speed (50+ mph) the highway driving, as expected given the speed limits, signalization, congestion, and other limitations of these three facility types. As expected, the frequency of the idle (OpMode 1) and braking (OpMode 0) modes decreased from city to arterial to highway. The highest frequency of EDO propulsion for the HEV occurred during idling and braking OpModes, but considerable EDO operation also occurred in OpModes with VSP less than 9 kW/ton (i.e., up to OpMode 14 at low speeds and up to OpMode 24 at moderate speeds; **Figure 3-6**). The large error bars in **Figure 3-6** for highway operation were due to the limited activity experienced in the lower speed modes (OpModes = 12, 13) on this facility type.

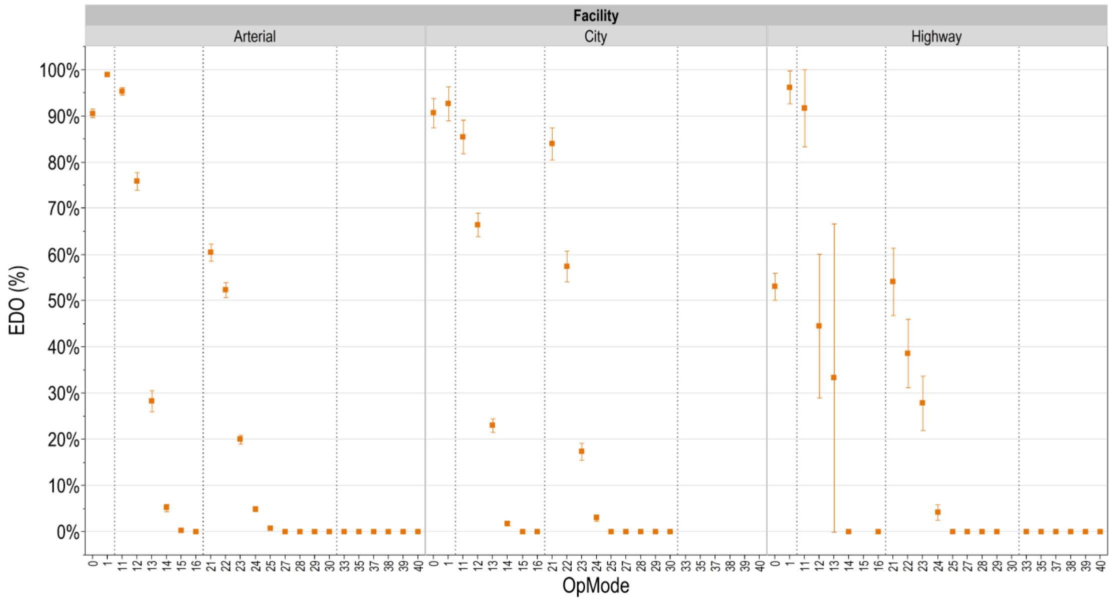

Figure 3-6. Percent time EDO propulsion for HEV across all MOVES Operating Modes by facility type. Mean ± standard error represented by the point and error bars for a given OpMode.

Vehicle Operation and Ambient Temperature

Although driver-dictated vehicle activities (e.g. target speed, acceleration rates, overall VSP, OpMode frequencies) were not expected to change based on season, the operation of each vehicle to meet the driver's demands was expected to have some response to ambient conditions. Data were collected only in dry weather to isolate the effects of temperature and relative humidity on the vehicle operation, fuel economy and emissions for each vehicle. Inclement weather (resulting in wet or snow-covered roads), particularly for cold seasonal temperatures, would be expected to significantly change vehicle activity (e.g. low speeds on highway during snow squalls) and thus invalidate inter-seasonal comparisons between the two vehicles.

Temperature effects on EDO propulsion were highest during operation in the city, where the median EDO changed by about 11% between cold and cool temperatures. **Figure 3-7A** demonstrates the high variability introduced in EDO operation under cold ambient temperature conditions, particularly for city driving, with a 23% interquartile range (i.e., spanning from 40% to 63% in **Figure 3-7A**). This variability indicates that, under cold temperature operation, it may be more difficult to predict the EDO propulsion during city driving with certainty. For other driving conditions, EDO% by temperature class spanned a maximum of 12%, indicating that the all-electric operation was more consistent (**Figure 3-7A**).

Battery state of charge (SOC, **Figure 3-7B**), a parameter indicating the performance of the HEV electrical energy storage system, trended with ambient temperature and facility type. State of charge consistently decreased as temperature increased across each facility type. This trend was in contrast to EDO%, which tended to peak with warm temperatures for city driving, decreased slightly with increasing temperature for arterial driving, and remained within 3% EDO for highway driving (**Figure 3-7A**).

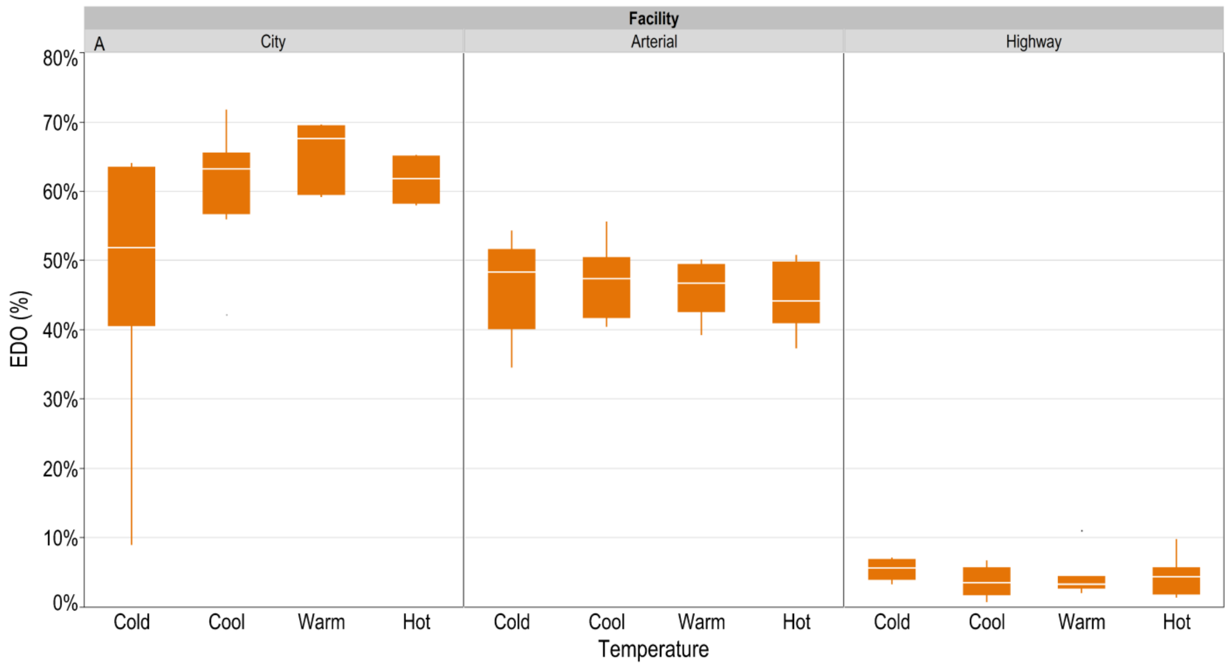

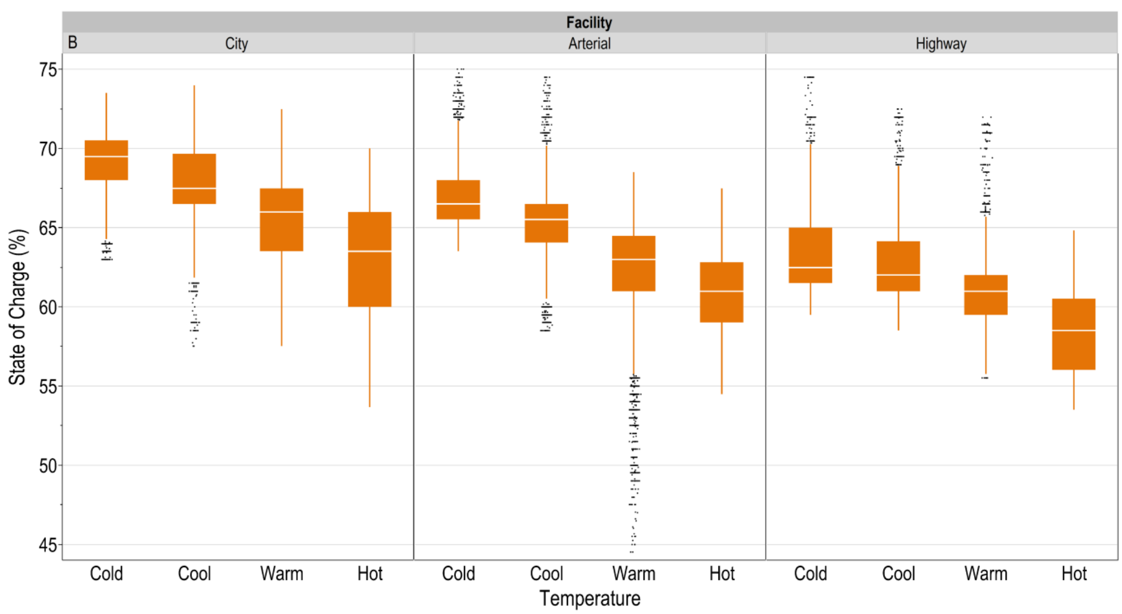

Figure 3-7. Boxplots of (A) Electric Drive Only HEV operation (across average EDO per run) and (B) battery state of charge by facility type and ambient temperature bin. Note: boxplots represent the interquartile range and whiskers represent 1.5 times the interquartile range.

Fuel Consumption Rates and Fuel Economy

Generally, across the full driving route, the HEV consumed less fuel than the CV across all facility types and temperature conditions as shown in **Table 3-4**. As expected, fuel economy of the HEV followed a trend with VSP that was similar to that for EDO operation: low VSP (< 0 kW/ton) was associated with high mile-per-gallon instantaneous fuel economy (FE) that decreased exponentially above 0 kW/ton VSP (**Figure 3-8**). For the HEV, the fuel economy pattern with VSP was consistent across the three facility types, with generally high fuel economy (>80 mpg) for negative VSP, dropping off significantly at VSP greater than zero. At the high end of the VSP distribution (VSP > 20 kW/ton), there was approximately a 10 mpg discrepancy between city and highway facility types, which is significant given that there is more activity in the high VSP bins for highway than city driving. The instantaneous fuel economy of the CV was much lower than that for the HEV for VSP <0 kW/ton and the difference between vehicle types diminished from city to highway driving (**Figure 3-8**). The maximum difference in instantaneous fuel economy between CV and HEV was about 50 MPG for city, 30 MPG for arterial and 20 MPG for highway driving and occurred at negative VSP operation (**Figure 3-8**). These trends in FE are likely explained by the % EDO propulsion of the HEV. With increasing positive VSP (VSP >0 kW/ton), the CV's fuel economy showed an exponentially decreasing pattern similar to that observed for the HEV.

Table 3-4. Comparison of HEV and CV Fuel Economy and Fuel Consumption Rate by Descriptive Statistics

Parameter	Vehicle	Mean	Std Dev	Min	Max
Fuel Economy	CV	28.8	26.2	0	100
(mpg)	HEV	48.8	40.9	0	100
Fuel Consumption Rate	CV	0.00048	0.00051	0	0.00415
(gal/sec)	HEV	0.00033	0.00046	0	0.00414

The VSP at which the fuel economy for both vehicles was equal varied with facility type. The "cross-over" VSP (at which CV = HEV fuel economy) was 20, 9 and 21 kW/ton for the city, arterial, and highway facility types, respectively (**Figure 3-8**). The lower cross-over VSP for arterial driving may reflect the relatively hilly driving at moderate speeds along the route that may have resulted in battery recharging events to a higher degree than was possible either under highway or city driving. Higher battery recharging would enable more EDO propulsion at higher VSP (in agreement with the **Figure 3-5** data for arterial). More detailed investigation of the HEV's energy status and performance is warranted to better quantify arterial driving behavior.

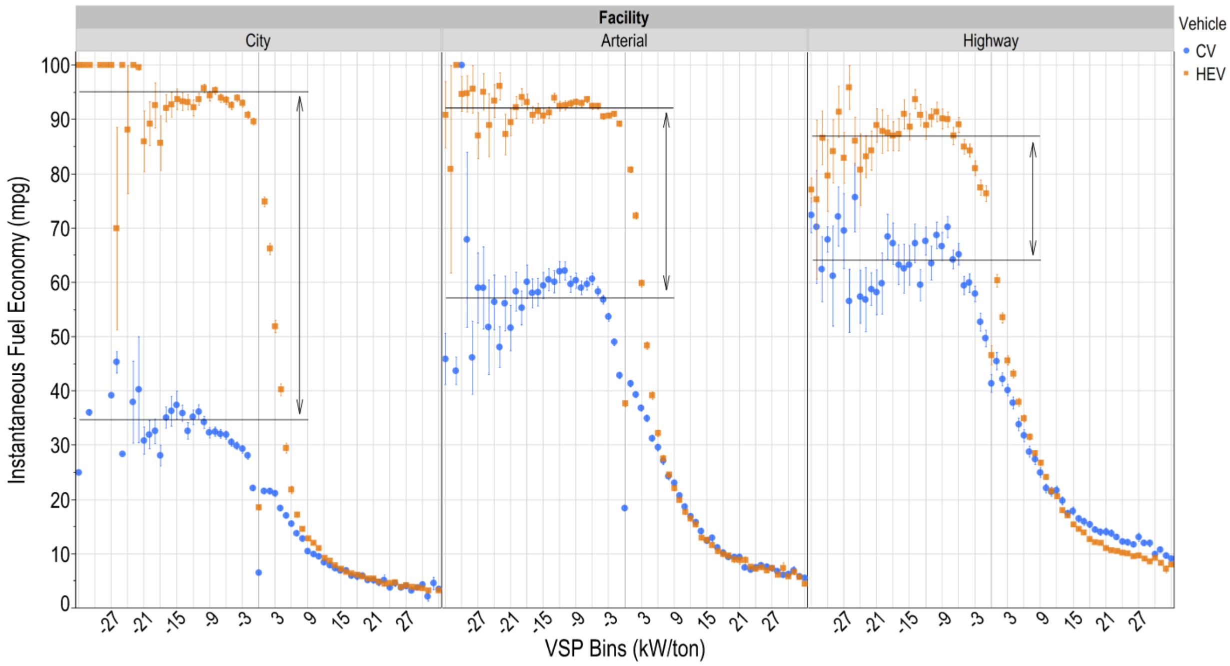

Figure 3-8. Instantaneous fuel economy for each vehicle type across all VSP bins, where the fuel economy is estimated by the carbon balance method. Points represent the mean and error bars represent the standard error.

As observed for relationships to VSP, the fuel economy pattern with OpMode also followed the EDO pattern of the HEV, with the highest mile-per-gallon achieved in operating modes corresponding to the greatest EDO occurrences (**Figure 3-9**). For both vehicles, fuel economy generally decreased as OpMode (and VSP) increased across each speed regime. The fuel economy of the HEV was typically higher than that for the CV, especially for the low and moderate speed OpModes with VSP less than 6 kW/ton (11-13 and 21-23). For OpModes 11 and 21, where coasting occurred, FE could reach 90 mpg for the HEV, but the maximum CV mean fuel economy was about 60 mpg (coasting at moderate speed or OpMode 21 during arterial driving; see **Figure 3-9**).

The data shown in **Figure 3-8** and **Figure 3-9** indicate that there exist a number of higher power operating regimes where the CV has better instantaneous fuel consumption than the HEV. For city and arterial driving, equivalent fuel economy between the two vehicles occurred at OpModes 24-28. For arterial driving at speeds >50 mph (in OpModes 33-40), the CV had higher (better) mean fuel economy than the HEV. For highway travel, the HEV had better (higher) mean fuel economy at all OpModes <37, but the difference between vehicles decreased with increasing VSP in a speed category. The differences between arterial vs. highway instantaneous fuel economy pattern for the high speed category (speed > 50 mph) OpModes (OpMode>33) may be attributed to the: (i) higher road grade experienced on the arterial portion of the route vs. highway; (ii) higher overall ICE power demand at highway speeds; (iii) HEV battery state-of-charge recharge/discharge pattern differences by facility type. Further work is needed to quantitatively evaluate the HEV energy performance and its effect on fuel consumption as a function of facility type, road grade and prior operating history.

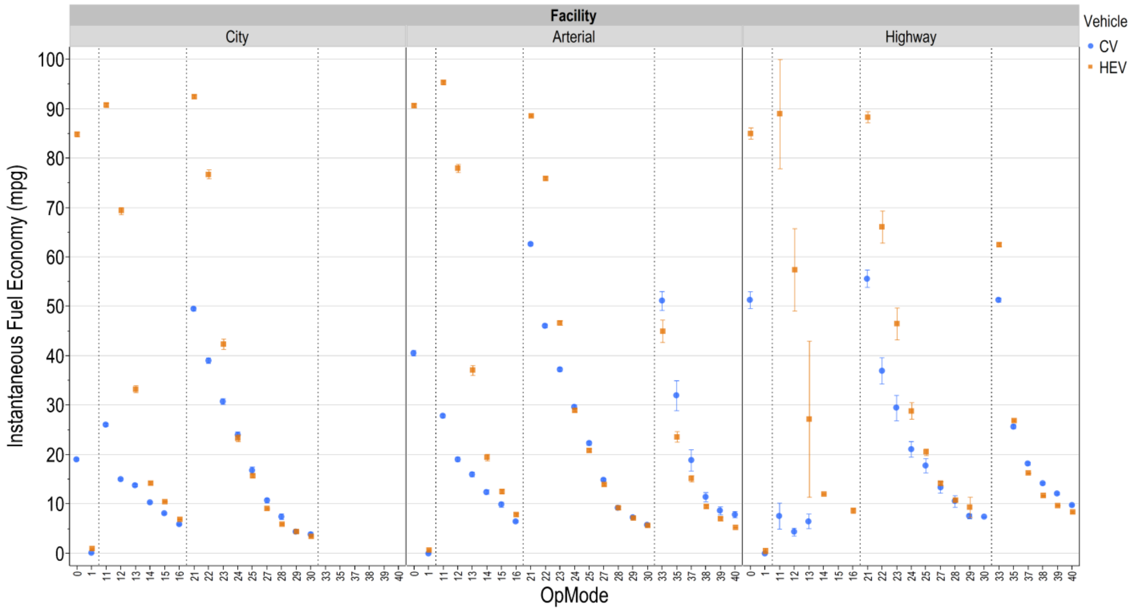

Figure 3-9. Instantaneous fuel economy estimated by carbon balance across all MOVES OpModes for the two vehicle types. Points and error bars represent the mean ± the standard error for each given OpMode and vehicle type.

The sensitivity of fuel economy to ambient temperature was also evaluated for the two test vehicles (**Figure 3-10**). The highest median mile-per-gallon FE rating was achieved for the HEV during city operation in warm test conditions. Median fuel economy by temperature class was greatest for arterial driving for both vehicle types (**Figure 3-10**). On the highway, the HEV fuel economy was within 5 mpg across the temperature classes, whereas the variation was greater for the CV. Although median fuel economy tended to decrease with increasing temperature for city (~5 mpg decrease across the temperature range) and arterial (~10 mpg decrease across the temperature range) driving for the HEV, the CV fuel economy for these two facility types remained fairly constant (within 3 mpg) with temperature. Thus, ambient temperature may affect the fuel use by the HEV differently than it does the CV. Given the relationships between HEV operation (i.e. SOC and EDO) and temperature, this result is not surprising. However, given the large range of FE (e.g. height of boxplot, Figure 3-10) for the HEV during city and arterial driving, it is difficult to decipher a statistically significant relationship between temperature class and fuel economy.

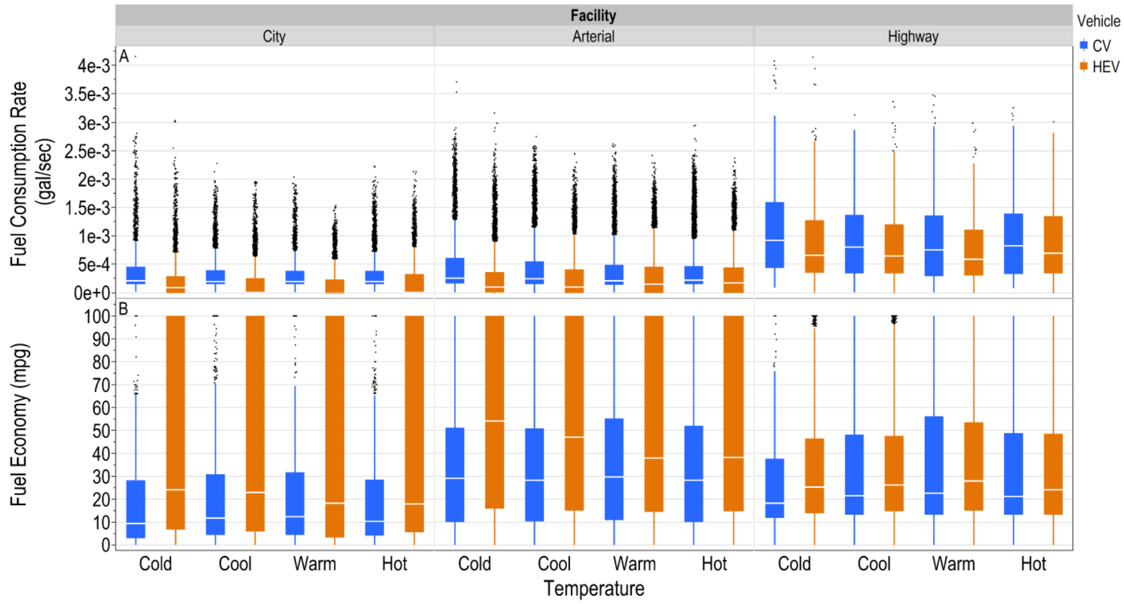

Figure 3-10. Comparison of HEV (orange) and CV (blue) (A) instantaneous fuel consumption rates and (B) instantaneous fuel economy (mpg) as a function of ambient temperature and facility type. Note: box represents interquartile range and whiskers represent 1.5 times the interquartile range.

3.3 Tailpipe Emissions

On average over the entire driving route, the CV mean *gas*-phase tailpipe emission rates were greater than that of the HEV as shown in **Table 3-5**. Mean *particle* number emission rates over the full route, however, were higher for the HEV than the CV. A more disaggregate comparison of tailpipe emissions between the two vehicle types by temperature class, facility and operating mode helped elucidate the quantitative emissions differences between the CV and HEV. The disaggregate comparisons can be used to estimate the benefits of driving the HEV over any composite drive cycle.

3.3.1 CV and HEV Tailpipe Emissions by Facility Type and Ambient Temperature

Comparison of emission rates over the route as a function of temperature and facility type was conducted for a selection of pollutants and aggregate pollutant types (**Figure 3-11**). The variability demonstrated by large standard deviations on the plotted mean emission rates indicate the range of real-world, transient operating conditions experienced within each temperature class. These transient, high emission events have been characterized for the particle number data in more detail elsewhere[69].

From **Figure 3-11** it is evident that the CV (blue) emission rates exceeded those of the HEV (orange) for many of the pollutants across the facility and temperature bins, but not for all scenarios. For instance, cold temperature, highway driving produced higher mean HEV methane (CH_4) and nitrous oxide (N_2O) emissions, as well as large standard deviations. This result suggests uncharacteristically high emissions of some greenhouse gases for the cold temperature, highway operation of the HEV, but CO_2 did not show a similar pattern.

Table 3-5. Full Run HEV and CV Tailpipe Pollutant Emission Rates

		Mean Emission Rates (μg/s unless otherwise indicated)	
		CV	HEV
	Pollutant Summations	Mean ± Std Dev	Mean ± Std Dev
Criteria Pollutants	Carbon Monoxide (mg/s)	4.3 ± 49.7	1.2 ± 37.2
	NMHC	1060.3 ± 1045.4	864.1 ± 1115.0
	NO_x	72.6 ± 235.7	48.4 ± 363.5
Greenhouse Gases	Carbon Dioxide (mg/s)	4230.6 ± 4475.8	2955.8 ± 4040.8
	Methane	46.5 ± 118.6	42.6 ± 98.0
	Nitrous Oxide	23.2 ± 40.0	19.9 ± 33.2
Mobile Source Air Toxics	Acetaldehyde	228.9 ± 243.5	181.3 ± 267.6
	Acrolein	148.7 ± 162.1	113.1 ± 165.4
	Benzene	628.7 ± 680.2	483.4 ± 634.1
	1,3-Butadiene	89.0 ± 96.1	74.8 ± 103.7
	Formaldehyde	31.4 ± 31.2	21.9 ± 27.4
	Alkanes	496.7 ± 483.0	439.7 ± 646.3
	Alkenes	220.5 ± 223.0	163.2 ± 208.4
	Alkynes	227.2 ± 265.7	167.6 ± 222.1
	Dienes	116.0 ± 121.3	93.7 ± 126.2
	Aromatics	3340.5 ± 3566.5	2385.7 ± 3057.7
	Ammonia	66.9 ± 312.1	31.8 ± 658.5
Particles	Particle Number (EEPS, #/s)	1.48E+10 ± 7.36E+10	1.61E+10 ± 5.05E+10
	Particle Number (CPC, #/s)	1.28E+10 ± 6.94E+10	1.30E+10 ± 5.33E+10

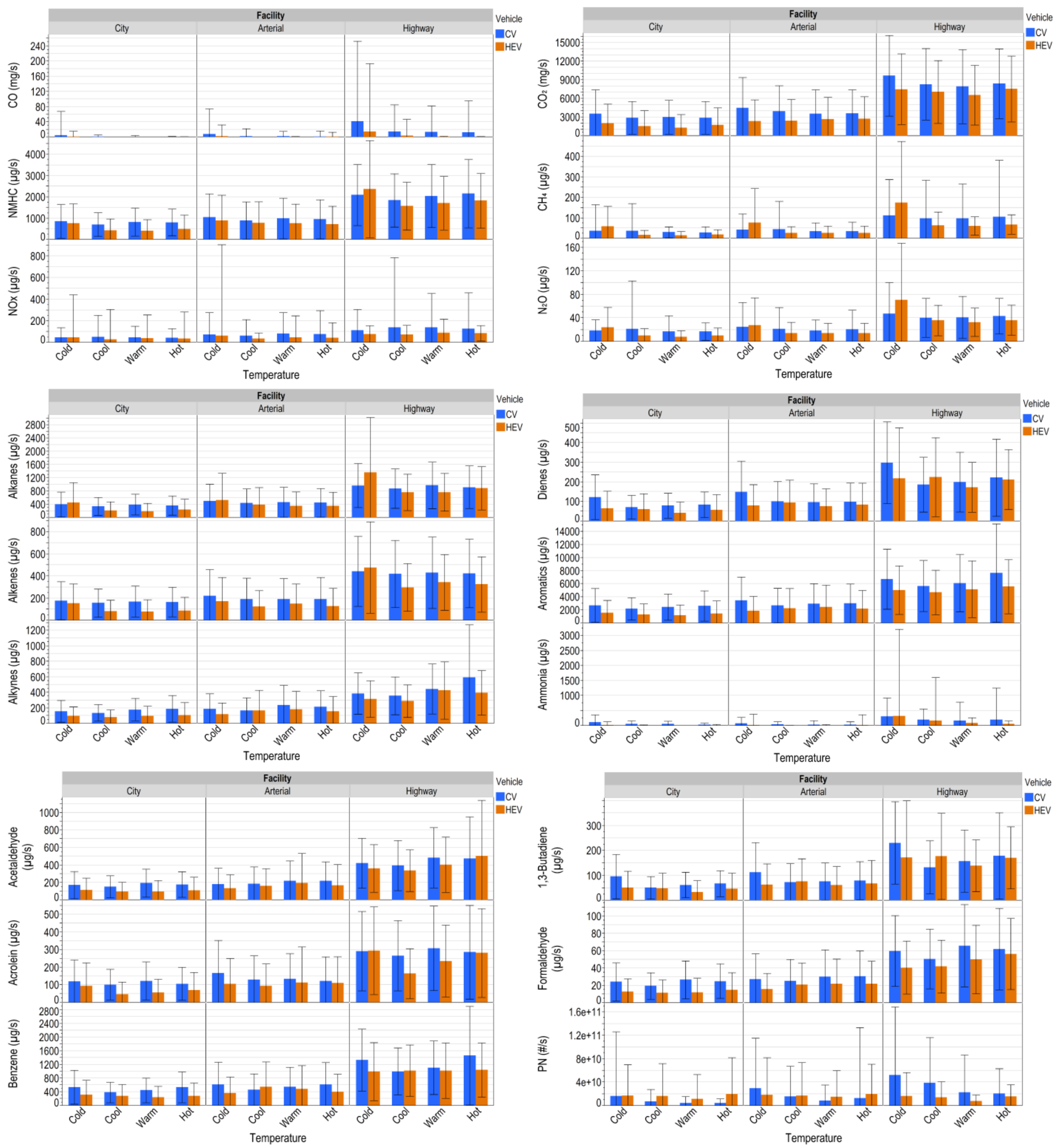

Figure 3-11. Mean CV and HEV tailpipe emission rates as a function of facility type and ambient temperature: (A) criteria pollutants, (B) greenhouse gases, (C,D) gas-phase analytes, (E) mobile source air toxics, and (F) particle number. Each bar represents the mean emission rate with the corresponding error bar representing the standard deviation for the given facility type and run ambient temperature class.

Table 3-6. Comparison of CV and HEV Mean Emission Rates by Facility Type

		Mean Emission Rates (µg/s unless otherwise indicated)					
		City		Arterial		Highway	
		CV	HEV	CV	HEV	CV	HEV
	Pollutant Summations	Mean ± Std Dev	Mean ± Std Dev	Mean ± Std Dev	Mean ± Std Dev	Mean ± Std Dev	Mean ± Std Dev
Criteria Pollutants	Carbon Monoxide (mg/s)	1.1 ± 25.1	0.4 ± 6.2	2.5 ± 29.1	0.7 ± 16.5	17.4 ± 108.9	4.3 ± 87.4
	NMHC	782.7 ± 644.3	501.6 ± 666.6	953.2 ± 942.0	787.8 ± 999.9	2023.4 ± 1455.3	1836.9 ± 1548.2
	NO_x	45.8 ± 135.8	34.8 ± 285.0	72.4 ± 193.1	47.4 ± 453.2	130.1 ± 439.7	79.9 ± 94.7
Greenhouse Gases	Carbon Dioxide (mg/s)	2999.4 ± 2877.5	1573.8 ± 2621.7	3778.1 ± 4097.3	2536.3 ± 3479.9	8426.8 ± 5896.0	7102.4 ± 5208.2
	Methane	32.6 ± 91.9	24.6 ± 51.0	38.9 ± 85.8	39.9 ± 93.1	102.4 ± 214.2	87.8 ± 156.1
	Nitrous Oxide	18.4 ± 48.4	12.0 ± 19.5	20.6 ± 33.3	17.8 ± 28.8	42.4 ± 36.8	42.8 ± 52.8
Mobile Source Air Toxics	Acetaldehyde	171.1 ± 146.1	101.2 ± 130.6	202.9 ± 209.9	164.7 ± 248.7	441.6 ± 371.8	395.7 ± 392.5
	Acrolein	110.5 ± 99.9	63.7 ± 95.6	132.9 ± 146.3	105.6 ± 162.2	285.1 ± 235.0	237.5 ± 217.8
	Benzene	467.9 ± 405.0	274.2 ± 362.3	557.2 ± 583.5	446.9 ± 615.2	1218.1 ± 1050.1	1017.9 ± 798.9
	1,3-Butadiene	65.3 ± 59.0	43.7 ± 59.2	81.0 ± 83.8	66.5 ± 84.9	167.5 ± 146.9	164.2 ± 163.3
	Formaldehyde	23.4 ± 19.6	12.6 ± 16.6	28.4 ± 28.5	20.0 ± 24.9	58.8 ± 43.0	46.9 ± 36.1
	Alkanes	367.4 ± 305.2	256.1 ± 379.5	452.8 ± 448.3	404.3 ± 577.0	924.5 ± 646.9	921.9 ± 968.2
	Alkenes	165.0 ± 139.8	96.4 ± 128.5	195.1 ± 199.5	145.5 ± 180.0	426.6 ± 311.7	355.1 ± 294.2
	Alkynes	165.4 ± 145.4	93.9 ± 125.2	199.5 ± 208.5	155.3 ± 212.6	454.9 ± 455.6	353.4 ± 288.0
	Dienes	84.9 ± 75.2	55.2 ± 75.4	105.8 ± 108.6	82.8 ± 104.5	217.4 ± 177.3	206.5 ± 191.2
	Aromatics	2460.6 ± 2135.7	1350.4 ± 1765.1	2954.7 ± 3002.5	2191.7 ± 2903.2	6553.7 ± 5520.6	5081.5 ± 3903.3
	Ammonia	51.7 ± 128.3	7.2 ± 51.8	36.6 ± 123.3	10.7 ± 247.5	205.1 ± 730.4	148.3 ± 1575.7
Particles	Particle Number (EEPS, #/s)	7.0E+09 ± 4.5E+10	1.6E+10 ± 5.3E+10	1.5E+10 ± 8.5E+10	1.7E+10 ± 5.4E+10	3.2E+10 ± 7.5E+10	1.3E+10 ± 2.6E+10
	Particle Number (CPC, #/s)	3.2E+09 ± 2.2E+10	1.4E+10 ± 5.1E+10	1.4E+10 ± 7.4E+10	1.4E+10 ± 5.8E+10	2.8E+10 ± 1.1E+11	9.4E+09 ± 3.9E+10

The relationship of particle number size distribution to ambient temperature and facility type is shown in **Figure 3-12**. HEV particle number emission rate exceeded that of the CV in most conditions across city and arterial driving for most of the measured particle diameters (**Figure 3-12**). During city driving, the HEV's emission rate for accumulation mode particle diameters (Dp = 25 to 80 nm) increased in magnitude with increasing temperature. In contrast, the CV accumulation mode particle emission rate tended to decrease with increasing temperature. These changes in the particle number distribution may have some relation to the change in EDO across the temperature bins. More detailed investigation is needed to elucidate these relationships between particle number distribution and vehicle operating mode.

The relationships between emission rates and disaggregate vehicle activity (VSP or OpMode) may provide more insight into the overall variability captured in the aggregate plots of emission rate by temperature class in **Figure 3-11**.

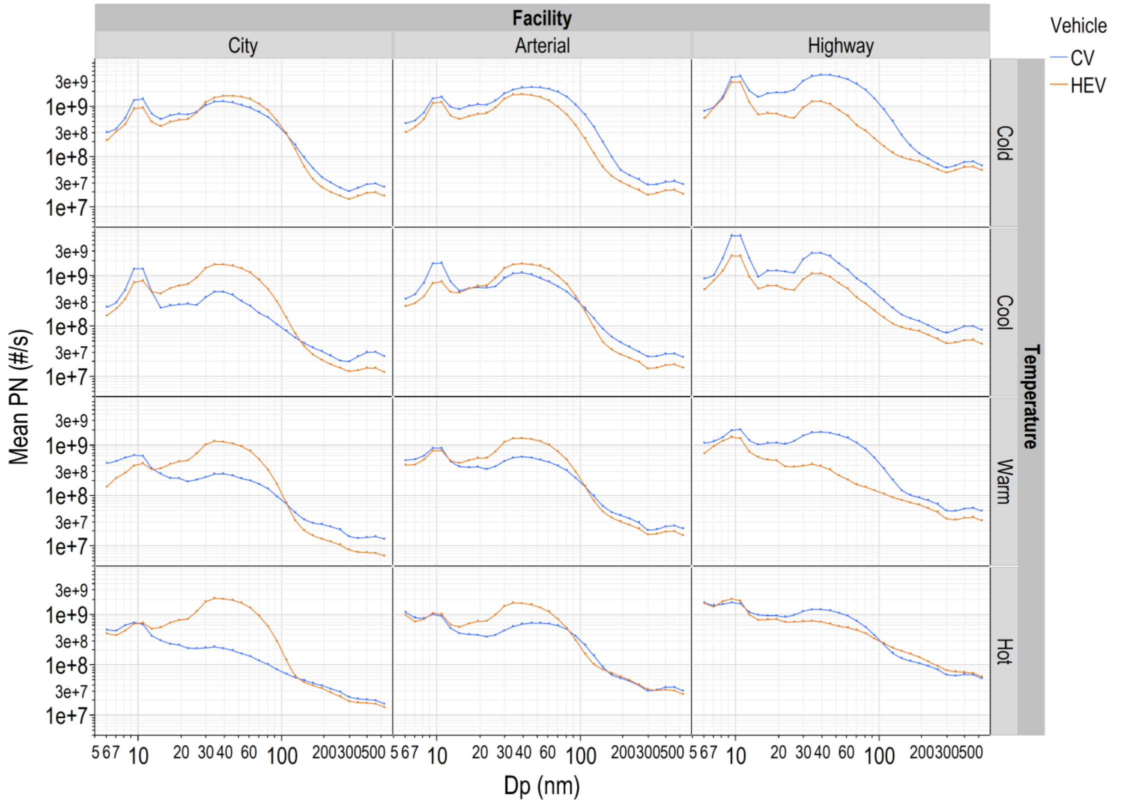

Figure 3-12. Comparison of HEV and CV mean particle number distributions as a function of facility type and seasonal temperature. Note the log-log axes scales.

3.3.2 Tailpipe Emissions by Activity (VSP and OpMode)

Criteria pollutant, gas-phase emissions (e.g. CO, NMHC, NOx) were generally higher for CV than HEV, particularly for any VSP activity less than 0 kW/ton (**Figure 3-13**). With increasing VSP, the VSP bin at which a pollutant's average HEV emission rate began to exceed that of the CV was referred to as the "cross-over" VSP. This cross-over VSP corresponds to the activity at which the HEV no longer provided a reduction in emissions compared to its conventional vehicle counterpart. The cross-over point varied depending on the pollutant. For instance, there was a consistent "HEV benefit" (i.e., lower emissions from HEV vs. CV) in NOx emissions up to VSP = 11 kW/ton (**Figure 3-13**). For activity with VSP greater than 11 kW/ton, the HEV and CV mean VSP-weighted NOx emission rates were roughly equivalent. Particle number had two cross-over points (**Figure 3-13**) that suggest a unique relationship between particle number emissions and VSP to give two positive VSP regimes —one from 0 – 15 kW/ton where HEV emission rates exceeded that of the CV and the second at >15 kW/ton where the CV emissions were lower than that for the HEV. Little vehicle activity occurred at VSP>31 kW/ton making it difficult to quantitatively interpret the relative emissions between the two vehicles.

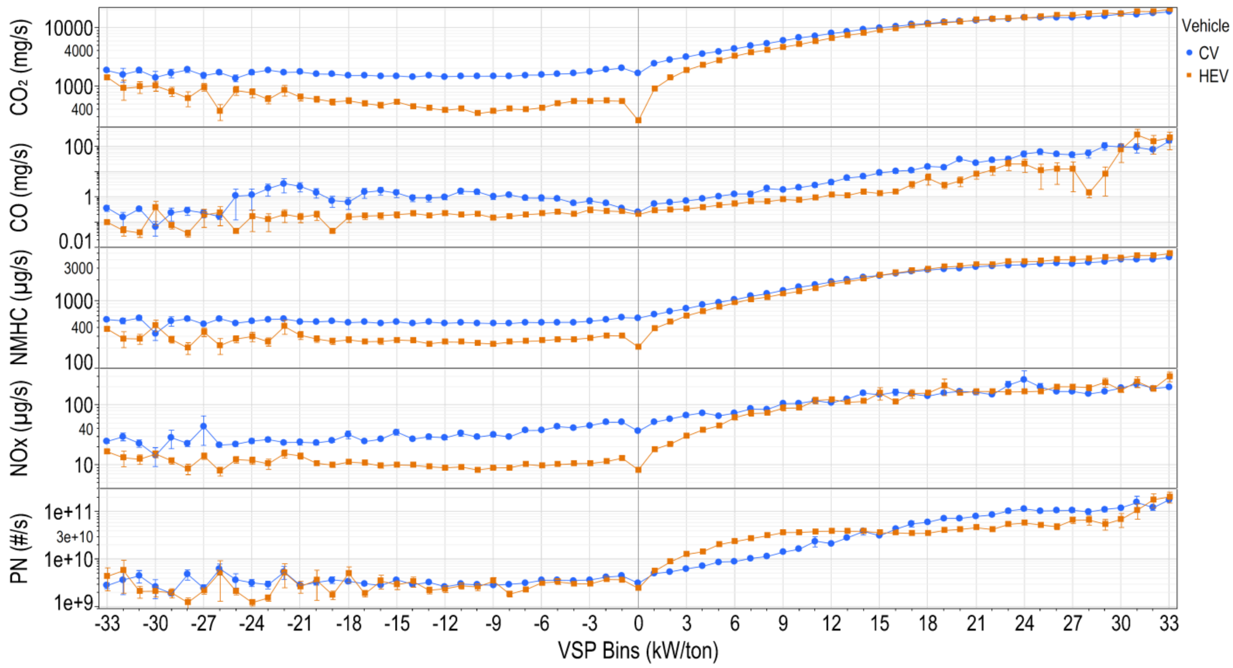

Figure 3-13. Comparison HEV and CV carbon dioxide, criteria gas-phase pollutants, and total particle number emission rates as a function of VSP. Note the log y-scale with symbols representing mean emission rates and error bars corresponding to standard error.

Analysis of the emission rates as a function of MOVES operating modes showed that gas-phase, criteria pollutant emission rates from the CV typically exceeded that of the HEV, especially for the idle, braking, and low VSP operating modes (**Figure 3-14**). The cross-over point by OpMode between the CV and HEV also depended on the pollutant. For instance, NOx had two cross-over points – between OpModes 13/14 and 38/39 – but carbon monoxide, did not cross over until OpModes 30 and 40. Particle number emission rates again presented a different scenario from the gas-phase pollutants. For PN, the combination of low speed and low VSP driving was associated with HEV particle number emission rates exceeding that of the CV up until the cross-over between OpMode 25 and 27. It is clear from this relationship that operating modes where the HEV was able to make reductions in gas-phase emissions relative to the CV created an anomaly in terms of particle number emissions. We have previously attributed this phenomena to internal combustion engine "restart" events occurring for the HEV during low speed, low VSP operation.[84, 85]

The complex patterns of mean pollutant emission rate data as a function of VSP and MOVES OpMode suggest that the net "benefits" of driving the HEV will critically depend on driver behavior. In other words,

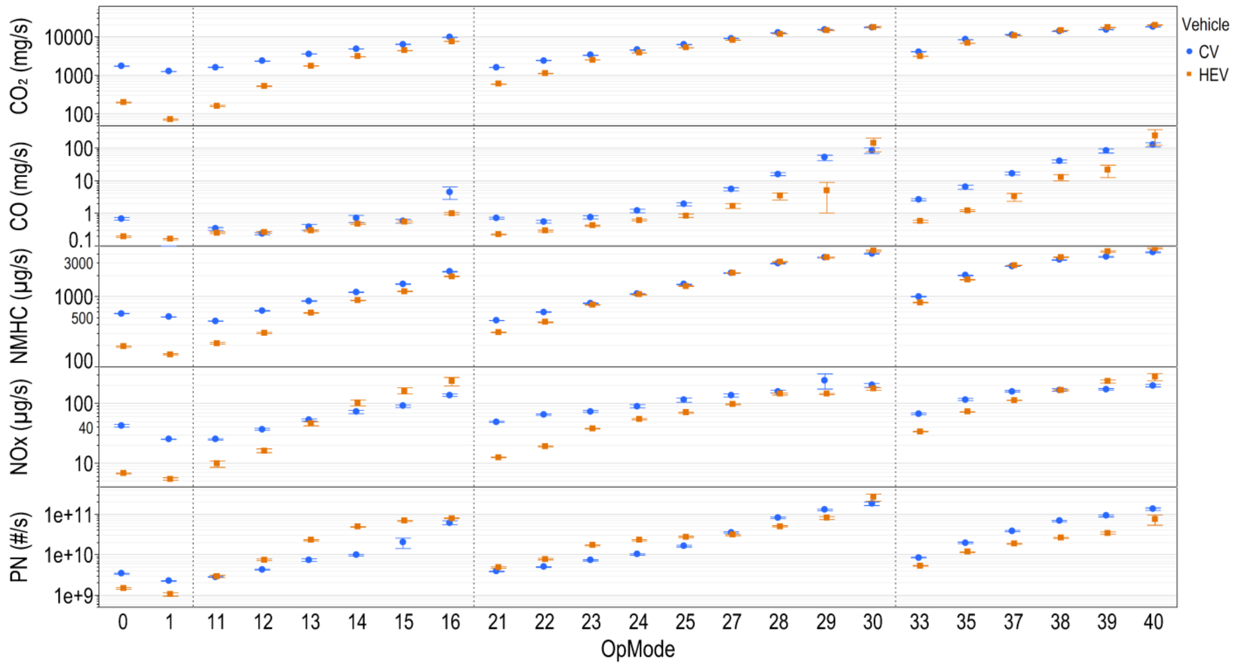

Figure 3-14. Comparison of HEV and CV carbon dioxide (top left), carbon monoxide (top right), non-methane hydrocarbons (middle left), oxides of nitrogen (middle right), and total particle number (bottom) emission rates as a function of OpMode. Symbols represent the mean, error bars correspond to the standard error, and note the log y-scale.

4. Conclusions and Future Work

This report summarizes the techniques used to complete the first successful comparison study of the emissions and performance of a HEV to its CV counterpart of the same make/model. Sufficient replicate runs were collected using the TOTEMS instrumentation package to quantify gas- and particle-phase emission rate and fuel consumption differences as a function of VSP and MOVES operating mode during real-world driving under ambient temperatures between -13°C to 40°C, relative humidity ranging from 19% to 90%, and -13.2% to +11.5% road grade.

Ambient Temperature Effects. Two vehicle performance metrics of the HEV varied with ambient temperature during the run: EDO% and battery SOC%. Relatively high variability was observed in EDO% during cold season operation indicating that it may be more difficult to predict the EDO propulsion during city driving with certainty under cold temperature winter driving.

Fuel consumption. Aggregating all the route data together over all seasons, the HEV fuel economy averaged 48.8 MPG compared to 28.8 for the CV, indicating a distinct advantage for the HEV platform. Instantaneous fuel consumption varied with VSP (or OpMode) as well as facility type and fuel economy advantages for the HEV were most significant for city driving at VSP ranging from approximately -27 to +8 kW/ton. The pattern of fuel consumption differences between the two vehicles as a function of facility and VSP mirrored the VSP trends for HEV EDO propulsion driving proportion.

PN Distributions and Total Particle Number. Unlike the gas-phase pollutants, particle number emissions were higher for HEV than for the CV during low power VSP operation (VSP range 2-13kW/ton) where the HEV had gas-phase emissions benefits over the CV. Observed changes in the particle number distributions by temperature season may have some relation to the change in EDO% across the temperature bins. More detailed investigation is needed to elucidate the relationships between particle number distribution and vehicle operating mode. Specifically, future work should include detailed analysis of particle number distributions at higher temporal resolution to delineate HEV "restart" emission relationships between gases and particles.

Road grade was not explicitly examined as an explanatory variable in this preliminary set of analyses of the TOTEMS on-board emissions data. Road grade is however a key component in the calculation of VSP and MOVES OpMode. Future work should examine the effect that use of laboratory drive cycles emissions data (where road grade is assumed to equal zero) in mobile source emissions modeling has on the accuracy of such emissions estimates for real-world driving in hilly terrain. The dataset created here for both the CV and HEV can be combined to answer this question.

Gas-phase Emissions by FTIR. In this preliminary study the manufacturer's default analysis methods were employed. Future analysis should include re-analysis of the raw FTIR spectral data to enable development of a refined FTIR analysis method for low-emitting gasoline vehicle exhaust characterization.

References Cited

1. *National Transportation Statistics*. n.d. February 6, 2014]; Available from: http://www.rita.dot.gov/bts/sites/rita.dot.gov.bts/files/publications/national_transportation_statistics/index.html.
2. DOE, *Alternative Fuels Data Center: AFVs in Use."*, in *Energy Efficiency & Renewable Energy*. 2012a.
3. *Light-Duty Automotive Technology, Carbon Dioxide Emissions, and Fuel Economy Trends: 1975 Through 2011*. 2012.
4. DOE, *Alternative Fuels Data Center: U.S. HEV Sales by Model*, in *Energy Efficiency & Renewable Energy*. 2012b.
5. EPA, *Light-Duty Automotive Technology, Carbon Dioxide Emissions, and Fuel Economy Trends: 1975 Through 2011*. 2012, Transportation and Climate Division Office of Transportation and Air Quality U.S. Environmental Protection Agency. p. 1-102.
6. *Inventory of U.S. Greenhouse Gas Emissions and Sinks: 1990-2011*. 2013.
7. Toyota. *Hybrid Systems*. 2011; Toyota Innovation Technology File]. Available from: http://www.toyota-global.com/innovation/environmental_technology/technology_file/.
8. Toyota, *Toyota Hybrid Sales Diagnosis*. 2009: Toyota Motor Sales, USA, Inc.
9. Holmén, B.A. and D.A. Niemeier, *Characterizing the effects of driver variability on real-world vehicle emissions.* Transportation Research Part D: Transport and Environment, 1998. **3**(2): p. 117-128.
10. Jackson, E., et al., *Driver and Road Type Effects on Light-Duty Gas and Particulate Emissions.* Transportation Research Record: Journal of the Transportation Research Board, 2006(1987).
11. Boriboonsomsin, K. and M. Barth, *Impacts of Road Grade on Fuel Consumption and Carbon Dioxide Emissions Evidenced by Use of Advanced Navigation Systems.* Transportation Research Record: Journal of the Transportation Research Board, 2009. **2139**(-1): p. 21-30.
12. Jackson, E. and L. Aultman-Hall, *Analysis of Real-World Lead Vehicle Operation for Modal Emissions and Traffic Simulation Models.* Transportation Research Record: Journal of the Transportation Research Board, 2010. **2158**(-1): p. 44-53.
13. Barth, M. and K. Boriboonsomsin, *Real-World Carbon Dioxide Impacts of Traffic Congestion.* Transportation Research Record: Journal of the Transportation Research Board, 2008. **2058**(-1): p. 163-171.
14. Song, G., L. Yu, and X. Zhang, *Emission Analysis at Toll Station Area in Beijing with Portable Emission Measurement System.* Transportation Research Record: Journal of the Transportation Research Board, 2008. **2058**(-1): p. 106-114.
15. Unal, A., N.M. Rouphail, and H.C. Frey, *Effect of arterial signalization and level of service on measured vehicle emissions.* Transportation Research Record: Journal of the Transportation Research Board, 2003. **1842**(-1): p. 47-56.
16. Coelho, M.C., et al., *Assessing methods for comparing emissions from gasoline and diesel light-duty vehicles based on microscale measurements.* Transportation Research Part D: Transport and Environment, 2009. **14**(2): p. 91-99.
17. Gierczak, C.A., et al., *Laboratory Evaluation of the SEMTECH-G® Portable Emissions Measurement System (PEMS) For Gasoline Fueled Vehicles*. 2006, SAE International: Warrendale, PA.
18. Barth, M., et al., *Measuring and modeling emissions from extremely low-emitting vehicles.* Transportation Research Record: Journal of the Transportation Research Board, 2006. **1987**(-1): p. 21-31.

19. Collins, J.F., et al., *Measurements of In-Use Emissions from Modern Vehicles Using an On-Board Measurement System.* Environmental Science & Technology, 2007. **41**(18): p. 6554-6561.
20. Jetter, J., et al., *Development of an On-Board Analyzer for Use on Advanced Low Emission Vehicles*. 2000, SAE International: Warrendale, PA.
21. Li, H., et al., *Comparisons of the Exhaust Emissions for Different Generations of SI Cars under Real World Urban Driving Conditions*. 2008, SAE International: Warrendale, PA.
22. Truex, T.J., et al., *Measurement of Ambient Roadway and Vehicle Exhaust Emissions-An Assessment of Instrument Capability and Initial On-Road Test Results with an Advanced Low Emission Vehicle*. 2000, SAE International: Warrendale, PA.
23. Robinson, M.K., K.M. Sentoff, and B.A. Holmén, *Particle Number and Size Distribution Emissions During Light-Duty Vehicle Cold Start: Data from the Total Onboard Tailpipe Emissions Measurement System.* Transportation Research Record No. 2158, 2010. **Environment 2010**: p. 86 - 94.
24. *California Exhaust Emissions Standards and Test Procedures for 2005 and Subsequent Model Zero-Emissions Vehicles, and 2001 and Subsequent Model Hybrid Electric Vehicles, in the Passenger Car, Light-Duty Truck and Medum-Duty Vehicle Classes*. 1999.
25. Engineers, S.o.A., *Recommended practice for measureing fuel economy and emissions of hybrid-electric and conventional heavy-duty vehicles.* Surface Vehicle Recommended Practice No. SAE - J2711, 2002.
26. Christenson, M., D. Karman, and L.A. Graham, *The Effect of Driving Conditions and Ambient Temperature on Light Duty Gasoline-Electric Hybrid Vehicles (1): Particulate Matter Emission Rates and Size Distribution.* SAE Paper Number 2007-01-2136, 2007.
27. Jimenez, J.L., *Understanding and Quantifying Motor Vehicle Emissions with Vehicle Specific Power and TILDAS Remote Sensing*. 1999, Massachusetts Institute of Technology: Massachusetts Institute of Technology. p. 361.
28. Koupal, J., et al., *MOVES2004 Energy and Emission Inputs Draft Report*. 2005.
29. Frey, C.H., et al., *On-Road Measurement of Vehicle Tailpipe Emissions Using a Portable Instrument.* Air and Waste Management, 2003(53): p. 992 - 1002.
30. Lee, H., C.-L. Myung, and S. Park, *Time-resolved particle emission and size distribution characteristics during dynamic engine operation conditions with ethanol-blended fuels.* Fuel, 2009. **88**(9): p. 1680-1686.
31. Kittelson, D.B., et al., *On-road and laboratory evaluation of combustion aerosols--Part 2:: Summary of spark ignition engine results.* Journal of Aerosol Science, 2006. **37**(8): p. 931-949.
32. Farnlund, J. and C. Holman, *Emissions of Ultrafine Particles from Different Types of Light Duty Vehicles*. 2001: Salemsvagen.
33. Kayes, D. and S. Hochgreb, *Mechanisms of Particulate Matter Formation in Spark-Ignition Engines. 2. Effect of Fuel, Oil, and Catalyst Parameters.* Environmental Science and Technology, 1999. **33**(22): p. 3968-3977.
34. Kayes, D. and S. Hochgreb, *Mechanisms of Particulate Matter Formation in Spark-Ignition Engines. 1. Effect of Engine Operating Conditions.* Environmental Science & Technology, 1999. **33**(22): p. 3957-3967.
35. Graham, L.A., S.L. Belisle, and C.-L. Baas, *Emissions from light duty gasoline vehicles operating on low blend ethanol gasoline and E85.* Atmospheric Environment, 2008. **42**(19): p. 4498-4516.
36. Kittelson, D.B., W.F. Watts, and J.P. Johnson, *Nanoparticle emissions on Minnesota highways.* Atmospheric Environment, 2004. **38**(1): p. 9-19.

37. Ristimaki, J., et al., *Cold Temperature PM Emissions Measurement; Method Evaluation and Application to Light Duty Vehicles.* Environmental Science & Technology, 2005. **39**(24): p. 9424-9430.
38. Kleeman, M.J., et al., *Lubricating Oil and Fuel Contributions To Particulate Matter Emissions from Light-Duty Gasoline and Heavy-Duty Diesel Vehicles.* Environmental Science & Technology, 2008. **42**(1): p. 235-242.
39. EPA, *Our Nation's Air - Status and Trends through 2010*. 2012a.
40. EPA, *EPA Will Propose Historic Greenhouse Gas Emissions Standards for Light-Duty Vehicles*. 2009, Office of Transportation and Air Quality.
41. Christenson, M., et al., *The Effect of Driving Conditions and Ambient Temperature on Light Duty Gasoline-Electric Hybrid Vehicles (2): Fuel Consumption and Gaseous Pollutant Emission Rates*. 2007, SAE International: Warrendale, PA.
42. Fontaras, G., P. Pistikopoulos, and Z. Samaras, *Experimental evaluation of hybrid vehicle fuel economy and pollutant emissions over real-world simulation driving cycles.* Atmospheric Environment, 2008. **42**(18): p. 4023-4035.
43. Graham, L.A., *Chemical characterization of emissions from advanced technology light-duty vehicles.* Atmospheric Environment, 2005. **39**(13): p. 2385-2398.
44. Reyes, F., et al., *Tecnical Note: Analysis of non-regulated vehicular emissions by extractive FTIR spectrometry: tests on a hybrid car in Mexico City.* Atmospheric Chemistry and Physics, 2006. **6**(12): p. 5339-5346.
45. Alvarez, R. and M. Weilenmann, *Effect of Low Ambient Temperature on Fuel Consumption and Pollutant and CO2 Emissions of Hybrid Electric Vehicles in Real-world Conditions.* Fuel, 2012. **97**(July): p. 119-124.
46. Sentoff, K., *Characterization of Gas-Phase Emissions from Comparable Conventional and Hybrid Gasoline Vehicles during Real-World Operation*. 2012, University of Vermont: Burlington, VT. p. 147.
47. *National Ambient Air Quality Standards*. 2008; Available from: www.epa.gov/air/criteria.html.
48. Brook, R.D., et al., *Air Pollution and Cardiovascular Disease: A Statement for Healthcare Professionals From the Expert Panel on Population and Prevention Science of the American Heart Association.* Circulation, 2004. **109**: p. 2655-2671.
49. Kittelson, D.B., *Engines and Nanoparticles: A Review.* Journal of Aerosol Science, 1998. **29**(5/6): p. 575-588.
50. kittelson, D.B., W.F. Watts, and J.P. Johnson, *Diesel Aerosol Sampling Methodology—CRC E-43 Final Report*, in *Coordinating Research Council*. 2002: Alpharetta, GA.
51. Gauderman, W.J., et al., *The Effect of Air Pollution on Lung Development from 10 to 18 Years of Age.* The New England Journal of Medicine, 2004. **351**(11): p. 1057-1067.
52. Pope III, C.A., et al., *Lung Cancer, Cardiopulmonary Mortality, and Long-term Exposure to Fine Particulate Air Pollution.* JAMA, 2002. **287**(9): p. 1132-1141.
53. Pope III, C.A., M. Ezzati, and D.W. Dockery, *Fine-Particulate Air Pollution and Life Expectancy in the United States.* The New England Journal of Medicine, 2009. **360**(4): p. 376-386.
54. Pope III, C.A., et al., *Ischemic Heart Disease Events Triggered by Short-Term Exposure to Fine Particulate Air Pollution.* Circulation, 2006. **114**: p. 2443-2448.
55. Pope III, C.A., et al., *Relation of Heart Failure Hospitalization to Exposure to Fine Particulate Air Pollution.* The American Journal of Cardiology, 2008. **102**(9): p. 1230-1234.
56. MacNee, W. and K. Donaldson, *Mechanism of lung injury caused by PM10 and ultrafine particles with special reference to COPD.* Eur Respir J, 2003. **21**(40_suppl): p. 47S-51.

57. Morawska, L., et al., *Quantification of Particle Number Emission Factors for Motor Vehicles from On-Road Measurements.* Environmental Science & Technology, 2005. **39**(23): p. 9130-9139.
58. Sawyer, R.F., et al., *Mobile sources critical review: 1998 NARSTO assessment.* Atmospheric Environment, 2000. **34**(12-14): p. 2161-2181.
59. Harris, S.J. and M.M. Maricq, *Signature size distributions for diesel and gasoline engine exhaust particulate matter.* Journal of Aerosol Science, 2001. **32**: p. 749-764.
60. Kasper, A., et al., *Particle Emissions from SI-Engines During Steady State and Transient Operating Conditions.* SAE Technical Paper No. 2005-01-3136, 2005.
61. Kayes, D., et al., *Particulate Matter Emission During Start-up and Transient Operation of a Spark-Ignition Engine(2): Effect of Speed, Load, and Real-World Driving Cycles.* SAE paper number 2000-01-1083, 2000.
62. Maricq, M.M., et al., *Vehicle Exhaust Particle Size Distributions: A Comparision Of Tailpipe And Dilution Tunnel Measurements.* SAE Technical Paper No. 011416, 1999.
63. Agus, E.L., et al., *Factors influencing particle number concentrations, size distributions and modal parameters at a roof-level and roadside site in Leicester, UK.* Science of the Total Environment, 2007. **386**(1-3): p. 65-82.
64. Gouriou, F., J.P. Morin, and M.E. Weill, *On-road measurements of particle number concentrations and size distributions in urban and tunnel environments.* Atmospheric Environment, 2004. **38**(18): p. 2831-2840.
65. El-Shawarby, I., K. Ahn, and H. Rakha, *Comparative field evaluation of vehicle cruise speed and acceleration level impacts on hot stabilized emissions.* Transportation Research Part D: Transport and Environment, 2005. **10**(1): p. 13-30.
66. Wehner, B., et al., *Aerosol number size distributions within the exhaust plume of a diesel and a gasoline passenger car under on-road conditions and determination of emission factors.* Atmospheric Environment, 2009. **43**(6): p. 1235-1245.
67. Christenson, M., et al., *The Effect of Driving Conditions and Ambient Temperature on Light Duty Gasoline-Electric Hybrid Vehicles (2): Fuel Consumption and Gaseous Pollutant Emission Rates.* SAE Paper Number 2007-01-2137, 2007.
68. Robinson, M.K. and B.A. Holmen, *Onboard, Real-World Second-by-Second Particle Number Emissions from a 2010 Hybrid and Comparable Conventional Vehicle.* Transportation Research Record, 2011. **2233**(Environment): p. 63-71.
69. Robinson, M.K., *Second-by-Second On-Board Real-World Particle Number Emissions for Comparable Conventional and Hybrid-Electric Gasoline Vehicles in a City Driving Environment*, in *Civil and Environmental Engineering*. 2011, University of Vermont.
70. Seigneur, C., *Current Understanding of Ultrafine Particulate Matter Emitted from Mobile Sources.* Journal of Air and Waste Management Association, 2009. **59**(1): p. 3-17.
71. CARB, *Toyota Motor Corporation New Passenger Cars, Light-Duty Trucks and Medium-Duty Vehicles: Gasoline Plus Battery-Assist Passenger Car*. 2008a.
72. CARB, *Toyota Motor Corporation New Passenger Cars, Light-Duty Trucks and Medium-Duty Vehicles: Gasoline Passenger Car*. 2008b.
73. Toyota, *Toyota Technical Training: Engine Control System II Course 874 Technician Handbook*. 2010a, Toyota Motor Sales, USA, Inc.
74. Toyota, *Toyota Technical Training: Engine Control Systems I Course 852*. 2010b.
75. Holmén, B.A., et al., *Signature Project 2 Proof-of-Concept Report: The On-Board Tailpipe Emissions Meaurement System (TOTEMS)*. 2010, *Technical Report #10-015;* The University of Vermont.
76. TSI, I., *Model 3090 Engine Exhaust Particle Sizer Spectrometer: Operation and Service Manual*. 2006: Shoreview.
77. TSI, *MD19-2E Rotating Disk Diluter for Particulate Emissions Operating Manual*. 2006.

78. TSI, *Calibration Certificate*. 2008.
79. Skoog, D.A. and J.J. Leary, *Principles of instrumental analysis.* 1992, Fort Worth: Saunders College Pub.
80. Smith, B.C., *Fundamentals of Fourier transform infrared spectroscopy*. 1996, Boca Raton: CRC Press.
81. CFR, *Protection of the Environment Fuel Economy Regulations for 1978 and Later Model Year Automobiles Test Procedures*, in *Code of Federal Regulations*. 2007.
82. EPA, *Fuel Economy Labeling of Motor Vehicles: Revisions To Improve Calculation of Fuel Economy Estimates*, in *40 CFR Parts 86 and 600*. 2006.
83. Zhai, H., H.C. Frey, and N.M. Rouphail, *Development of a modal emissions model for a hybrid electric vehicle.* Transportation Research Part D: Transport and Environment, 2011. **16**: p. 444-450.
84. Conger, M.B. and B.A. Holmén, *Real-World Engine Cold Start and "Restart" Particle Number Emissions from a 2010 Hybrid and Comparable Conventional Vehicle.* Transportation Research Board 91st Annual Meeting, 2012. **No. 12-4570**.
85. Robinson, M. and B.A. Holmén, *Onboard, Real-World Second-by-Second Particle Number Emissions from 2010 Hybrid and Comparable Conventional Vehicles.* Transportation Research Record: Journal of the Transportation Research Board, 2011. **2233**: p. 63-71.

Appendices

Information on TOTEMS instrument setup details, standard operating procedures for data collection and quality assurance/quality control are provided in the following appendices.

Appendix A. Sample Collection & Database Development Detail

Table A.1. Sampling Run Summary

Run No.	Vehicle ID	Driver	Date (DD-MMM-YY)	HEV initial SOC*	Delta SOC (final - initial)*	Avg Temp. (˚C)**	Avg RH (%)**	Odometer Start	Odometer Stop	Fuel Used @ Pump (gal)	Economy Pump Estimated (MPG)
1	Minivan		1-Apr-09	N/A	N/A	9	58	148424	148483	2.323	25.4
1.5	Minivan		12-May-09	N/A	N/A	15	40	Not	Not	N/A	N/A
1.75	Minivan		14-May-09	N/A	N/A	15	69	Not	Not	N/A	N/A
2	Minivan		17-May-09	N/A	N/A	19	28	148619	148661	2.466	17.0
3	Minivan		21-May-09	N/A	N/A	34	23	148661	148702	1.808	22.7
4	Minivan		22-May-09	N/A	N/A	23	42	148702	148743	1.324	31.0
4.1	Minivan		24-Jun-09	N/A	N/A	31	46	148812	148854	N/A	N/A
4.2	Minivan		25-Jun-09	N/A	N/A	34	39	148854	148895	N/A	N/A
PITOT TUBE AND TAILPIPE ADAPTER CHANGED WHEN SAMPLING BEGAN ON TOYOTA CAMRY'S											
4.3	CV		26-Jan-10	N/A	N/A	12	35	3001	3035	N/A	N/A
4.4	CV		28-Jan-10	N/A	N/A	-1	88	3035	3038	N/A	N/A
4.5	CV		4-Feb-10	N/A	N/A	-5	38	3038	3074	1.611	22.3
SP2 SAMPLING BEGINS											
5	CV	KMS	9-Feb-10	N/A	N/A	-2	47	3074	3110	1.418	25.4
6	CV	KMS	11-Feb-10	N/A	N/A	-1	49	3110	3145	1.511	23.2
7	CV	KMS	12-Feb-10	N/A	N/A	-5	41	3145	3181	1.667	21.6
8	CV	KMS	17-Feb-10	N/A	N/A	4	48	3181	3217	1.351	26.6
9	CV	KMS	18-Feb-10	N/A	N/A	2	60	3217	3253	1.567	23.0
10	CV	KMS	2-Mar-10	N/A	N/A	5	54	3262	3297	1.821	19.2
11	CV	KMS	3-Mar-10	N/A	N/A	3	62	3298	3333	1.556	22.5
12	CV	KMS	4-Mar-10	N/A	N/A	2	51	3334	3369	1.61	21.7
PITOT TUBE CALIBRATION PERFORMED ON MARCH 5, 2010											
13	HEV	KMS	9-Mar-10	60.5	7.0	4	46	4242	4276	1.177	28.9
14	HEV	KMS	10-Mar-10	66.5	1.5	5	40	4278	4312	1.163	29.2
15	HEV	KMS	11-Mar-10	67.0	1.0	7	39	4313	4348	1.323	26.5
16	HEV	KMS	16-Mar-10	69.5	-2.5	3	46	4349	4384	1.038	33.7
17	HEV	KMS	17-Mar-10	67.0	1.0	5	55	4384	4420	0.995	36.2
18	HEV	KMS	18-Mar-10	67.5	2.5	9	47	4421	4456	1.151	30.4
19	HEV	KMS	29-Jun-10	61.0	-3.0	19	68	4552	4587	0.991	35.3
20	HEV	KMS	30-Jun-10	67.0	-5.5	22	42	4588	4623	0.863	40.6
21	HEV	KMS	2-Jul-10	62.0	2.0	21	52	4624	4659	1.022	34.2
22	HEV	KMS	6-Jul-10	65.0	-5.0	35	48	4660	4695	0.869	40.3
23	HEV	KMS	7-Jul-10	64.0	-5.5	35	48	4696	4731	0.586	59.7
24	HEV	KMS	8-Jul-10	53.0	2.0	36	47	4732	4767	0.642	54.5
25	HEV	KMS	9-Jul-10	63.5	-3.0	31	57	4768	4802	0.952	35.7
26	HEV	KMS	15-Jul-10	52.5	6.5	32	48	4809	4843	0.594	57.2
27	HEV	KMS	20-Jul-10	54.0	12.0	28	57	4844	4879	1.124	31.1
PITOT TUBE CALIBRATION PERFORMED ON JULY 28, 2010 (LABVIEW BATTERY LOW, SIMILAR TO RUNS 22 TO 27)											
PITOT TUBE CALIBRATION PERFORMED ON JULY 30, 2010 (FULL BATTERY)											
28	HV	KMS	1-Sep-10	51.0	8.5	36	39	4907	4942	0.833	42.0
29	HV	KMS	2-Sep-10	39.0	20.0	33	46	4943	4978	1.13	31.0
30	HV	KMS	3-Sep-10	46.0	13.0	30	57	4979	5014	0.917	38.2
PITOT TUBE CALIBRATION PERFORMED ON SEPTEMBER 13, 2010											
31	CV	KMS	18-Sep-10	N/A	N/A	24	36	4042	4078	1.189	30.3
32	CV	KMS	20-Sep-10	N/A	N/A	20	20	4079	4114	0.647	54.1
33	CV	KMS	23-Sep-10	N/A	N/A	18	50	4115	4150	1.649	21.2
34	CV	KMS	11-Oct-10	N/A	N/A	11	56	4151	4186	1.247	28.1
35	CV	KMS	13-Oct-10	N/A	N/A	7	72	4187	4221	1.498	22.7
36	CV	KMS	18-Oct-10	N/A	N/A	11	41	4222	4257	1.221	28.7
37	CV	KMS	20-Oct-10	N/A	N/A	9	62	4258	4293	1.397	25.1
38	CV	KMS	3-Nov-10	N/A	N/A	9	47	4294	4329	1.32	26.5
39	CV	KMS	10-Nov-10	N/A	N/A	4	67	4330	Not	N/A	N/A
40	CV	KMS	12-Nov-10	N/A	N/A	13	40	4364	4398	1.35	25.2
PITOT TUBE CALIBRATION PERFORMED ON NOVEMBER 19, 2010											
41	HEV	KMS	22-Nov-10	64.5	0	9	79	5223	5258	1.375	25.5
42	HEV	KMS	29-Nov-10	63.5	1	4	57	5258	5294	1.091	33.0
43	HEV	KMS	3-Dec-10	66.0	0.0	4	57	5295	5330	0.889	39.4
44	HEV	KMS	31-Jan-11	60.0	5.0	-10	32	5345	5380	1.24	28.2
45	HEV	KMS	22-Feb-11	66.5	0.5	-10	51	5382	5417	1.107	31.6
46	HEV	KMS	23-Feb-11	57.5	8.5	-1	24	5418	5453	0.953	36.7
47	HEV	KMS	24-Feb-11	60.0	5.5	2	33	5454	5489	0.813	43.1
48	HEV	KMS	29-Mar-11	56.0	10.5	4	41	5489	5525	0.819	44.0
49	HEV	KMS	30-Mar-11	57.5	71.5	10	28	5527	5561	0.854	39.8
50	HEV	KMS	31-Mar-11	63.0	1.5	11	32	5564	5598	0.859	39.6
51	HEV	KMS	9-Apr-11	57.0	7.5	12	34	5599	5634	0.889	39.4
52	HEV	KMS	14-Apr-11	50.5	10.0	8	70	5635	5670	1.017	34.4
53	HEV	KMS	15-Apr-11	58.0	7.5	2	30	5671	5706	1.105	31.7
VEHICLE INSPECTIONS and OIL CHANGE ON CAMRY HEV AND CV											
PITOT TUBE CALIBRATION PERFORMED ON APRIL 21, 2011											
54	CV	KMS	11-May-11	N/A	N/A	23	40	5664	5698	1.265	26.9
55	CV	KMS	25-May-11	N/A	N/A	22	46	5699	5733	1.05	32.4
56	CV	KMS	31-May-11	N/A	N/A	33	36	5735	5769	0.993	34.2
57	CV	KMS	15-Jun-11	N/A	N/A	25	46	5771	5805	1.299	26.2
58	CV	KMS	16-Jun-11	N/A	N/A	33	33	5807	5841	0.914	37.2
59	CV	KMS	21-Jun-11	N/A	N/A	28	37	5843	5877	1.009	33.7
60	CV	KMS	22-Jun-11	N/A	N/A	22	66	5879	5913	0.987	34.4
61	CV	KMS	27-Jun-11	N/A	N/A	33	32	5914	5948	1.09	31.2
62	CV	KMS	30-Jun-11	N/A	N/A	24	48	5950	5984	1.12	30.4
63	CV	KMS	5-Jul-11	N/A	N/A	34	34	5986	6020	1	34.0
64	CV	KMS	11-Jul-11	N/A	N/A	33	46	6022	6056	0.835	40.7
65	CV	KMS	12-Jul-11	N/A	N/A	32	52	6058	6092	0.868	39.2
66	CV	KMS	19-Jul-11	N/A	N/A	29	39	6094	6128	0.955	35.6
67	CV	KMS	20-Jul-11	N/A	N/A	27	53	6130	6164	1.195	28.5
PITOT TUBE CALIBRATION PERFORMED ON AUGUST 2, 2011											
68	HEV	KMS	5-Aug-11	59.0	3.0	33	39	7783	7817	0.68	50.0
69	HEV	KMS	11-Aug-11	60.0	3.0	25	42	7821	7855	0.815	41.7
70	HEV	KMS	12-Aug-11	56.0	7.5	29	39	7857	7891	0.785	43.3
71	HEV	KMS	16-Aug-11	54.0	6.5	27	53	7893	7927	0.951	35.8
72	HEV	KMS	17-Aug-11	57.0	5.0	30	38	7929	7963	0.757	44.9
73	HEV	KMS	19-Aug-11	56.5	1.0	30	52	7965	7999	0.793	42.9
74	HEV	KMS	24-Aug-11	55.0	7.5	25	47	8001	8035	0.861	39.5
75	HEV	KMS	26-Aug-11	51.5	12.5	26	50	8037	8071	0.93	36.6
76	HEV	KMS	27-Aug-11	57.5	6.0	29	48	8073	8107	0.786	43.3
77	HEV	KMS	30-Aug-11	58.5	-3.5	27	48	8109	8143	0.789	43.1
78	HEV	KMS	31-Aug-11	56.0	1.5	28	49	8145	8179	0.874	38.9
79	HEV	KMS	6-Sep-11	58.0	-1.0	20	63	8181	8215	1.149	29.6
PITOT TUBE CALIBRATION PERFORMED ON SEPTEMBER 13, 2011											

Table A.2. Raw Files Acquired During Data Collection

Filename	Description	Instrument	Headers (row #) Headerlines	Column Headers	Time Format	Time Cell Location Row	Column	Time Cell Information
YYMMDD_LAB1.txt	Labview Device 1 File	Labview Device 1 (LAB1)	None	None	24-hour format	all	1	N/A (HH:MM:SS.MMMM)
YYMMDD_LAB2.txt	Labview Device 2 File	Labview Device 2 (LAB2)	None	None	24-hour format	all	1	N/A (HH:MM:SS.MMMM)
YYMMDD_CSCN.CSV	Conventional Vehicle Scantool File	Toyota Techstream	8	7 and 8	AM/PM format	6	2	Stop Time (MM/DD/YYYY HH:MM:SS)
YYMMDD_HSCN.CSV	Hybrid Vehicle Scantool File	Toyota Techstream	8	7 and 8	AM/PM format	6	2	Stop Time (MM/DD/YYYY HH:MM:SS)
YYMMDD_GAR.TXT	Garmin Fugawi GPS File	Fugawi Garmin (GAR)	9	None	24-hour format	all	4	N/A (HHMMSS)
YYMMDD_GEO.csv	Geologger GPS File	GeoStats Geologger (GEO)	None	None	24-hour format	all	6	N/A (HHMMSS)
YYMMDD_CPC1.txt	CPC Pre-Sampling Instrument Blank File	TSI CPC	14	14	24-hour format	all	2	N/A (HH:MM:SS AM/PM)
YYMMDD_CPC2.txt	CPC Pre-Sampling Tunnel Blank File							
YYMMDD_CPC3.txt	CPC Data Sampling File							
YYMMDD_CPC4.txt	CPC Post-Sampling Tunnel Blank File							
YYMMDD_CPC5.txt	CPC Post-Sampling Instrument Blank File							
YYMMDD_FTIR1.prn	FTIR Pre-Sampling Instrument Blank File	MKS MultiGas 2030HS (FTIR)	1	1	24-hour format	all	3	N/A (HH:MM:SS.mmm)
YYMMDD_FTIR2.prn	FTIR Pre-Sampling Tunnel Blank File							
YYMMDD_FTIR3.prn	FTIR Data Sampling File							
YYMMDD_FTIR4.prn	FTIR Post-Sampling Tunnel Blank File							
YYMMDD_FTIR5.prn	FTIR Post-Sampling Instrument Blank File							
YYMMDD_FTIRbkg.prn	FTIR Background Signal							
YYMMDD_EEPS1.txt	EEPS Pre-Sampling Instrument Blank File	TSI EEPS	15	14 and 15	AM/PM format	all	1	N/A (HH:MM:SS AM/PM)
YYMMDD_EEPS2.txt	EEPS Pre-Sampling Tunnel Blank File							
YYMMDD_EEPS3.txt	EEPS Data Sampling File							
YYMMDD_EEPS4.txt	EEPS Post-Sampling Tunnel Blank File							
YYMMDD_EEPS5.txt	EEPS Post-Sampling Instrument Blank File							
YYMMDD_RHT_IN.csv	Inside Vehicle Relative Humidity/Temperature File	Onset HOBO (RHT)	2	2	24-hour format	all	2	N/A (MM/DD/YYYY HH:MM:SS)
YYMMDD_RHT_OUT.csv	Outside Vehicle Relative Humidity/Temperature File	Onset HOBO (RHT)	2	2	24-hour format	all	2	N/A (MM/DD/YYYY HH:MM:SS)
YYMMDD_VID.avi	Video Camera File	Canon Optura 30 (VID)	N/A	N/A	N/A	N/A	N/A	Does not apply
YYMMDD_preEEPSoffsets.txt	EEPS offsets and RMS recorded pre-run	EEPS	1	1	N/A	N/A	N/A	No time in file
YYMMDD_postEEPSoffsets.txt	EEPS offsets and RMS recorded post-run	EEPS	1	1	N/A	N/A	N/A	No time in file
YYMMDD_SNR1.txt	FTIR signal to noise recorded pre-run	FTIR	5	N/A	AM/PM format	1	3	Start time (HH:MM)
YYMMDD_SNR2.txt	FTIR signal to noise recorded post-run	FTIR	5	N/A	AM/PM format	1	3	Start time (HH:MM)
YYMMDD_SPECS.docx	FTIR screen shots of specifications pre/post-run	FTIR	N/A	N/A	N/A	N/A	N/A	Does not apply

NOTE: YELLOW HIGHLIGHTED FILES ARE COLLECTED DATA, BUT WILL NOT BE INCLUDED IN THE DATABASE
GREEN HIGHLIGHTED FILES INDICATE EITHER ONE OR THE OTHER WILL EXIST FOR A RUN

Table A.3. Database Parameters from TOTEMS Instrumentation

Parameter	Unit	Description	Make/Model	Notation	Expected Minimum Value	Expected Maximum Value
Parameters Created from SamplingSummary_DATE.xlsx						
Second of Year	seconds	Calculated second from 12 midnight, January 1 of the current year	N/A	SOY	1	31557600
Date	N/A	The date the data was collected on (YYMMDD)	N/A	DATE	N/A	N/A
Run Number	N/A	Run identification number assigned to each of the sampling runs	N/A	RUN_NO	5	79
Driver ID	N/A	The initial of the driver for each run	N/A	DRIVER_ID	N/A	N/A
Vehicle ID	N/A	To ID which vehicle was used: CV for Conventional in cells when conventional used (ID using scan tool data), HEV for Hybrid in cells when hybrid is used (ID using scan tool data).	N/A	VEH_ID	N/A	N/A
Labview Device 1 YYMMDD_LAB1.txt						
Time stamp with the resolution on seconds to four decimal places	HH:MM:SS.SSSS	Hours(24 hr time), minutes, seconds + fraction of seconds to four decimal places	N/A	LAB1_EXACT_TIME	N/A	N/A
Time stamp	HH:MM:SS AM/PM	Hours(12 hr time), minutes, seconds, AM/PM	N/A	LAB1_CLK_TIME	N/A	N/A
Temperature 1	°C	Temperature from Type T thermocouple on the end of heated line (at the cross)	Omega Type T	HL_TEMP	40	200
Temperature 2	°C	Temperature from Type J thermocouple at the end of the tailpipe	Omega Type J	EXH_TEMP	40	500
Temperature 3	°C	Temperature from Type T thermocouple at the inlet of the FTIR and the filters	Omega Type T	FTIR_TEMP	40	200
Temperature 4	°C	Temperature from Type T thermocouple at the split to the CPC and EEPS	Omega Type T	PART_TEMP	15	80
Total Pressure	Volts	Total pressure	Omega PX181-030G5V	TOT_PRESS	0.7	1.3
Accelerometer: x-axis	Volts	Crossbow x-axis acceleration: Starting value is 2.5, axis runs lengthwise along vehicle front to back.	Crossbow CXLO2LF3	LAB1_ACCx	2	3
Accelerometer: y-axis	Volts	Crossbow y-axis acceleration: starting value is 2.5, axis runs across the vehicle, left to right.	Crossbow CXLO2LF3	LAB1_ACCy	1.5	3.5
Accelerometer: z-axis	Volts	Crossbow z-axis acceleration: starting value is 1.5, axis runs vertically, pointing to the road/sky	Crossbow CXLO2LF3	LAB1_ACCz	0.25	2.5
Labview Device 2 YYMMDD_LAB2.txt						
Time stamp with the resolution on seconds to four decimal places	HH:MM:SS.SSSS	Hours(24 hr time), minutes, seconds + fraction of seconds to four decimal places	N/A	LAB2_EXACT_TIME	N/A	N/A
Time stamp	HH:MM:SS AM/PM	Hours(12 hr time), minutes, seconds, AM/PM	N/A	LAB2_CLK_TIME	N/A	N/A
Differential Pressure 1	Volts	Pitot sensor 1 (highest flow rate)	Omega PX277	LAB2_DIFFP1	0	7
Differential Pressure 2	Volts	Pitot sensor 2 (second highest flowrate)	Omega PX277	LAB2_DIFFP2	0	10
Differential Pressure 3	Volts	Pitot sensor 3 (third highest flowrate)	Omega PX277	LAB2_DIFFP3	0	10
Differential Pressure 4	Volts	Pitot sensor 4 (lowest flow rate)	Omega PX277	LAB2_DIFFP4	5.2	10
RDD pin 16	Volts	Voltage Proportional to Stage 1 Dilution Factor	Matter Engineering (MD19-2E)	LAB2_DIL16	9.85	10
RDD pin 2	Volts	Voltage Proportional to Sensor Flow	Matter Engineering (MD19-2E)	LAB2_DIL2	2.5	3.5
RDD pin 25	Volts	Exhaust probe block temperature	Matter Engineering (MD19-2E)	LAB2_DIL25	1	3
RDD pin 5	Volts	Tacho voltage, which corresponds to the rotation rate of the rotating disk	Matter Engineering (MD19-2E)	LAB2_DIL5	-9	-10
Scantool Conventional Only (Blank for Hybrid Vehicle Sampling Runs) YYMMDD_CSCN.csv						
Sample Time	MM:SS.mmm	Sample Time	Toyota Techstream	CSCN_TIME	N/A	N/A
AF Lambda B1S1	Dimensionless	Air to Fuel Ratio Lambda	Toyota Techstream	CSCN_LAMBDA	0.7	1.35
Ambient Temperature	°C	Ambient Temperature	Toyota Techstream	CSCN_AMBTEMP	-30	40
Calculate Load	%	Load Calculated by ECM	Toyota Techstream	CSCN_LOAD	0	100
Catalyst Temp B1S1	°C	Catalyst Temperature Bank 1 Sensor 1	Toyota Techstream	CSCN_CATTEMP1	0	1000
Catalyst Temp B1S2	°C	Catalyst Temperature Bank 1 Sensor 2	Toyota Techstream	CSCN_CATTEMP2	0	950
Coolant Temp	°C	Coolant Temp	Toyota Techstream	CSCN_COOLTEMP	0	120
Engine Speed	rpm	Engine Speed	Toyota Techstream	CSCN_RPM	0	5500
Injection Volum (Cylinder1)	ml	Fuel Injection Volume for One Cylinder	Toyota Techstream	CSCN_INJVOL	0	1.2
MAF	gm/s	Mass Air Flow	Toyota Techstream	CSCN_MAF	0.3	120
MIL ON Run Distance	Km	Run Distance	Toyota Techstream	CSCN_RUNDIST	Currently is not being accurately collected (due to poor software)	
Vehicle Speed	km/h	Vehicle Speed	Toyota Techstream	CSCN_SPEED	0	130
Scantool Hybrid Only (Blank for Conventional Vehicle Sampling Runs) YYMMDD_HSCN.csv						
Sample Time	MM:SS.mmm	Sample Time	Toyota Techstream	HSCN_TIME	N/A	N/A
Accel Sensor Main	%	Acceleration Sensor	Toyota Techstream	HSCN_ACCEL	Currently is not being accurately collected (due to poor software)	
Ambient Temperature	°C	Ambient Temperature	Toyota Techstream	HSCN_AMBTEMP	-30	40
Battery State of Charge	%	State of Charge (All Batteries)	Toyota Techstream	HSCN_SOC	40	85
Calculate Load	%	Calculated Load	Toyota Techstream	HSCN_LOAD	0	100
Engine Coolant Temp	°C	Engine Coolant Temperature	Toyota Techstream	HSCN_COOLTEMP	0	120
Engine Spd	rpm	Engine Revolutions	Toyota Techstream	HSCN_ICE_RPM	0	5500
Generator(MG1) Rev	rpm	Generator Revolutions	Toyota Techstream	HSCN_GEN_RPM	-8000	12000
Generator(MG1) Torq	Nm	Generator Torque	Toyota Techstream	HSCN_GEN_TRQ	-100	100
MIL on Run Distance	km	Run Distance	Toyota Techstream	HSCN_RUNDIST	Currently is not being accurately collected (due to poor software)	
Motor(MG2) Revolution	rpm	Motor Revolution	Toyota Techstream	HSCN_ELEC_RPM	-600	8561
Motor(MG2) Torq	Nm	Motor Torque	Toyota Techstream	HSCN_ELEC_TRQ	-200	300
Regenerative Brake Torq	Nm	Regenerative Brake Torque	Toyota Techstream	HSCN_BRAKE_TRQ	0	450
Vehicle Spd	km/h	Vehicle Speed	Toyota Techstream	HSCN_SPEED	0	130
WIN Control Power	W	Maximum Chargeable Power Out of HV Battery	Toyota Techstream	HSCN_WIN	-5000	-26000
WOUT Control Power	W	Maximum Chargeable Power to HV Battery	Toyota Techstream	HSCN_WOUT	20000	26000

(continued on next page)

Table A.3. continued (Page 2 of 4)

Parameter	Unit	Description	Make/Model	Notation	Expected Minimum Value	Expected Maximum Value
		Garmin GPS (Fugawi) YYMMDD_GAR.txt				
Latitude	decimal degrees	Latitude WGS84 (negative is south)	Garmin GPS (Fugawi)	GAR_LAT	44.3979857	44.4889443
Longitude	decimal degrees	Longitude WGS84 (negative is west)	Garmin GPS (Fugawi)	GAR_LONG	-73.2193227	-72.9930073
Local Date	yyyymmdd	Date	Garmin GPS (Fugawi)	GAR_DATE	N/A	N/A
Local Time	hhmmss	Time	Garmin GPS (Fugawi)	GAR_TIME	N/A	N/A
Speed	m/s	Speed	Garmin GPS (Fugawi)	GAR_SPEED	0	130
		Geologger GPS YYMMDD_GEO.csv				
Status	code	A = GPS ok (valid data), D = DGPS mode ok (valid data), V = first valid sentence after loss of signal or power	Geostats Geologger (Ver. 2.4)	GEO_ST	N/A	N/A
Latitude	decimal degrees	Latitude in the WGS84 reference datum	Geostats Geologger (Ver. 2.4)	GEO_LAT	44.3979857	44.4889443
Latitudinal orientation	N or S	North or South	Geostats Geologger (Ver. 2.4)	GEO_DIR_LAT	N (only)	N (only)
Longitude	decimal degrees	Longitude in the WGS84 reference datum	Geostats Geologger (Ver. 2.4)	GEO_LONG	73.2193227	72.9930073
Longitudinal direction	E or W	East or West	Geostats Geologger (Ver. 2.4)	GEO_DIR_LONG	W (only)	W (only)
Time stamp	HHMMSS	Hours(24 hr time), minutes, seconds	Geostats Geologger (Ver. 2.4)	GEO_TIME	N/A	N/A
Date stamp	DDMMYY	Day(could be one or two digits), month, year	Geostats Geologger (Ver. 2.4)	GEO_DATE	N/A	N/A
Speed	mph	Calculated speed using delta distance between the present measurement and the last one	Geostats Geologger (Ver. 2.4)	GEO_SPD	0	130
Heading	degrees	Heading relative to North	Geostats Geologger (Ver. 2.4)	GEO_HDNG	0	359
Altitude	feet	Elevation above Mean Sea Level (MSL)	Geostats Geologger (Ver. 2.4)	GEO_ALT	80	1000
Horizontal Dilution of Precision	dimensionless constant	HDOP = $\sqrt{(dx^2 + dy^2)}$ can have values between 0.5 to 99.9, see Table 1 for interpretation of values	Geostats Geologger (Ver. 2.4)	GEO_HDOP	0.5	99.9
Number of satellites	integer value	available satellites, can range from 0 to 12	Geostats Geologger (Ver. 2.4)	GEO_SAT	0	12
		CPC YYMMDD_CPC#.txt				
Elapsed time	seconds	seconds elapsed since began recording	CPC model 3025A	CPC_ET	N/A	N/A
Time stamp	HH:MM:SS	Hours(24 hr time0, minutes, seconds	CPC model 3025A	CPC_TIME	N/A	N/A
Total Concentration	#/cm^3	Total particle concentration reported from the UCPC	CPC model 3025A	CPC_CONC	0	99900
		FTIR YYMMDD_FTIR#.prn				
Spectrum	name of file	name of the configuration file that was used	MKS Multigas 2030 HS	FTIR_SPEC	N/A	N/A
Date stamp	mm/dd/yyyy	month, day, and year	MKS Multigas 2030 HS	FTIR_DATE	N/A	N/A
Time stamp	HH:MM:SS.FFF	hours(24 hr time), minutes, and seconds + fraction of seconds to three decimal places	MKS Multigas 2030 HS	FTIR_TIME	N/A	N/A
1,2,4-Trimethylbenzene	ppm	Concentration of 1,2,4-Trimethylbenzene	MKS Multigas 2030 HS	FTIR_TRI124	-10	100000
1,2-Propadiene	ppm	Concentration of 1,2-Propadiene	MKS Multigas 2030 HS	FTIR_PROP12	-10	100000
1,3,5-Trimethylbenzene	ppm	Concentration of 1,3,5-Trimethylbenzene	MKS Multigas 2030 HS	FTIR_TRI135	-10	100000
1,3-Butadiene	ppm	Concentration of 1,3-Butadiene	MKS Multigas 2030 HS	FTIR_BUTA13	-10	100000
2-Methylpropene	ppm	Concentration of 2-Methylpropene	MKS Multigas 2030 HS	FTIR_MTHYL2	-10	100000
Acetaldehyde	ppm	Concentration of Acetaldehyde	MKS Multigas 2030 HS	FTIR_ACETAL	-10	100000
Acetylene	ppm	Concentration of Acetylene	MKS Multigas 2030 HS	FTIR_ACETYL	-10	100000
Acrolein	ppm	Concentration of Acrolein	MKS Multigas 2030 HS	FTIR_ACROLE	-10	100000
Benzene	ppm	Concentration of Benzene	MKS Multigas 2030 HS	FTIR_BENZ	-10	100000
CH4	ppm	Concentration of Methane	MKS Multigas 2030 HS	FTIR_CH4	-10	100000
CO ppm	ppm	Concentration of Carbon Monoxide	MKS Multigas 2030 HS	FTIR_COPPM	-10	100000
CO%	%	Percent Concentration of Carbon Monoxide	MKS Multigas 2030 HS	FTIR_COPCT	-1	50
CO2%	%	Percent Concentration of Carbon Dioxide	MKS Multigas 2030 HS	FTIR_CO2PCT	-1	50
Ethane	ppm	Concentration of Ethane	MKS Multigas 2030 HS	FTIR_ETHANE	-10	100000
Ethanol	ppm	Concentration of Ethanol	MKS Multigas 2030 HS	FTIR_ETHANO	-10	100000
Ethylene	ppm	Concentration of Ethylene	MKS Multigas 2030 HS	FTIR_ETHYLE	-10	100000
Formaldehyde	ppm	Concentration of Formaldehyde	MKS Multigas 2030 HS	FTIR_FORMAL	-10	100000
H2O%	%	Percent Concentration of Water	MKS Multigas 2030 HS	FTIR_H2OPCT	-1	50
IsoOctane	ppm	Concentration of IsoOctane	MKS Multigas 2030 HS	FTIR_ISOOCT	-10	100000
m-Xylene	ppm	Concentration of m-Xylene	MKS Multigas 2030 HS	FTIR_MXYLEN	-10	100000
MeOH	ppm	Concentration of Methanol	MKS Multigas 2030 HS	FTIR_MEOH	-10	100000
N2O	ppm	Concentration of Nitrous Oxide	MKS Multigas 2030 HS	FTIR_N2O	-10	100000
NH3	ppm	Concentration of Ammonia	MKS Multigas 2030 HS	FTIR_NH3	-10	100000
NO	ppm	Concentration of Nitric Oxide	MKS Multigas 2030 HS	FTIR_NO	-10	100000
NO2	ppm	Concentration of Nitrogen Dioxide	MKS Multigas 2030 HS	FTIR_NO2	-10	100000
Octane	ppm	Concentration of Octane	MKS Multigas 2030 HS	FTIR_OCTANE	-10	100000
Propane	ppm	Concentration of Propane	MKS Multigas 2030 HS	FTIR_PROPAN	-10	100000
Propylene	ppm	Concentration of Propylene	MKS Multigas 2030 HS	FTIR_PROPYL	-10	100000
Propyne	ppm	Concentration of Propyne	MKS Multigas 2030 HS	FTIR_PROPYN	-10	100000
SO2	ppm	Concentration of Sulfur Dioxide	MKS Multigas 2030 HS	FTIR_SO2	-10	100000
Toluene	ppm	Concentration of Toluene	MKS Multigas 2030 HS	FTIR_TOLUEN	-10	100000
Temp (C)	°C	Temperature of sample cell	MKS Multigas 2030 HS	FTIR_TEMP	181	201
Pressure (atm)	atm	Pressure in sample cell	MKS Multigas 2030 HS	FTIR_PRESS	0.8	1.2
Igram DC		Interferogram preamp setup measure	MKS Multigas 2030 HS	FTIR_IGDC	-10	10
Igram PP		Interferogram signal measure, 2° to Single Beam @ 2500	MKS Multigas 2030 HS	FTIR_IGPP	0	6
Phase angle	°	Laser alignment phase angle	MKS Multigas 2030 HS	FTIR_ANGLE	55	120
Laser PP	V	Laser voltage	MKS Multigas 2030 HS	FTIR_LASPP	2	9
Laser DC	V	Laser health indicator	MKS Multigas 2030 HS	FTIR_LASDC	-9	-2
Bad scan counter		Modulator unable to scan, should be less than 10 per day	MKS Multigas 2030 HS	FTIR_BADSCN	0	10
Centerburst location	cm^{-1}	Interferogram measure, 3° to other igram measures	MKS Multigas 2030 HS	FTIR_CTRLOC	560	580
Linearizer check		Linearizer Check	MKS Multigas 2030 HS	FTIR_LINCHK	0	0.005
SNR 2500		Signal to noise ratio at 2500 cm-1, should be 90% of original daily value taken during SNR check	MKS Multigas 2030 HS	FTIR_SNR	100	1500
sBeam @2500	AU	Single beam signal intensity at 2500cm-1, more useful as a check with N2 flow	MKS Multigas 2030 HS	FTIR_SBEAM	0	1

Table A.3. continued (page 3 of 4)

Parameter	Unit	Description	Make/Model	Notation	Expected Minimum Value	Expected Maximum Value
EEPS YYMMDD_EEPS#.txt						
Time stamp	HH:MM:SS AM/PM	12-Hour Time AM/PM	TSI EEPS Model 3090	EEPS_CLK_TIME	N/A	N/A
Channel 1	#/cm^3	Particle concentration in the range 5.6234 - 6.4938 nanometers	TSI EEPS Model 3090	EEPS_1	0	100000 to 10000000
Channel 2	#/cm^3	Particle concentration in the range 6.4938 - 7.4989 nanometers	TSI EEPS Model 3090	EEPS_2	0	100000 to 10000000
Channel 3	#/cm^3	Particle concentration in the range 7.4989 - 8.6596 nanometers	TSI EEPS Model 3090	EEPS_3	0	100000 to 10000000
Channel 4	#/cm^3	Particle concentration in the range 8.6596 - 10.000 nanometers	TSI EEPS Model 3090	EEPS_4	0	100000 to 10000000
Channel 5	#/cm^3	Particle concentration in the range 10.000 - 11.5478 nanometers	TSI EEPS Model 3090	EEPS_5	0	100000 to 10000000
Channel 6	#/cm^3	Particle concentration in the range 11.5478 - 13.3352 nanometers	TSI EEPS Model 3090	EEPS_6	0	100000 to 10000000
Channel 7	#/cm^3	Particle concentration in the range 13.3352 - 15.3393 nanometers	TSI EEPS Model 3090	EEPS_7	0	100000 to 10000000
Channel 8	#/cm^3	Particle concentration in the range 15.3393 - 17.7828 nanometers	TSI EEPS Model 3090	EEPS_8	0	100000 to 10000000
Channel 9	#/cm^3	Particle concentration in the range 17.7828 - 20.5353 nanometers	TSI EEPS Model 3090	EEPS_9	0	100000 to 10000000
Channel 10	#/cm^3	Particle concentration in the range 20.5353 - 23.7137 nanometers	TSI EEPS Model 3090	EEPS_10	0	100000 to 10000000
Channel 11	#/cm^3	Particle concentration in the range 23.7137 - 27.3842 nanometers	TSI EEPS Model 3090	EEPS_11	0	100000 to 10000000
Channel 12	#/cm^3	Particle concentration in the range 27.3842 - 31.6228 nanometers	TSI EEPS Model 3090	EEPS_12	0	100000 to 10000000
Channel 13	#/cm^3	Particle concentration in the range 31.6228 - 36.5174 nanometers	TSI EEPS Model 3090	EEPS_13	0	100000 to 10000000
Channel 14	#/cm^3	Particle concentration in the range 36.5174 - 42.1697 nanometers	TSI EEPS Model 3090	EEPS_14	0	100000 to 10000000
Channel 15	#/cm^3	Particle concentration in the range 42.1697 - 48.6968 nanometers	TSI EEPS Model 3090	EEPS_15	0	100000 to 10000000
Channel 16	#/cm^3	Particle concentration in the range 48.6968 - 56.2341 nanometers	TSI EEPS Model 3090	EEPS_16	0	100000 to 10000000
Channel 17	#/cm^3	Particle concentration in the range 56.2341 - 64.9832 nanometers	TSI EEPS Model 3090	EEPS_17	0	100000 to 10000000
Channel 18	#/cm^3	Particle concentration in the range 64.9832 - 74.9894 nanometers	TSI EEPS Model 3090	EEPS_18	0	100000 to 10000000
Channel 19	#/cm^3	Particle concentration in the range 74.9894 - 86.5964 nanometers	TSI EEPS Model 3090	EEPS_19	0	100000 to 10000000
Channel 20	#/cm^3	Particle concentration in the range 86.5964 - 100.000 nanometers	TSI EEPS Model 3090	EEPS_20	0	100000 to 10000000
Channel 21	#/cm^3	Particle concentration in the range 100.000 - 115.478 nanometers	TSI EEPS Model 3090	EEPS_21	0	100000 to 10000000
Channel 22	#/cm^3	Particle concentration in the range 115.478 - 133.352 nanometers	TSI EEPS Model 3090	EEPS_22	0	100000 to 10000000
Channel 23	#/cm^3	Particle concentration in the range 133.352 - 153.992 nanometers	TSI EEPS Model 3090	EEPS_23	0	100000 to 10000000
Channel 24	#/cm^3	Particle concentration in the range 153.992 - 177.827 nanometers	TSI EEPS Model 3090	EEPS_24	0	100000 to 10000000
Channel 25	#/cm^3	Particle concentration in the range 177.827 - 205.352 nanometers	TSI EEPS Model 3090	EEPS_25	0	100000 to 10000000
Channel 26	#/cm^3	Particle concentration in the range 205.352 - 237.137 nanometers	TSI EEPS Model 3090	EEPS_26	0	100000 to 10000000
Channel 27	#/cm^3	Particle concentration in the range 237.137 - 273.842 nanometers	TSI EEPS Model 3090	EEPS_27	0	100000 to 10000000
Channel 28	#/cm^3	Particle concentration in the range 273.842 - 316.227 nanometers	TSI EEPS Model 3090	EEPS_28	0	100000 to 10000000
Channel 29	#/cm^3	Particle concentration in the range 316.227 - 365.174 nanometers	TSI EEPS Model 3090	EEPS_29	0	100000 to 10000000
Channel 30	#/cm^3	Particle concentration in the range 365.174 - 421.696 nanometers	TSI EEPS Model 3090	EEPS_30	0	100000 to 10000000
Channel 31	#/cm^3	Particle concentration in the range 421.696 - 486.976 nanometers	TSI EEPS Model 3090	EEPS_31	0	100000 to 10000000
Channel 32	#/cm^3	Particle concentration in the range 486.976 - 562.341 nanometers	TSI EEPS Model 3090	EEPS_32	0	100000 to 10000000
Time stamp 1	HH:MM:SS AM/PM	12-Hour Time AM/PM	TSI EEPS Model 3090	EEPS_TIME1	N/A	N/A
Total Concentration	#/cm^3	Total particle concentration from all channels combined	TSI EEPS Model 3090	EEPS_TOT_CONC	0	N/A (channel dependent)
Time stamp 2	HH:MM:SS AM/PM	12-Hour Time AM/PM	TSI EEPS Model 3090	EEPS_TIME2	N/A	N/A
Column Pressure	mbar	Pressure within electrometer column	TSI EEPS Model 3090	EEPS_P	920	1050
Time stamp 3	HH:MM:SS AM/PM	12-Hour Time AM/PM	TSI EEPS Model 3090	EEPS_TIME3	N/A	N/A
Sample Temperature	˚C	Temperature of sample going into instrument	TSI EEPS Model 3090	EEPS_SAMP_T	15	45
Time Stamp 4	HH:MM:SS AM/PM	12-Hour Time AM/PM	TSI EEPS Model 3090	EEPS_TIME4	N/A	N/A
Raw Channel 1	femtoamp	Raw Channel 1 Current	TSI EEPS Model 3090	EEPS_R1	-15	15
Raw Channel 2	femtoamp	Raw Channel 2 Current	TSI EEPS Model 3090	EEPS_R2	-15	15
Raw Channel 3	femtoamp	Raw Channel 3 Current	TSI EEPS Model 3090	EEPS_R3	-20	20
Raw Channel 4	femtoamp	Raw Channel 4 Current	TSI EEPS Model 3090	EEPS_R4	-120	120
Raw Channel 5	femtoamp	Raw Channel 5 Current	TSI EEPS Model 3090	EEPS_R5	-120	300
Raw Channel 6	femtoamp	Raw Channel 6 Current	TSI EEPS Model 3090	EEPS_R6	-120	300
Raw Channel 7	femtoamp	Raw Channel 7 Current	TSI EEPS Model 3090	EEPS_R7	-120	500
Raw Channel 8	femtoamp	Raw Channel 8 Current	TSI EEPS Model 3090	EEPS_R8	-120	700
Raw Channel 9	femtoamp	Raw Channel 9 Current	TSI EEPS Model 3090	EEPS_R9	-120	900
Raw Channel 10	femtoamp	Raw Channel 10 Current	TSI EEPS Model 3090	EEPS_R10	-100	1200
Raw Channel 11	femtoamp	Raw Channel 11 Current	TSI EEPS Model 3090	EEPS_R11	-200	4000
Raw Channel 12	femtoamp	Raw Channel 12 Current	TSI EEPS Model 3090	EEPS_R12	-200	4500
Raw Channel 13	femtoamp	Raw Channel 13 Current	TSI EEPS Model 3090	EEPS_R13	-200	4000
Raw Channel 14	femtoamp	Raw Channel 14 Current	TSI EEPS Model 3090	EEPS_R14	-200	3000
Raw Channel 15	femtoamp	Raw Channel 15 Current	TSI EEPS Model 3090	EEPS_R15	-200	2000
Raw Channel 16	femtoamp	Raw Channel 16 Current	TSI EEPS Model 3090	EEPS_R16	-200	1000
Raw Channel 17	femtoamp	Raw Channel 17 Current	TSI EEPS Model 3090	EEPS_R17	-200	500
Raw Channel 18	femtoamp	Raw Channel 18 Current	TSI EEPS Model 3090	EEPS_R18	-200	300
Raw Channel 19	femtoamp	Raw Channel 19 Current	TSI EEPS Model 3090	EEPS_R19	-200	200
Raw Channel 20	femtoamp	Raw Channel 20 Current	TSI EEPS Model 3090	EEPS_R20	-200	200
Raw Channel 21	femtoamp	Raw Channel 21 Current	TSI EEPS Model 3090	EEPS_R21	-500	400
Raw Channel 22	femtoamp	Raw Channel 22 Current	TSI EEPS Model 3090	EEPS_R22	-1000	2000

Table A.3. continued (page 4 of 4)

Parameter	Unit	Description	Make/Model	Notation	Expected Minimum Value	Expected Maximum Value
Relative Humidity and Temperature Logger [Inside vehicle] YYMMDD_RHT_IN.csv						
Sample Number	integer value	Sample number since started recording	Onset HOBO U23-001	RHT_IN_SAMP	N/A	N/A
Date/Time stamp	mm/dd/yyyy HH:MM:SS	Date (month/day/yr) and time (hours in 24 hr time, minutes, seconds)	Onset HOBO U23-001	RHT_IN_DT	N/A	N/A
Temperature (IN)	˚C	Temperature inside car in Celcius	Onset HOBO U23-001	RHT_IN_T	10	30
Relative Humidity (IN)	%	Relative humidity inside the car	Onset HOBO U23-001	RHT_IN_RH	10	90
Relative Humidity and Temperature Logger [Outside vehicle] YYMMDD_RHT_OUT.csv						
Sample Number	integer value	Sample number since started recording	Onset HOBO U23-001	RHT_OUT_SAMP	N/A	N/A
Date/Time stamp	mm/dd/yyyy HH:MM:SS	Date (month/day/yr) and time (hours in 24 hr time, minutes, seconds)	Onset HOBO U23-001	RHT_OUT_DT	N/A	N/A
Temperature (OUT)	˚C	Temperature outside car in Celcius	Onset HOBO U23-001	RHT_OUT_T	-30	40
Relative Humidity (OUT)	%	Relative humidity outside the car	Onset HOBO U23-001	RHT_OUT_RH	10	95
Video Camera YYMMDD_VID.avi						

Table A.4. Constants for Database Parameter Calculations

Constants			
Parameter	**Unit**	**Value**	**Notation**
Calibration Factor	*unitless*	1523	X
Temperature Correction Factor	°C	1	f
Gravitational constant	m/s^2	9.81	g
Coefficient of Drag: CV	unitless	0.28	$Conv\_C_D$
Coefficient of Drag: HEV	unitless	0.27	Hyb_C_D
Mass of loaded conventional	kg	1996	Conv_m
Mass of loaded hybrid	kg	2136	Hyb_m
cross-sectional area of convention	m^2	2.48	Conv_A
cross-sectional area of hybrid	m^2	2.45	Hyb_A
Universal Gas Constant	L.atm/mol.K	0.0821	R
Volumetric Conversion for %		0.1	V_PCT
Volumetric Conversion for ppm		1	V_PPM

Table A.5. Calculated Parameters Descriptions (Page 1 of 4)

Data Name	Parameter	Unit	Equation	Description
DATE	Date of data collection	YYMMDD		Date the data was collected on in the format YYMMDD
TIME	Time of data collection	HH:MM:SS		Time associated with the adjusted data in the format of HH:MM:SS
VEH_ID	Vehicle used for data collection	N/A	**VEH_ID** = CV *for Conventional Vehicle* HV *for Hybrid Vehicle*	To ID which vehicle was used: CV (conventional vehicle) in cells when conventional used (ID using scan tool data), HV (hybrid vehicle) in cells when hybrid is used (ID using scan tool data).
DRIVER_ID	Vehicle driver's initials	N/A	**DRIVER_ID** = KMS	The initials of the driver for each run; KMS unless otherwise noted
PHASE_ID	Phase of run	N/A	**PHASE_ID** = IB_1 *for PHASE_NUM = 1* TB_1 *for PHASE_NUM = 2* WARM *for PHASE_NUM = 3* RUN_OUT *for PHASE_NUM = 4* PARK *for PHASE_NUM = 5* RUN_IN *for PHASE_NUM = 6* POST *for PHASE_NUM = 7* TB_2 *for PHASE_NUM = 8* IB_2 *for PHASE_NUM = 9*	The phases of the sampling run, in order, include: instrument blank (pre-sampling), tunnel blank (pre-sampling), warm-up driving, outbound sampling, parking at the Richmond Park-and-Ride, inbound sampling, post-sampling driving to gas station, tunnel blank (post-sampling), and instrument blank (post-sampling).
RUN_NUM	Run Number	N/A	**RUN_NO** = 5 thru 75	Run number associated with each sampling set; 5 thru 75 for data collection runs on HV and CV
PHASE_NUM	Phase of run	N/A	**PHASE_NO** = 1 *for Pre-Run Instrument Blank* 2 *for Pre-Run Tunnel Blank* 3 *for Run Warm-Up* 4 *for Stablized Outbound Phase Data* 5 *for Idle at the Richmond Park and Ride* 6 *for Stabilized Inbound Phase Data* 7 *for Run Post Route Travel* 8 *for Post-Run Tunnel Blank* 9 *for Post-Run Instrument Blank*	The phases of the sampling run are numbered one through nine, corresponding to instrument blank (pre-sampling), tunnel blank (pre-sampling), warm-up driving, outbound sampling, parking at the Richmond Park-and-Ride, inbound sampling, post-sampling driving to gas station, tunnel blank (post-sampling), and instrument blank (post-sampling), respectively.
VEH_NO	Vehicle Identification Number	N/A	**VEH_NO** = 1 *for CV* 2 *for HV*	Vehicle identification number for use when character type data may not be feasible.
SOY	seconds of the year	seconds	See soyassign_final.m for algorithm.	Calculated second from 12 midnight, January 1 of 2010, continuous through all future dates and times, accounting for leap year and daylight savings.
Exhaust Flow Rate Calculated Parameters				
EST_EXHTEMP	Predicted Exhaust Temperature for missing exhaust temperature data	°C	**EST_EXHTEMP** = 1.18298 * SCN_SPEED + 0.02821 * SCN_RPM + 92.5954 *for CV* 0.02531 * SCN_RPM + 0.12429 * SCN_MOTORRPM - 8.02728 * SCN_SPEED - 0.06838 * SCN_CALCLOAD + 100.7577 *for HEV*	
REC_EXHTEMP	Recommended Exhaust Temperature for missing exhaust temperature data	°C	**REC_EXHTEMP** = EST_EXHTEMP *if* -40 < LAB1_EXHTEMP < 400 EST_EXHTEMP *if* [LAB1_EXHTEMP$_t$ - LAB1_EXHTEMP$_{t-1}$] < -80 EST_EXHTEMP *if* [LAB1_EXHTEMP$_t$ - LAB1_EXHTEMP$_{t-1}$] > 80 LAB1_EXHTEMP *else*	
FLAG_EXHTEMP		N/A	**EXHTEMP_FLAG** = 1 *if REC_EXHTEMP = LAB1_EXHTEMP* 2 *if REC_EXTEMP = PRE_EXHTEMP*	
FLOWRATE_4	Differential Pressure Sensor 4	LPM	**FLOWRATE_4** = (83609.257 * (LAB2_DIFFP4 - 5))$^{1/2}$	Where m = 83609.257 and b = 0; see PitotCalibrationEquations tab for more information.
FLOWRATE_3	Differential Pressure Sensor 3	LPM	**FLOWRATE_3** = (394516.8 * LAB2_DIFFP3)$^{1/2}$	Where m = 394516.8 and b = 0; see PitotCalibrationEquations tab for more information.
FLOWRATE_2	Differential Pressure Sensor 2	LPM	**FLOWRATE_2** = (2129720.5 * LAB2_DIFFP2)$^{1/2}$	Where m = 2129720.5 and b = 0; see PitotCalibrationEquations tab for more information.
FLOWRATE_1	Differential Pressure Sensor 1	LPM	**FLOWRATE_1** = (14499240 * LAB2_DIFFP1)$^{1/2}$	Where m = 14499240 and b = 0; see PitotCalibrationEquations tab for more information.
EST_CHOSENFLOW			**EST_CHOSENFLOW** = -219.2309 + 0.7634308 * SCN_RPM + 0.0003573 * (SCN_RPM - 947.284)^2	See EST_CHOSENFLOW tab for regression information.
CHOSEN_FLOW	Tailpipe Flow Rate selection based on the usage range of each of the Differential Pressure Sensors	LPM	**CHOSEN_FLOW** = EST_CHOSENFLOW if RUN_NO = 19, 23, 24, 25, 26, 27, 74 PHASE 4 only FLOWRATE_4 *if* 0.4 ≤ (LAB2_DIFFP4 - 5) < 4.6 FLOWRATE_3 *if* 0.4 ≤ LAB2_DIFFP3 < 9.6 FLOWRATE_2 *if* 0.4 ≤ LAB2_DIFFP2 < 9.6 FLOWRATE_1 *if* 0.4 ≤ LAB2_DIFFP1 < 9.6 FLOWRATE_4 *if* 0 ≤ (LAB2_DIFFP4 - 5) < 0.4	Flowrate calculated from one of the four differential pressure sensors, selected based on the usage ranges for each sensor. If the uppermost condition is not met, the conditional moves to the next uppermost condition and so on. The final condition is a consideration for extrapolation beyond the usage range of the most sensitive sensor.
FLAG_FLOW	Flag for Chosen Flow	N/A	**FLOW_FLAG** = 1 *if CHOSEN_FLOW = FLOWRATE_1* 2 *if CHOSEN_FLOW = FLOWRATE_2* 3 *if CHOSEN_FLOW = FLOWRATE_3* 4 *if CHOSEN_FLOW = FLOWRATE_4* 5 *if CHOSEN_FLOW = FLOWRATE_4 && LAB2_DIFFP4 < 0.4* 6 *if CHOSEN_FLOW = EST_CHOSENFLOW*	Indicates the input for the final flow calculation
TC_FLOW	Temperature compensated exhaust flow rate	LPM	**TC_FLOW** = CHOSEN_FLOW * ((REC_EXHTEMP + 273.15) / 298.15))	Calculated_Flow is the calculated flow from the pressure sensors: EXH_TEMP is the Temperature from the Type J thermocouple in Kelvins

Table A.5. Calculated Parameters Descriptions (p. 2 of 4)

Data Name	Parameter	Unit	Equation	Description
Environmental Conditions				
DEWPT_OUT	Dewpoint for Ambient Conditions	°C	**DEWPT_OUT** = $\dfrac{\ln((\mathrm{RHT\_OUT\_RH} / 100) * 0.611 * \exp(17.3 * \mathrm{RHT\_OUT\_T} / (\mathrm{RHT\_OUT\_T} + 237.3))) + 0.4926}{0.0708 - 0.00421 * \ln((\mathrm{RHT\_OUT\_RH} / 100) * 0.611 * \exp(17.3 * \mathrm{RHT\_OUT\_T} / (\mathrm{RHT\_OUT\_T} + 237.3)))}$	
DEWPT_IN	Dewpoint for Vehicle Cabin	°C	**DEWPT_IN** = $\dfrac{\ln((\mathrm{RHT\_IN\_RH} / 100) * 0.611 * \exp(17.3 * \mathrm{RHT\_IN\_T} / (\mathrm{RHT\_IN\_T} + 237.3))) + 0.4926}{0.0708 - 0.00421 * \ln((\mathrm{RHT\_IN\_RH} / 100) * 0.611 * \exp(17.3 * \mathrm{RHT\_IN\_T} / (\mathrm{RHT\_IN\_T} + 237.3)))}$	
Fuel Consumption Calculated Parameters				
HEV_MAF	Hybrid vehicle mass air flow	g/sec	**HEV_MAF** = 0.018832 * SCN_RPM - 14.603 if VEH_ID = HV & SCN_RPM > 775.435 0 if VEH_ID = HV & SCN_RPM < 775.435	Due to scan tool limitations, MAF must be estimated for the hybrid vehicle using RPM data; HSCN_ICE_RPM of 775.435 is the point at which the ICE turns off and below that RPM would be reported as a negative MAF otherwise.
FUEL_RATE	Fuel Rate	gal/sec	**FUEL_RATE** = $\dfrac{0.273 * \mathrm{FTIR\_CO2PCT\_ER} * 10^{-3} + 0.429 * \mathrm{FTIR\_COPCT\_ER} * 10^{-3} + 0.817 * \mathrm{FTIR\_PROPAN\_ER} * 10^{-6}}{2421}$	Carbon balance method to calculating Fuel Consumption; see FuelConsumption_4NOV10.docx for explanation.
FUEL_ECON_Bal	Fuel Economy Balance	mi/gal	**FUEL_ECON_Bal** = $\dfrac{\mathrm{SCN\_SPEED} * 2421 * 0.621}{0.273 * \mathrm{FTIR\_CO2PCT\_ER} * 10^{-3} + 0.429 * \mathrm{FTIR\_COPCT\_ER} * 10^{-3} + 0.817 * \mathrm{FTIR\_PROPAN\_ER} * 10^{-3}}$	
FUEL_ECON	Fuel Economy	mi/gal	**FUEL_ECON** = $\dfrac{\mathrm{SCN\_SPEED} * 0.6 * 6.15 * 14.7}{\mathrm{SCN\_MAF} * 60 * (1 / 453.592) * 60}$ if SCN_MAF > 0 $\dfrac{\mathrm{HEV\_SPEED} * 0.6 * 6.15 * 14.7}{\mathrm{HEV\_MAF} * 60 * (1 / 453.592) * 60}$ if HEV_MAF > 0 100 if SCN_MAF = 0 100 if HEV_MAF = 0 100 if FUEL_ECON > 100	CSCN_SPEED or HSCN_SPEED [km/hr] from the scantool; CSCN_MAF [g/sec] is mass air flow from the scan tool; HSCN_MAF [g/sec] is obtained by the RPM/MAF regression equation; 14.7 is assumed stoichiometry; 0.6 [mi/km] conversion; 6.15 [lb/gal] conversion; 1/453.592 [lb/g] conversion; 60 [min/hr] conversion. FUEL_ECON = 100 mi/gal is an arbitrary value indicating the highest possible fuel economy achieved.
Acceleration Rate				
ACCEL	Scantool Calculated Acceleration	m/s^2	**ACCEL** = $\dfrac{\mathrm{SCN\_SPEED}_t - \mathrm{SCN\_SPEED}_{t-1}}{\mathrm{SCN\_TIME}_t - \mathrm{SCN\_TIME}_{t-1}}$	Where: i = current data record (starting at the second record); i-1 = data at the previous data record
ACCx	Acceleration in the x-direction	m/s^2	**ACCx** = (LAB1_ACCx - 2.5) * 9.80665	Conversion of raw mV signals measured in the x-direction by the Crossbow accelerometer and converted to gravitational units and then to km/hr.s.
ACCy	Acceleration in the y-direction	m/s^2	**ACCy** = (LAB1_ACCy - 2.5) * 9.80665	Conversion of raw mV signals measured in the y-direction by the Crossbow accelerometer and converted to gravitational units and then to km/hr.s.
ACCz	Acceleration in the z-direction	m/s^2	**ACCz** = (LAB1_ACCz - 1.0) * 9.80665	Conversion of raw mV signals measured in the z-direction by the Crossbow accelerometer and converted to gravitational units and then to km/hr.s.
Grade				
REC_CHAINAGE	Chainage of route	meters	For details on development of these parameters and joining of grade from the Vermont Agengy of Transportation's Automatic Road Analyzer (ARAN) vehicle to the data set, see **SOP_GradeJoin_Chainage_31SEP12.doc**.	Cumulative distance of the full route.
REC_GRADE	Recommended Road Grade	% grade		Slope of road way along the route in the direction the vehicle is traveling.
REC_LAT	Recommended Latitude	decimal degrees		Latitude recommended for the full route.
REC_LONG	Recommended Longitude	decimal degrees		Longitude recommended for the full route.
FLAG_GRADE	Flag for Grade Choice	N/A	**GRADE_FLAG** = 1 *if GAR and GEO measured* 2 *if GEO only measured (GAR estimated)* 3 *if GAR only measured (GEO estimated)* 4 *if GAR and GEO estimated under 15s* 5 *if GEO estimated under 15s (GAR estimated greater than 15s)* 6 *if GAR estimated under 15s (GEO estimated greater than 15s)* 7 *if Vehicle Detour -neither device available*	
VSP parameters				
AIR_DENS	ρ_a	kg/m^3	**AIR_DENS** (ρ_a) = $\dfrac{352.977}{\mathrm{RHT\_OUT\_T} + 273.15}$	A calculation of the air density using second-by-second temperature
ELEC_HP	Electric motor horsepower	hp	**ELEC_HP** = $\dfrac{\mathrm{SCN\_MOTORTRQ} * \mathrm{SCN\_MOTORRPM}}{7121}$	HSCN parameters described in "Database DataDictionary" worksheet)
ELEC_GEN_HP	Electric Generator Horsepower	hp	**ELEC_GENHP** = $\dfrac{\mathrm{SCN\_GENTRQ} * \mathrm{SCN\_GENRPM}}{7121}$	HSCN parameters described in "Database DataDictionary" worksheet)
VSP_K	Vehicle Specific Power: Kinetic	kW/metric ton	**VSP_K** = 1.1 * SCN_SPEED * (1 / 3.6) * ACCx	Where **RawData** include: HSCN_SPEED or CSCN_SPEED = vehicle speed (km/hr); where **CalculatedParameters** include: ACCx = acceleration (m/s^2) from Crossbow in x-direction; where coefficients include: $\varepsilon = 0.1$ as recommended by Jimenez (1999) making the adapted equation of $1+\varepsilon = 1.1$
VSP_P	Vehicle Specific Power: Potential	kW/metric ton	**VSP_P** = g * (GRADE / 100) * SCN_SPEED * (1 / 3.6)	Where **RawData** include: HSCN_SPEED or CSCN_SPEED = vehicle speed (km/hr); where **CalculatedParameters** include: GRADE = road grade (%); where **Constants** include: g = Gravitational Constant (m/s^2)
VSP_R	Vehicle Specific Power: Rolling Resistance	kW/metric ton	**VSP_R** = 0.13244 * SCN_SPEED * (1 / 3.6)	Where **RawData** include: HSCN_SPEED or CSCN_SPEED = vehicle speed (km/hr); where coefficients include: $C_R = 0.0135$ as recommended by Jimenez (1999) making the value of $C_R * g = 0.13244$ (m/s^2)
VSP_D	Vehicle Specific Power: Drag	kW/metric ton	**VSP_D** = $(1 / 2) * \rho_a * [(C_{Dcv} * A_{cv}) / m_{cv}] * [\mathrm{SCN\_SPEED} * (1 / 3.6)]^3$	Where **RawData** include: HSCN_SPEED or CSCN_SPEED = vehicle speed (km/hr); where **CalculatedParameters** include: ρ_a = air density (kg/m^3); where **Constants** include: C_{DHyb} or C_{DConv} = Coefficient of Drag of Vehicle, A_{Hyb} or A_{Conv} = Cross-Sectional Area of Vehicle (m^2), m_{Hyb} or m_{Conv} = Mass of Vehicle (kg)
VSP	Vehicle Specific Power	kW/metric ton	**VSP** = VSP_K + VSP_P + VSP_R + VSP_D	Equation adapted from Jimenez (1999).
OpMode	Operating Mode	N/A	**OpMode** = f(VSP, SCN_SPEED)	According to EPA MOVES OpMode definition

Table A.5. Calculated Parameters Descriptions (p. 3 of 4)

Data Name	Parameter	Unit	Equation	Description
Dilution System Calculated Parameters				
DF	Dilution Factor (including MD19-2E and ASET dilution)	N/A	**DF** = [(X * f) / (10 * LAB2_DIL16)] * 7.1	X is the calibration factor, f is the temperature correction (See the "Constants" worksheet)
SFLOW	Sensor Flow	LPM	**SFLOW** = 0.5 * LAB2_DIL2	Sensor flow corresponds to the flow being pulled by the connected measurement device. This is the ASET for Sig Proj. 2
BTEMP	Exhaust Probe Block Temperature on MD19-2E	°C	**BTEMP** = -235 + 133 * LAB2_DIL25 + 15.6 * LAB2_DIL25 ^ 2	Corresponds to the temperature the heating block is at on the MD19-2E
ROTRATE	Tachometer Voltage on MD19-2E	1/s	**ROTRATE** = -0.25 * LAB2_DIL5	Corresponds to the rotation rate of the 10-cavity disk
Particle Number Emission Rates				
	EEPS Protocol		If (EEPS_# - EEPS_DL_#) > 0, follow equations below. If < 0 use only (EEPS_DL _#) in equation and not (EEPS_# - EEPS_DL_#).	
EEPS_1_ER	Particle emission rates in the range 5.6234 - 6.4938 nanometers	#/sec	**EEPS1_ER** = (EEPS1 - EEPS1_DL) * TC_FLOW * DF * (1000 / 60)	DF obtained from Dilution system calculated parameter listed above.
EEPS_2_ER	Particle emission rates in the range 6.4938 - 7.4989 nanometers	#/sec	**EEPS2_ER** = (EEPS2 - EEPS2_DL) * TC_FLOW * DF * (1000 / 60)	DF obtained from Dilution system calculated parameter listed above.
EEPS_3_ER	Particle emission rates in the range 7.4989 - 8.6596 nanometers	#/sec	**EEPS3_ER** = (EEPS3 - EEPS3_DL) * TC_FLOW * DF * (1000 / 60)	DF obtained from Dilution system calculated parameter listed above.
EEPS_4_ER	Particle emission rates in the range 8.6596 - 10.000 nanometers	#/sec	**EEPS4_ER** = (EEPS4 - EEPS4_DL) * TC_FLOW * DF * (1000 / 60)	DF obtained from Dilution system calculated parameter listed above.
EEPS_5_ER	Particle emission rates in the range 10.000 - 11.5478 nanometers	#/sec	**EEPS5_ER** = (EEPS5 - EEPS5_DL) * TC_FLOW * DF * (1000 / 60)	DF obtained from Dilution system calculated parameter listed above.
EEPS_6_ER	Particle emission rates in the range 11.5478 - 13.3352 nanometers	#/sec	**EEPS6_ER** = (EEPS6 - EEPS6_DL) * TC_FLOW * DF * (1000 / 60)	DF obtained from Dilution system calculated parameter listed above.
EEPS_7_ER	Particle emission rates in the range 13.3352 - 15.3393 nanometers	#/sec	**EEPS7_ER** = (EEPS7 - EEPS7_DL) * TC_FLOW * DF * (1000 / 60)	DF obtained from Dilution system calculated parameter listed above.
EEPS_8_ER	Particle emission rates in the range 15.3393 - 17.7828 nanometers	#/sec	**EEPS8_ER** = (EEPS8 - EEPS8_DL) * TC_FLOW * DF * (1000 / 60)	DF obtained from Dilution system calculated parameter listed above.
EEPS_9_ER	Particle emission rates in the range 17.7828 - 20.5353 nanometers	#/sec	**EEPS9_ER** = (EEPS9 - EEPS9_DL) * TC_FLOW * DF * (1000 / 60)	DF obtained from Dilution system calculated parameter listed above.
EEPS_10_ER	Particle emission rates in the range 20.5353 - 23.7137 nanometers	#/sec	**EEPS10_ER** = (EEPS10 - EEPS10_DL) * TC_FLOW * DF * (1000 / 60)	DF obtained from Dilution system calculated parameter listed above.
EEPS_11_ER	Particle emission rates in the range 23.7137 - 27.3842 nanometers	#/sec	**EEPS11_ER** = (EEPS11 - EEPS11_DL) * TC_FLOW * DF * (1000 / 60)	DF obtained from Dilution system calculated parameter listed above.
EEPS_12_ER	Particle emission rates in the range 27.3842 - 31.6228 nanometers	#/sec	**EEPS12_ER** = (EEPS12 - EEPS12_DL) * TC_FLOW * DF * (1000 / 60)	DF obtained from Dilution system calculated parameter listed above.
EEPS_13_ER	Particle emission rates in the range 31.6228 - 36.5174 nanometers	#/sec	**EEPS13_ER** = (EEPS13 - EEPS13_DL) * TC_FLOW * DF * (1000 / 60)	DF obtained from Dilution system calculated parameter listed above.
EEPS_14_ER	Particle emission rates in the range 36.5174 - 42.1697 nanometers	#/sec	**EEPS14_ER** = (EEPS14 - EEPS14_DL) * TC_FLOW * DF * (1000 / 60)	DF obtained from Dilution system calculated parameter listed above.
EEPS_15_ER	Particle emission rates in the range 42.1697 - 48.6968 nanometers	#/sec	**EEPS15_ER** = (EEPS15 - EEPS15_DL) * TC_FLOW * DF * (1000 / 60)	DF obtained from Dilution system calculated parameter listed above.
EEPS_16_ER	Particle emission rates in the range 48.6968 - 56.2341 nanometers	#/sec	**EEPS16_ER** = (EEPS16 - EEPS16_DL) * TC_FLOW * DF * (1000 / 60)	DF obtained from Dilution system calculated parameter listed above.
EEPS_17_ER	Particle emission rates in the range 56.2341 - 64.9832 nanometers	#/sec	**EEPS17_ER** = (EEPS17 - EEPS17_DL) * TC_FLOW * DF * (1000 / 60)	DF obtained from Dilution system calculated parameter listed above.
EEPS_18_ER	Particle emission rates in the range 64.9832 - 74.9894 nanometers	#/sec	**EEPS18_ER** = (EEPS18 - EEPS18_DL) * TC_FLOW * DF * (1000 / 60)	DF obtained from Dilution system calculated parameter listed above.
EEPS_19_ER	Particle emission rates in the range 74.9894 - 86.5964 nanometers	#/sec	**EEPS19_ER** = (EEPS19 - EEPS19_DL) * TC_FLOW * DF * (1000 / 60)	DF obtained from Dilution system calculated parameter listed above.
EEPS_20_ER	Particle concentration in the range 86.5964 - 100.000 nanometers	#/sec	**EEPS20_ER** = (EEPS20 - EEPS20_DL) * TC_FLOW * DF * (1000 / 60)	DF obtained from Dilution system calculated parameter listed above.
EEPS_21_ER	Particle emission rates in the range 100.000 - 115.478 nanometers	#/sec	**EEPS21_ER** = (EEPS21 - EEPS21_DL) * TC_FLOW * DF * (1000 / 60)	DF obtained from Dilution system calculated parameter listed above.
EEPS_22_ER	Particle emission rates in the range 115.478 - 133.352 nanometers	#/sec	**EEPS22_ER** = (EEPS22 - EEPS22_DL) * TC_FLOW * DF * (1000 / 60)	DF obtained from Dilution system calculated parameter listed above.
EEPS_23_ER	Particle emission rates in the range 133.352 - 153.992 nanometers	#/sec	**EEPS23_ER** = (EEPS23 - EEPS23_DL) * TC_FLOW * DF * (1000 / 60)	DF obtained from Dilution system calculated parameter listed above.
EEPS_24_ER	Particle emission rates in the range 153.992 - 177.827 nanometers	#/sec	**EEPS24_ER** = (EEPS24 - EEPS24_DL) * TC_FLOW * DF * (1000 / 60)	DF obtained from Dilution system calculated parameter listed above.
EEPS_25_ER	Particle emission rates in the range 177.827 - 205.352 nanometers	#/sec	**EEPS25_ER** = (EEPS25 - EEPS25_DL) * TC_FLOW * DF * (1000 / 60)	DF obtained from Dilution system calculated parameter listed above.
EEPS_26_ER	Particle emission rates in the range 205.352 - 237.137 nanometers	#/sec	**EEPS26_ER** = (EEPS26 - EEPS26_DL) * TC_FLOW * DF * (1000 / 60)	DF obtained from Dilution system calculated parameter listed above.
EEPS_27_ER	Particle emission rates in the range 237.137 - 273.842 nanometers	#/sec	**EEPS27_ER** = (EEPS27 - EEPS27_DL) * TC_FLOW * DF * (1000 / 60)	DF obtained from Dilution system calculated parameter listed above.
EEPS_28_ER	Particle emission rates in the range 273.842 - 316.227 nanometers	#/sec	**EEPS28_ER** = (EEPS28 - EEPS28_DL) * TC_FLOW * DF * (1000 / 60)	DF obtained from Dilution system calculated parameter listed above.
EEPS_29_ER	Particle emission rates in the range 316.227 - 365.174 nanometers	#/sec	**EEPS29_ER** = (EEPS29 - EEPS29_DL) * TC_FLOW * DF * (1000 / 60)	DF obtained from Dilution system calculated parameter listed above.
EEPS_30_ER	Particle emission rates in the range 365.174 - 421.696 nanometers	#/sec	**EEPS30_ER** = (EEPS30 - EEPS30_DL) * TC_FLOW * DF * (1000 / 60)	DF obtained from Dilution system calculated parameter listed above.
EEPS_31_ER	Particle emission rates in the range 421.696 - 486.976 nanometers	#/sec	**EEPS31_ER** = (EEPS31 - EEPS31_DL) * TC_FLOW * DF * (1000 / 60)	DF obtained from Dilution system calculated parameter listed above.
EEPS_32_ER	Particle emission rates in the range 486.976 - 562.341 nanometers	#/sec	**EEPS32_ER** = (EEPS32 - EEPS32_DL) * TC_FLOW * DF * (1000 / 60)	DF obtained from Dilution system calculated parameter listed above.
EEPS_TOT_ER	Total particle emission rates from all EEPS channels combined	#/sec	**EEPS_TOT_ER** = (EEPS_TOT - EEPS_TOT_DL) * TC_FLOW * DF * (1000 / 60)	DF obtained from Dilution system calculated parameter listed above.
CPC_TOT_ER	Total particle emission rates from the CPC	#/sec	**CPC_TOT_ER** = (CPC_TOT - CPC_TOT_DL) * TC_FLOW * DF * (1000/60)	DF obtained from Dilution system calculated parameter listed above.

Table A.5. Calculated Parameters Descriptions (p. 4 of 4)

Data Name	Parameter	Unit	Equation	Description
Gas-Phase Emissions Rate				
	FTIR Protocol		$FTIR\_GAS_i = FTIR\_GAS - DL\_GAS_i$ If $FTIR\_GAS_i > 0$, follow equations below, if $FTIR\_GAS_i < 0$ use only (DL_GAS_i) in equation	Where i = RUN_NO Tunnel Blanks
FTIR_TRI124_ER	Emissions Rate for 1,2,4-Trimethylbenzene	µg/sec	**FTIR_TRI124_ER** = (FTIR_TRI124 * MW_TRI124 * TC_FLOW * FTIR_PRESS) [R * (FTIR_TEMP + 273.15) * V_PPM * 60]	Molecular Weight, temperature, and time conversions are numerical; R is the universal gas constant; V_PPM is a volumetric conversion
FTIR_PROP12_ER	Emissions Rate for 1,2-Propadiene	µg/sec	**FTIR_PROP12_ER** = (FTIR_PROP12 * MW_PROP12 * TC_FLOW * FTIR_PRESS) [R * (FTIR_TEMP + 273.15) * V_PPM * 60]	Molecular Weight, temperature, and time conversions are numerical; R is the universal gas constant; V_PPM is a volumetric conversion
FTIR_TRI135_ER	Emissions Rate for 1,3,5-Trimethylbenzene	µg/sec	**FTIR_TRI135_ER** = (FTIR_TRI135 * MW_TRI135 * TC_FLOW * FTIR_PRESS) [R * (FTIR_TEMP + 273.15) * V_PPM * 60]	Molecular Weight, temperature, and time conversions are numerical; R is the universal gas constant; V_PPM is a volumetric conversion
FTIR_BUTA13_ER	Emissions Rate for 1,3-Butadience	µg/sec	**FTIR_BUTA13_ER** = (FTIR_BUTA13 * MW_BUTA13 * TC_FLOW * FTIR_PRESS) [R * (FTIR_TEMP + 273.15) * V_PPM * 60]	Molecular Weight, temperature, and time conversions are numerical; R is the universal gas constant; V_PPM is a volumetric conversion
FTIR_MTHYL2_ER	Emissions Rate for 2-Methylpropene	µg/sec	**FTIR_MTHYL2_ER** = (FTIR_MTHYL2 * MW_MTHYL2 * TC_FLOW * FTIR_PRESS) [R * (FTIR_TEMP + 273.15) * V_PPM * 60]	Molecular Weight, temperature, and time conversions are numerical; R is the universal gas constant; V_PPM is a volumetric conversion
FTIR_ACETAL_ER	Emissions Rate for Acetaldehyde	µg/sec	**FTIR_ACETAL_ER** = (FTIR_ACETAL * MW_ACETAL * TC_FLOW * FTIR_PRESS) [R * (FTIR_TEMP + 273.15) * V_PPM * 60]	Molecular Weight, temperature, and time conversions are numerical; R is the universal gas constant; V_PPM is a volumetric conversion
FTIR_ACETYL_ER	Emissions Rate for Acetylene	µg/sec	**FTIR_ACETYL_ER** = (FTIR_ACETYL * MW_ACETYL * TC_FLOW * FTIR_PRESS) [R * (FTIR_TEMP + 273.15) * V_PPM * 60]	Molecular Weight, temperature, and time conversions are numerical; R is the universal gas constant; V_PPM is a volumetric conversion
FTIR_ACROLE_ER	Emissions Rate for Acrolein	µg/sec	**FTIR_ACROLE_ER** = (FTIR_ACROLE * MW_ACROLE * TC_FLOW * FTIR_PRESS) [R * (FTIR_TEMP + 273.15) * V_PPM * 60]	Molecular Weight, temperature, and time conversions are numerical; R is the universal gas constant; V_PPM is a volumetric conversion
FTIR_BENZ_ER	Emissions Rate for Benzene	µg/sec	**FTIR_BENZ_ER** = (FTIR_BENZ * MW_BENZ * TC_FLOW * FTIR_PRESS) [R * (FTIR_TEMP + 273.15) * V_PPM * 60]	Molecular Weight, temperature, and time conversions are numerical; R is the universal gas constant; V_PPM is a volumetric conversion
FTIR_CH4_ER	Emissions Rate for Methane	µg/sec	**FTIR_CH4_ER** = (FTIR_CH4 * MW_CH4 * TC_FLOW * FTIR_PRESS) [R * (FTIR_TEMP + 273.15) * V_PPM * 60]	Molecular Weight, temperature, and time conversions are numerical; R is the universal gas constant; V_PPM is a volumetric conversion
FTIR_COPPM_ER	Emissions Rate for Carbon Monoxide	µg/sec	**FTIR_COPPM_ER** = (FTIR_COPPM * MW_COPPM * TC_FLOW * FTIR_PRESS) [R * (FTIR_TEMP + 273.15) * V_PPM * 60]	Molecular Weight, temperature, and time conversions are numerical; R is the universal gas constant; V_PPM is a volumetric conversion
FTIR_COPCT_ER	Emissions Rate for Carbon Monoxide (%)	mg/sec	**FTIR_COPCT_ER** = (FTIR_COPCT * MW_COPCT * TC_FLOW * FTIR_PRESS) [R * (FTIR_TEMP + 273.15) * V_PCT * 60]	Molecular Weight, temperature, and time conversions are numerical; R is the universal gas constant; V_PCT is a volumetric conversion
FTIR_CO2PCT_ER	Emissions Rate for Carbon Dioxide (%)	mg/sec	**FTIR_CO2PCT_ER** = (FTIR_CO2PCT * MW_CO2PCT * TC_FLOW * FTIR_PRESS) [R * (FTIR_TEMP + 273.15) * V_PCT * 60]	Molecular Weight, temperature, and time conversions are numerical; R is the universal gas constant; V_PCT is a volumetric conversion
FTIR_ETHANE_ER	Emissions Rate for Ethane	µg/sec	**FTIR_ETHANE_ER** = (FTIR_ETHANE * MW_ETHANE * TC_FLOW * FTIR_PRESS) [R * (FTIR_TEMP + 273.15) * V_PPM * 60]	Molecular Weight, temperature, and time conversions are numerical; R is the universal gas constant; V_PPM is a volumetric conversion
FTIR_ETHANO_ER	Emissions Rate for Ethanol	µg/sec	**FTIR_ETHANO_ER** = (FTIR_ETHANO * MW_ETHANO * TC_FLOW * FTIR_PRESS) [R * (FTIR_TEMP + 273.15) * V_PPM * 60]	Molecular Weight, temperature, and time conversions are numerical; R is the universal gas constant; V_PPM is a volumetric conversion
FTIR_ETHYLE_ER	Emissions Rate for Ethylene	µg/sec	**FTIR_ETHYLE_ER** = (FTIR_ETHYLE * MW_ETHYLE * TC_FLOW * FTIR_PRESS) [R * (FTIR_TEMP + 273.15) * V_PPM * 60]	Molecular Weight, temperature, and time conversions are numerical; R is the universal gas constant; V_PPM is a volumetric conversion
FTIR_FORMAL_ER	Emissions Rate for Formaldehyde	µg/sec	**FTIR_FORMAL_ER** = (FTIR_FORMAL * MW_FORMAL * TC_FLOW * FTIR_PRESS) [R * (FTIR_TEMP + 273.15) * V_PPM * 60]	Molecular Weight, temperature, and time conversions are numerical; R is the universal gas constant; V_PPM is a volumetric conversion
FTIR_H2OPCT_ER	Emissions Rate for H2O (%)	mg/sec	**FTIR_H2OPCT_ER** = (FTIR_H2OPCT * MW_H2OPCT * TC_FLOW * FTIR_PRESS) [R * (FTIR_TEMP + 273.15) * V_PCT * 60]	Molecular Weight, temperature, and time conversions are numerical; R is the universal gas constant; V_PCT is a volumetric conversion
FTIR_ISOOCT_ER	Emissions Rate for IsoOctane	µg/sec	**FTIR_ISOOCT_ER** = (FTIR_ISOOCT * MW_ISOOCT * TC_FLOW * FTIR_PRESS) [R * (FTIR_TEMP + 273.15) * V_PPM * 60]	Molecular Weight, temperature, and time conversions are numerical; R is the universal gas constant; V_PPM is a volumetric conversion
FTIR_MXYLEN_ER	Emissions Rate for m-Xylene	µg/sec	**FTIR_MXYLEN_ER** = (FTIR_MXYLEN * MW_MXYLEN * TC_FLOW * FTIR_PRESS) [R * (FTIR_TEMP + 273.15) * V_PPM * 60]	Molecular Weight, temperature, and time conversions are numerical; R is the universal gas constant; V_PPM is a volumetric conversion
FTIR_MEOH_ER	Emissions Rate for Methanol	µg/sec	**FTIR_MEOH_ER** = (FTIR_MEOH * MW_MEOH * TC_FLOW * FTIR_PRESS) [R * (FTIR_TEMP + 273.15) * V_PPM * 60]	Molecular Weight, temperature, and time conversions are numerical; R is the universal gas constant; V_PPM is a volumetric conversion
FTIR_N2O_ER	Emissions Rate for Nitrous Oxide	µg/sec	**FTIR_N2O_ER** = (FTIR_N2O * MW_N2O * TC_FLOW * FTIR_PRESS) [R * (FTIR_TEMP + 273.15) * V_PPM * 60]	Molecular Weight, temperature, and time conversions are numerical; R is the universal gas constant; V_PPM is a volumetric conversion
FTIR_NH3_ER	Emissions Rate for Ammonia	µg/sec	**FTIR_NH3_ER** = (FTIR_NH3 * MW_NH3 * TC_FLOW * FTIR_PRESS) [R * (FTIR_TEMP + 273.15) * V_PPM * 60]	Molecular Weight, temperature, and time conversions are numerical; R is the universal gas constant; V_PPM is a volumetric conversion
FTIR_NO_ER	Emissions Rate for Nitric Oxide	µg/sec	**FTIR_NO_ER** = (FTIR_NO * MW_NO * TC_FLOW * FTIR_PRESS) [R * (FTIR_TEMP + 273.15) * V_PPM * 60]	Molecular Weight, temperature, and time conversions are numerical; R is the universal gas constant; V_PPM is a volumetric conversion
FTIR_NO2_ER	Emissions Rate for Nitrogen Dioxide	µg/sec	**FTIR_NO2_ER** = (FTIR_NO2 * MW_NO2 * TC_FLOW * FTIR_PRESS) [R * (FTIR_TEMP + 273.15) * V_PPM * 60]	Molecular Weight, temperature, and time conversions are numerical; R is the universal gas constant; V_PPM is a volumetric conversion
FTIR_OCTANE_ER	Emissions Rate for Octane	µg/sec	**FTIR_OCTANE_ER** = (FTIR_OCTANE * MW_OCTANE * TC_FLOW * FTIR_PRESS) [R * (FTIR_TEMP + 273.15) * V_PPM * 60]	Molecular Weight, temperature, and time conversions are numerical; R is the universal gas constant; V_PPM is a volumetric conversion
FTIR_PROPAN_ER	Emissions Rate for Propane	µg/sec	**FTIR_PROPAN_ER** = (FTIR_PROPAN * MW_PROPAN * TC_FLOW * FTIR_PRESS) [R * (FTIR_TEMP + 273.15) * V_PPM * 60]	Molecular Weight, temperature, and time conversions are numerical; R is the universal gas constant; V_PPM is a volumetric conversion
FTIR_PROPYL_ER	Emissions Rate for Propylene	µg/sec	**FTIR_PROPYL_ER** = (FTIR_PROPYL * MW_PROPYL * TC_FLOW * FTIR_PRESS) [R * (FTIR_TEMP + 273.15) * V_PPM * 60]	Molecular Weight, temperature, and time conversions are numerical; R is the universal gas constant; V_PPM is a volumetric conversion
FTIR_PROPYN_ER	Emissions Rate for Propyne	µg/sec	**FTIR_PROPYN_ER** = (FTIR_PROPYN * MW_PROPYN * TC_FLOW * FTIR_PRESS) [R * (FTIR_TEMP + 273.15) * V_PPM * 60]	Molecular Weight, temperature, and time conversions are numerical; R is the universal gas constant; V_PPM is a volumetric conversion
FTIR_SO2_ER	Emissions Rate for Sulfur Dioxide	µg/sec	**FTIR_SO2_ER** = (FTIR_SO2 * MW_SO2 * TC_FLOW * FTIR_PRESS) [R * (FTIR_TEMP + 273.15) * V_PPM * 60]	Molecular Weight, temperature, and time conversions are numerical; R is the universal gas constant; V_PPM is a volumetric conversion
FTIR_TOLUEN_ER	Emissions Rate for Toluene	µg/sec	**FTIR_TOLUEN_ER** = (FTIR_TOLUEN * MW_TOLUEN * TC_FLOW * FTIR_PRESS) [R * (FTIR_TEMP + 273.15) * V_PPM * 60]	Molecular Weight, temperature, and time conversions are numerical; R is the universal gas constant; V_PPM is a volumetric conversion

Appendix B. QA/QC Data

The raw blanks data were plotted by pollutant and run number. Due to the size of the QA/QC data files listed below, those interested in viewing the QA/QC data should contact Dr. Britt A. Holmén at britt.holmen@uvm.edu and request copies of the files listed in Table B.1. Each file contains individual Instrument Blank (IB) and Tunnel Blank (TB) raw data.

Table B.1 Instrument and Tunnel Blank Raw Data Filenames

FtirQaBoxplot_CompareQaPhases.PDF
FtirQaBoxplot_CompareAllRuns.PDF
PnQaTimeSeries_All.PDF
PnQaBoxplotFixed_All.PDF
PnQaBoxplot_All.PDF

The computed instrument detection limits (IDLs) are found in ascii files listed in Table B.2.

Table B.2 Instrument Detection Limit Filenames

FtirDL_AllIB_JUN14_Final.txt
FtirDL_AllTB_JUN14_Final.txt
FtirDL_PreTB_JUN14_Final.txt
CpcDL_AllIB_JUN14_Final.txt
CpcDL_AllTB_JUN14_Final.txt
CpcDL_PreTB_JUN14_Final.txt
EepsDL_AllIB_JUN14_Final.txt
EepsDL_AllTB_JUN14_Final.txt
EepsDL_PreTB_JUN14_Final.txt
FtirDL_AllIB_22SEP12_Final.txt
FtirDL_AllTB_22SEP12_Final.txt
FtirDL_PreTB_22SEP12_Final.txt
CpcDL_AllIB_22SEP12_Final.txt
CpcDL_PreTB_22SEP12_Final.txt
EepsDL_AllIB_22SEP12_Final.txt
EepsDL_AllTB_22SEP12_Final.txt
EepsDL_PreTB_22SEP12_Final.txt
CpcDL_AllTB_22SEP12_Final.txt

Appendix C. Daily Emissions Test Logsheets

Turn-by-turn driving route information is found on the TOTEMS Data Collection Logsheet (**Table C.2**).

Table C.1. Daily Sampling Logsheet

On-Board Emissions Log Sheet

University of Vermont Transportation Research Center Signature Project II

Date: ________ Run No. ________ Driver: ________

Vehicle ID: ________ Personnel: ________

Odometer Reading: ________ ________

Weather: ________ Battery Voltages: ________

Setup and Instrument Blank

Start Time: ________ Tire Pressure: DF ________ PF ________

End Time: ________ DR ________ PR ________

Pre-Run Tunnel Blank

Start Time: ________ *End Time:* ________

Sampling Run

Road Conditions: ________

Notes: ________

Pre-Run Gas Station Check

Gallons Added: ________ Odometer Reading: ________

Post-Run Gas Station Check

Gallons Added: ________ Odometer Reading: ________

Post-Run Tunnel Blank

Start Time: ________ *End Time:* ________

Post-Run Instrument Blank

Start Time: ________ Tire Pressure: DF ________ PF ________

End Time: ________ DR ________ PR ________

Notes: ________

____

____

____

Table C.2. Passenger Notes Logsheet by Route Turn Sequence

Signature Project 2 -- TOTEMS Data Collection RUN: __________ Date: ____________
Initials: ____________

Time	Direction	Facility Name	Notes
	--	ENGINE ON	*Start Phase 3
	L	Colchester Avenue	
	R	North Prospect Street	
	R	Riverside Avenue	
	R	Cumberland Farms Gulf Station	
	R	Riverside Avenue	
	R	Colchester Avenue	
	--	START OF RUN AT VOTEY HALL	*Start Phase 4
	R	Mansfield Avenue	
	L	Mansfield Avenue	
	C	North Street	
	R	North Willard Street	
	L	Archibald Street	
	L	Intervale Avenue	
	L	North Street	
	R	North Winooski Avenue	
	R	Pearl Street	
	R	Elmwood Avenue	
	L	Allen Street	
	R	Murray Street	
	L	North Street	
	L	Park Street	
	C	Battery Street	
	L	King Street	
	R	South Champlain Street	
	L	Maple Street	
	L	South Prospect Street	
	R	Main Street / US-2 E	
	R	I-89 South	
	R	Exit 11 for US-2	
	C	Richmond Park and Ride (entrance	*Start Phase 5
	L	West Main Street / US-2 E	*End Phase 5
	R	Bridge Street	
	R	Huntington Road	
	R	Hinesburg Road	
	C	East Hill Road	
	R	South Road	
	R	Oak Hill Road	
	L	US-2 / Williston Road	
	R	Patchen Road	
	C	Grove Street	
	L	Chase Street	
	C	Barrett Street	
	L	Colchester Avenue	
	--	END OF RUN AT VOTEY HALL	*End Phase 6
	--	ENGINE OFF	*End Phase 7

Appendix D. Tailpipe Flow Rate and Pitot Tube Apparatus

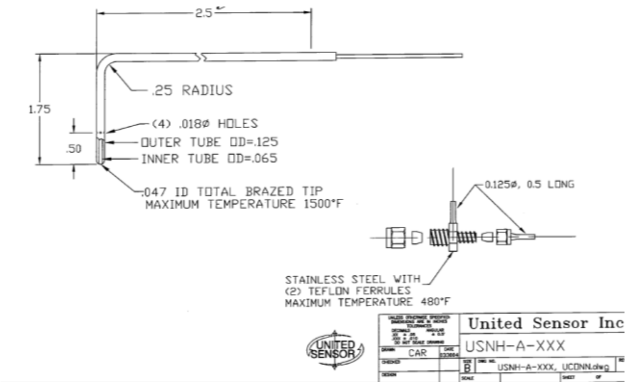

Figure D.1 Pitot tube schematic.

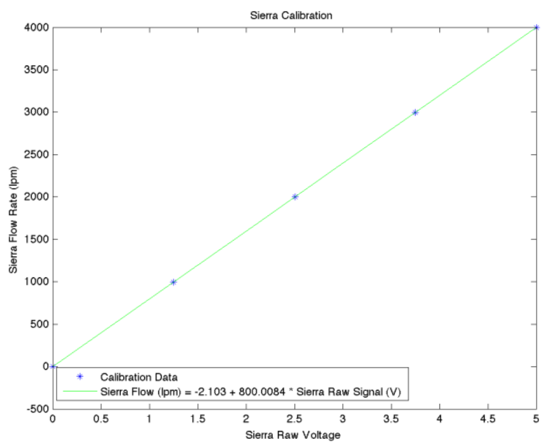

Figure D.2 Sierra Flowmeter Reference Calibration

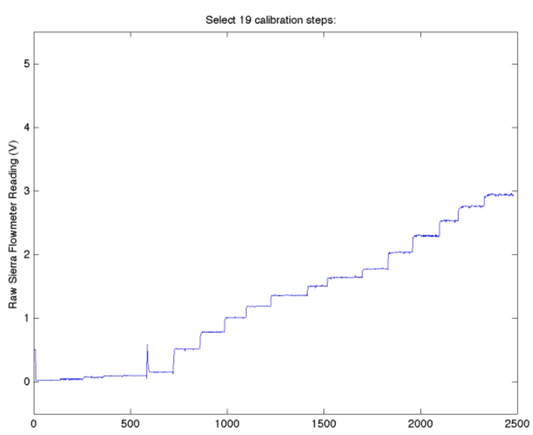

Figure D.3 Pitot calibration data from March 5, 2010.

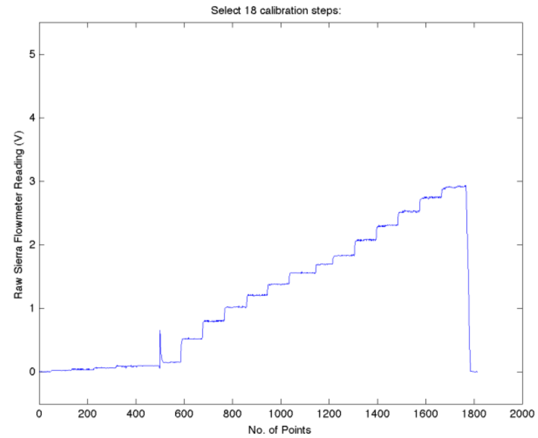

Figure D.4 Pitot calibration data from July 28, 2010.

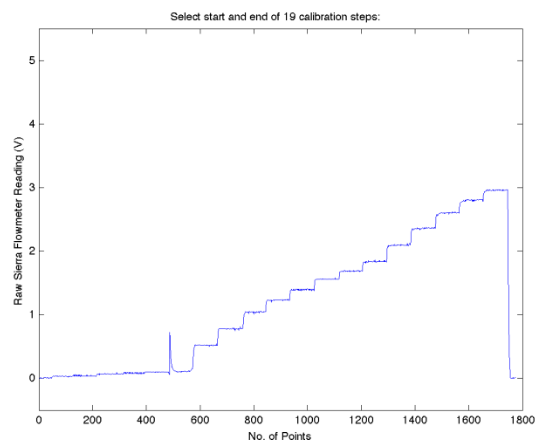

Figure D.5 Pitot calibration data from July 30, 2010.

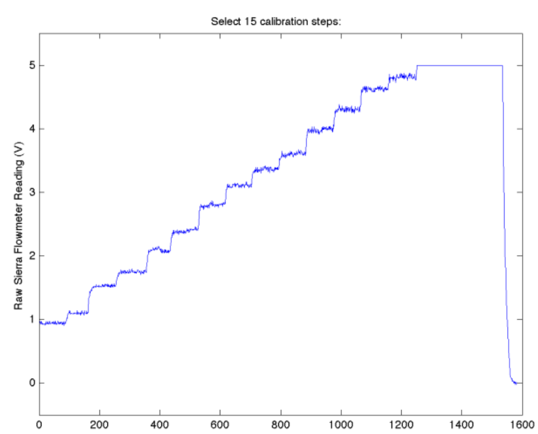

Figure D.6 Pitot calibration data from August 9, 2010.

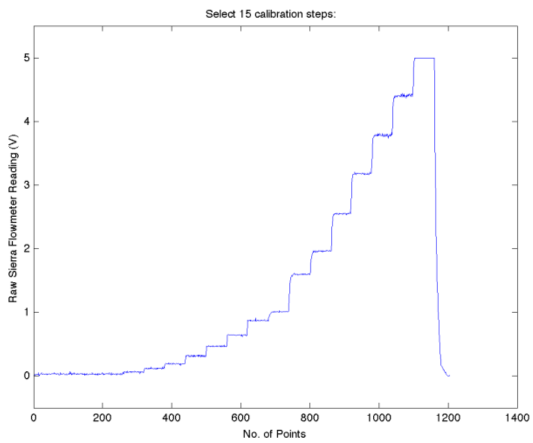

Figure D.7 Pitot calibration data from September 13, 2010.

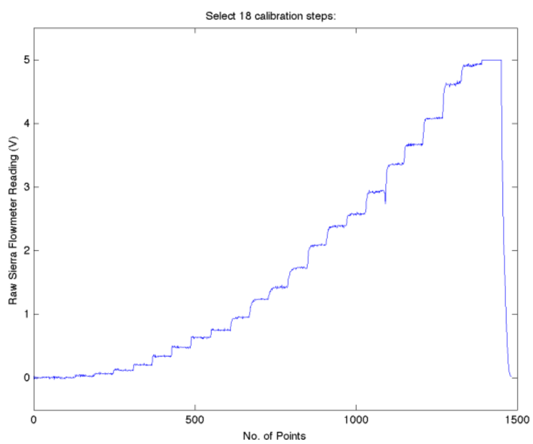

Figure D.8 Pitot calibration data from November 19, 2010.

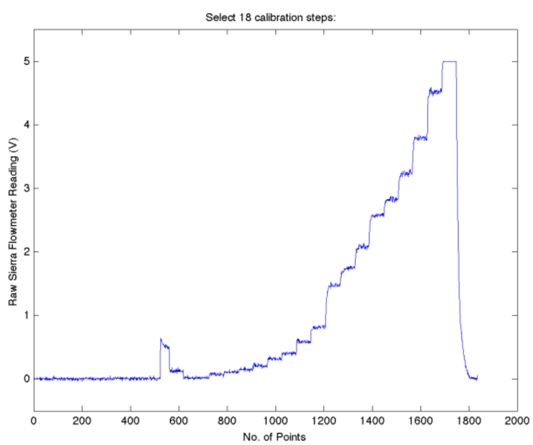

Figure D.9 Pitot calibration data from April 21, 2011.

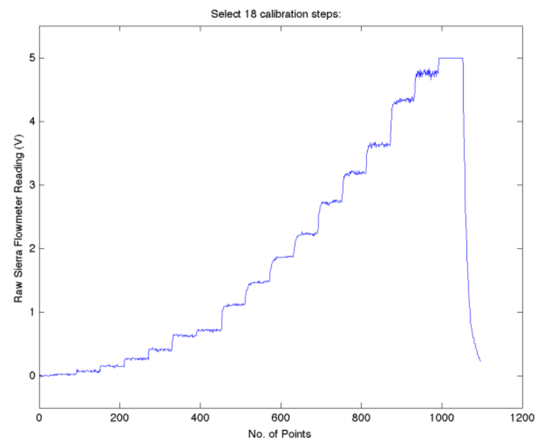

Figure D.10 Pitot calibration data from August 2, 2011.

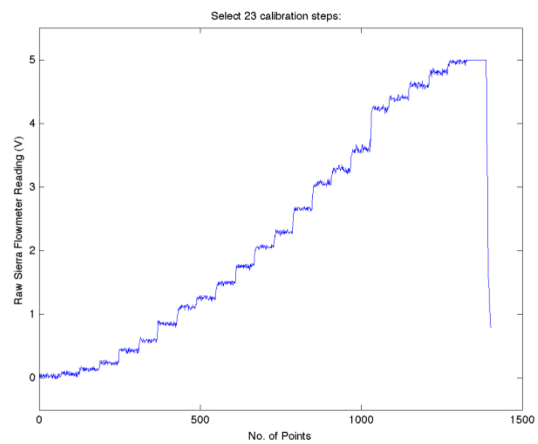

Figure D.11 Pitot calibration data from September 13, 2011.

Fit Y by X Group

Bivariate Fit of Q (lpm) By DiffP1 (Remove Max)

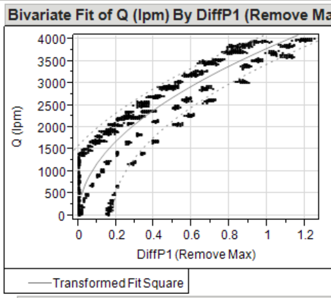

Transformed Fit Square

Square(Q (lpm)) = 0 + 14499240*DiffP1 (Remove Max)

Summary of Fit

RSquare	.
RSquare Adj	.
Root Mean Square Error	1314611
Mean of Response	3018622
Observations (or Sum Wgts)	8712

Analysis of Variance

Source	DF	Sum of Squares	Mean Square	F Ratio
Model	1	2.0625e+17	2.062e+17	119341.6
Error	8711	1.5054e+16	1.728e+12	Prob > F
C. Total	8712	2.213e+17		<.0001*

Tested against reduced model: Y=0

Parameter Estimates

Term		Estimate	Std Error	t Ratio	Prob>|t|
Intercept	Constrained	0	0	.	.
DiffP1 (Remove Max)		14499240	41970.99	345.46	<.0001*

Fit Measured on Original Scale

Sum of Squared Error	3.4095e+9
Root Mean Square Error	625.65721
RSquare	0.6952881
Sum of Residuals	1867716.3

Bivariate Fit of Q (lpm) By DiffP2 (Remove Max)

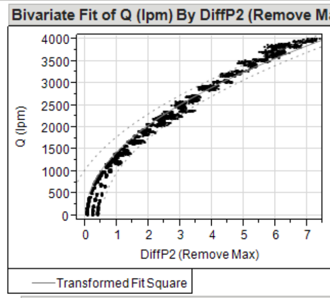

Transformed Fit Square

Square(Q (lpm)) = 0 + 2129720.5*DiffP2 (Remove Max)

Summary of Fit

RSquare	.
RSquare Adj	.
Root Mean Square Error	575329.3
Mean of Response	3018622
Observations (or Sum Wgts)	8712

Analysis of Variance

Source	DF	Sum of Squares	Mean Square	F Ratio
Model	1	2.1842e+17	2.184e+17	659864.0
Error	8711	2.8834e+15	3.31e+11	Prob > F
C. Total	8712	2.213e+17		<.0001*

Tested against reduced model: Y=0

Parameter Estimates

Term		Estimate	Std Error	t Ratio	Prob>|t|
Intercept	Constrained	0	0	.	.
DiffP2 (Remove Max)		2129720.5	2621.775	812.32	<.0001*

Fit Measured on Original Scale

Sum of Squared Error	659579814
Root Mean Square Error	275.1849
RSquare	0.9410525
Sum of Residuals	-1636018

Bivariate Fit of Q (lpm) By DiffP3 (Remove Max)

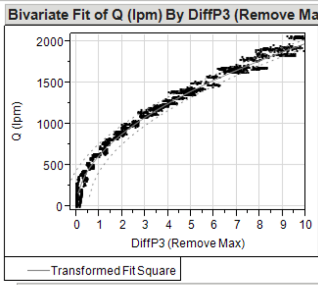

Transformed Fit Square

Square(Q (lpm)) = 0 + 394516.8*DiffP3 (Remove Max)

Summary of Fit

RSquare	.
RSquare Adj	.
Root Mean Square Error	103482.2
Mean of Response	887977.4
Observations (or Sum Wgts)	6237

Analysis of Variance

Source	DF	Sum of Squares	Mean Square	F Ratio
Model	1	1.2093e+16	1.209e+16	1129266
Error	6236	6.6779e+13	1.071e+10	Prob > F
C. Total	6237	1.216e+16		<.0001*

Tested against reduced model: Y=0

Parameter Estimates

Term		Estimate	Std Error	t Ratio	Prob>|t|
Intercept	Constrained	0	0	.	.
DiffP3 (Remove Max)		394516.8	371.2507	1062.7	<.0001*

Fit Measured on Original Scale

Sum of Squared Error	38676665
Root Mean Square Error	78.760104
RSquare	0.9833223
Sum of Residuals	144756.28

Bivariate Fit of Q (lpm) By DiffP4 (Remove Baseline)

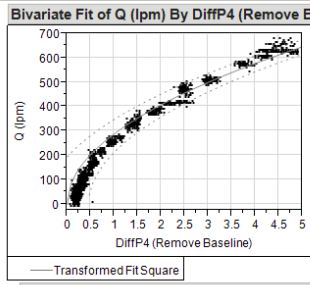

Transformed Fit Square

Square(Q (lpm)) = 0 + 83609.257*DiffP4 (Remove Baseline)

Summary of Fit

RSquare	.
RSquare Adj	.
Root Mean Square Error	19309.8
Mean of Response	81626.58
Observations (or Sum Wgts)	3268

Analysis of Variance

Source	DF	Sum of Squares	Mean Square	F Ratio
Model	1	6.8001e+13	6.8e+13	182372.2
Error	3267	1.2182e+12	372868312	Prob > F
C. Total	3268	6.9219e+13		<.0001*

Tested against reduced model: Y=0

Parameter Estimates

Term		Estimate	Std Error	t Ratio	Prob>|t|
Intercept	Constrained	0	0	.	.
DiffP4 (Remove Baseline)		83609.257	195.783	427.05	<.0001*

Fit Measured on Original Scale

Sum of Squared Error	16714335
Root Mean Square Error	71.537945
RSquare	0.8696638
Sum of Residuals	-182425.5

Figure D.12 Evaluation and development of global pitot tube calibration equations.

Test Set: Bivariate Fit of Chosen Flow By SCN_RPM

Polynomial Fit Degree=2
ChosenFlow = -219.2309 + 0.7634308*SCN_RPM + 0.0003573*(SCN_RPM-947.284)^2

Summary of Fit	
RSquare	0.945194
RSquare Adj	0.94519
Root Mean Square Error	214.003
Mean of Response	795.6862
Observations (or Sum Wgts)	25130

Analysis of Variance

Source	DF	Sum of Squares	Mean Square	F Ratio
Model	2	1.98E+10	9.92E+09	216672
Error	25127	1150748749	45797.3	**Prob > F**
C. Total	25129	2.10E+10		<.0001*

Parameter Estimates

Term	Estimate	Std Error	t Ratio	Prob>|t|
Intercept	-219.2309	2.051849	-106.8	<.0001*
SCN_RPM	0.7634308	0.00166	459.92	<.0001*
(SCN_RPM-947.284)^2	0.0003573	1.60E-06	223.41	<.0001*

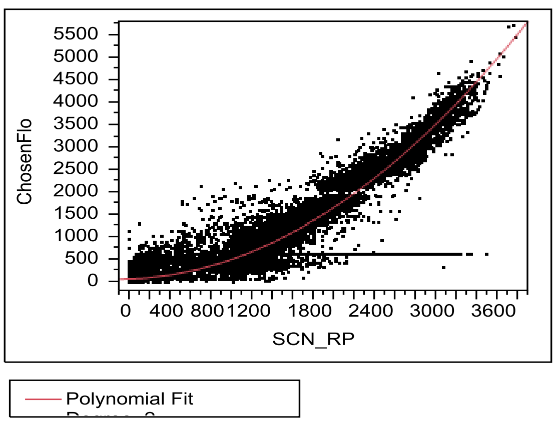

Figure D.13 Estimated chosen flow calculation to estimate tailpipe flow rate when not available from pitot tube and differential pressure transducers, according to engine speed (RPM).

Appendix E. MKS Inc. Multigas FTIR Instrumentation Details

In FTIR, an infrared source produces radiation directed into an interferometer, where the beam is split, reflected, and recombined. Splitting the beam allows approximately half of the signal to be reflected on a fixed mirror and half on a moving mirror. The position of the moving mirror is known precisely, and as it translates produces a signal that has a varying phase pattern. The signal reflected on the moving mirror is then recombined with the signal reflected from the fixed mirror, producing a modulated signal with peaks and troughs altered based on the interference of the two beams. In-phase signals constructively interfere, increasing the magnitude of peaks and troughs, whereas out-of-phase signals destructively interfere, canceling the recombined signals out. The interferometer produces a modulated signal ranging from completely constructive to completely destructive interferences between the two signals, referred to as an interferogram. It is this signal that is passed through a gas sample. A detector captures the resulting range of infrared frequencies simultaneously. The signal reaching the detector is encoded with the absorption of compounds in the sample across the wide range of frequencies in the modulated signal. The Fourier transform is used to decode the summation of signals, which contains all of the intensity information across the wavenumber range of interest. The transform produces a single beam spectrum, indicating transmittance across the wavenumber region.

Details of MKS MultiGas 2030 High-Speed Gas Analyzer (FTIR)

The FTIR used in this study was the MKS MultiGas 2030 HS unit, with specifications according to **Table E.1**. **Figure E.1** is a photograph of the internal components of the MKS MultiGas interferometer to highlight critical components of the unit. The silicon carbide source of radiation was housed next to **A**, maintaining a temperature of 1200 °C. Infrared radiation traveled along the line from **A** to **B**, the beamsplitter, where fifty percent transmitted along the path towards the static mirror, **C**, and the other portion reflected towards the moving mirror, **D**. The two paths recombined, at **E**, forming the modulated signal, and followed the path out of the interferometer housing towards the optics housing. The He-Ne laser source, **F (Figure 3.1)**, followed a path around the outside of the interferometer housing before following a path similar to the infrared radiation path. The wavelength of the He-Ne laser in the MKS unit is known precisely at 15798.2 cm^{-1} and the broad wavelength range for the infrared radiation is measured in reference to this signal.

Table E.1 Specifications of the MultiGas 2030 HS

Specification	Description
Infrared Source	Silicon Carbide @ 1200°C
Detector	Mercury Cadmium Telluride (Liquid Nitrogen Cooled)
Windows	Potassium Bromide
Path-Length	5.11 meters
Spectral Resolution	0.5 cm^{-1}
Scanning Rate	5 scans per second
Reference Laser	Helium Neon
Sample Temperature	191°C
Sample Handling	Particulate Filters on Inlet (2.0 μm and 0.1 μm pore-size)
Sample Flow Rate	12 liters per minute

Inside the optics housing, the modulated signal was reflected up and through the first KBr window of the sample cell, occurring behind the liquid nitrogen dewar, **F**. The modulated signal passed into the 200 mL volume gas sample cell through potassium bromide (KBr) windows and reflected between gold-plated mirrors to achieve a 5.11-meter path length. The gas cell contained the complex sample delivered from the tailpipe and maintained at 191°C through the heated inlet and gas cell components of the instrument, as the gas calibrations are specific to standards measured at 191°C. The resulting partially absorbed, modulated signal was directed down towards the detector, **G**, indicated by the flow path. The mercury cadmium telluride (MCT) detector was cooled by liquid nitrogen stored in the dewar, **F**, at a temperature of 77 K. A wavenumber resolution of 0.5 cm^{-1} was selected to scan the infrared spectra at a rate of approximately 5 scans per second, with the average of each second recorded to an individual spectral file.

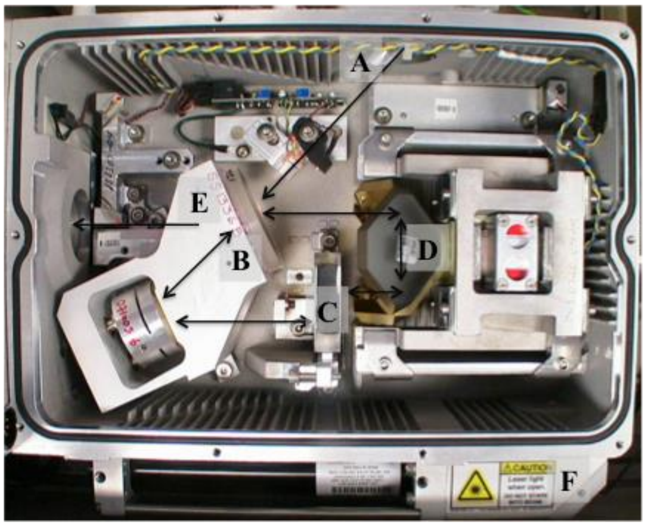

Figure E.1 Internal components of the MKS MultiGas Michelson interferometer. See text for identification of components labeled A-F.

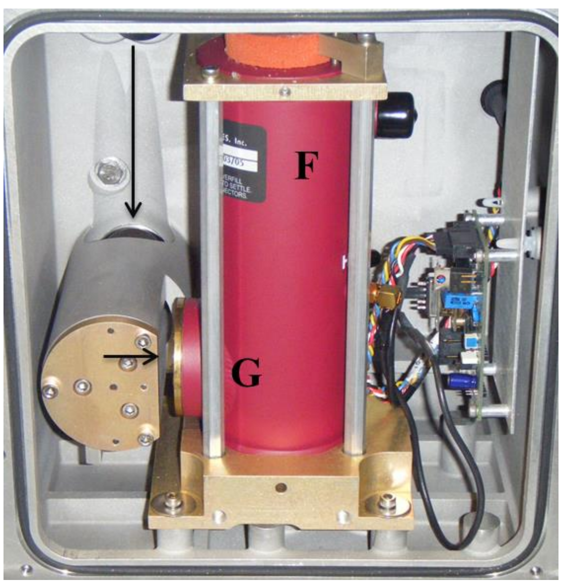

Figure E.2 Optics housing of MKS MultiGas instrument showing the detector (G) and liquid nitrogen dewar (F).

FTIR Emissions Check with Certified Emissions Mix from AirGas
A certified emissions mix was used periodically to check that the instrument was functioning properly. On average the quantification of the emissions mix contents was no more than 5% different than the certification.

Table E.2. FTIR Emissions Mix Check

Emissions Mix Assays	Carbon Monoxide (%)		Carbon Dioxide (%)		Nitic Oxide (ppm)		Propane (ppm)	
Mar-10	7.48	± 0.26	11.86	± 0.18	3195.17	± 40.38	3213.16	± 29.22
Mar-10	7.92	± 0.15	12.12	± 0.09	3172.39	± 16.69	3186.68	± 20.07
Jun-10	7.77	± 0.33	12.01	± 0.21	3142.17	± 62.42	3180.17	± 40.42
Oct-10	7.85	± 0.04	12.04	± 0.03	3159.75	± 9.02	3219.68	± 21.29
Sep-11	7.66	± 0.17	11.96	± 0.12	3225.27	± 20.59	3264.58	± 25.17
Target Certification (±Error Margin)	8.04	± 2%	12.22	± 2%	3030	± 2%	3230	± 2%
Average % Difference	-4%		-2%		5%		-1%	

In addition to checking the certified mix quantification, daily pre- and post-sampling checks of the FTIR against specifications were conducted for proper alignment, full width half height water trace, phase angle, laser frequency, signal to noise ratios, etc.

Table E.3 Mean Percentage of Non-Detects Across Sampling Runs for the Gas-Phase Emissions (with Standard Deviations)

		Outbound		Inbound	
Group	Compound	Mean	Std Dev	Mean	Std Dev
GHGs	Methane	80.5%	26.9%	80.9%	27.2%
	Carbon Dioxide	15.8%	19.6%	15.7%	16.7%
	Nitrous Oxide	81.8%	27.0%	81.5%	27.3%
NAAQs	Carbon Monoxide	50.0%	26.3%	63.1%	28.3%
	Nitric Oxide	78.2%	25.9%	71.4%	24.5%
	Nitrogen Dioxide	62.7%	24.6%	68.9%	25.6%
	Sulfur Dioxide	71.0%	24.1%	78.6%	26.7%
MSATs	Formaldehyde	82.0%	27.1%	81.4%	27.2%
	Acetaldehyde	81.7%	27.0%	81.0%	27.2%
	Acrolein	81.7%	27.0%	81.0%	27.1%
	1,3-Butadiene	81.9%	27.1%	81.6%	27.3%
	Benzene	81.8%	27.0%	81.1%	27.2%
Misc	Ammonia	24.8%	31.7%	44.7%	30.9%
	Water	13.2%	22.1%	16.6%	18.8%
Alcohols	Methanol	82.1%	27.1%	81.7%	27.3%
	Ethanol	82.1%	27.1%	81.7%	27.3%
Alkanes	Ethane	82.0%	27.1%	81.3%	27.2%
	Propane	82.0%	27.1%	81.5%	27.3%
	Octane	82.1%	27.1%	81.6%	27.3%
	IsoOctane	82.0%	27.1%	81.5%	27.3%
Alkenes	Ethylene	65.3%	28.1%	73.2%	27.8%
	Propylene	82.2%	27.1%	81.7%	27.3%
	2-Methylpropene	82.1%	27.1%	81.7%	27.3%
Alkynes	Acetylene	80.7%	26.9%	80.2%	27.0%
	Propyne	81.4%	26.9%	80.7%	27.1%
Dienes	1,2-Propadiene	82.2%	27.1%	81.7%	27.3%
Aromatics	Toluene	81.3%	26.9%	80.7%	27.1%
	m-Xylene	82.2%	27.1%	81.7%	27.3%
	1,2,4-Trimethylbenzene	82.1%	27.1%	81.7%	27.3%
	1,3,5-Trimethylbenzene	82.1%	27.1%	81.7%	27.3%

Table E.4 Pre- and Post-Sampling Specification Checks for the FTIR

	Pre-Run Specification Checks								Post-Run Specification Checks							
Run #	Phase Angle	Igram Max	Igram Min	DC Level	Phi A pp(V)	Calc. Laser Freq.	FWHH	Freq.	Phase Angle	Igram Max	Igram Min	DC Level	Phi A pp(V)	Calc. Laser Freq.	FWHH	Freq.
5	86.82	5.17	-0.85	3.15		15798.27	0.477	3920.09	87.53	5.18	-0.8	3.15		15798.28	0.4826	3920.09
6	86.82	5.23	-0.79	3.2		15798.28	0.4857	3920.09	87.53	5.19	-0.74	3.17		15798.28	0.4797	3920.09
7	87.53	5.23	-0.78	3.21		15798.29	0.4779	3920.09	87.53	5.16	-0.67	3.15		15798.26	0.479	3920.09
8	86.82	5.17	-0.4	3.2		15798.29	0.4721	3920.09	88.24	5.14	-0.26	3.19		15798.26	0.4806	3920.09
9		5.13	-0.28	3.19		15798.29	0.4781	3920.09		5.14	-0.43	3.17		15798.28	0.4807	3920.09
10	88.24	5.08	-0.81	3.07		15798.28	0.4776	3920.09	88.94	5.08	-0.85	3.05		15798.29	0.4805	3920.09
11	88.24	5.17	-0.8	3.15		15798.28	0.4801	3920.09	88.24	5.14	-0.86	3.12		15798.29	0.4833	3920.09
12	89.65	4.98	-0.82	3.03		15798.29	0.4758	3920.09	88.94	5.39	-0.68	3.35		15798.29	0.4809	3920.09
13	89.65	4.9	-0.52	3.06		15798.3	0.4771	3920.09	89.65	4.98	-0.41	3.04		15798.29	0.4754	3920.09
14	89.65	4.99	-0.37	3.05		15798.28	0.4786	3920.09	90.35	5	-0.57	3.03		15798.29	0.476	3920.09
15	89.65	4.98	-0.27	3.07		15798.28	0.4777	3920.09	89.65	5	-0.58	3.03		15798.26	0.4775	3920.09
16	90.35	4.93	-0.32	3.03		15798.28	0.4774	3920.09	90.35	4.95	-0.52	3		15798.33	0.4798	3920.09
17	90.35	4.96	-0.45	3.02		15798.28	0.4755	3920.09	90.35	4.93	-0.38	3.01		15798.27	0.4777	3920.09
18	91.06	5.04	-0.42	3.1		15798.28	0.4759	3920.09	91.06	5.03	-0.53	3.08		15798.28	0.4785	3920.09
19	100.94	5.16	-0.34	3.24	3.92	15798.18	0.4814	3920.09						15798.28	0.4881	3920.09
20	98.12	5.28	-0.15	3.35		15798.18	0.4829	3920.09	103.06	5.19	-0.19	3.29		15798.31	0.4883	3920.09
21	100.24	5.33	-0.4	3.36		15798.24	0.4832	3920.09						15798.24	0.4835	3920.09
22	100.94	5.18	-0.27	3.35		15798.19	0.4824	3920.09	101.65	5.04	-0.43	3.21		15798.35	0.4771	3920.09
23	98.12	5.18	-0.14	3.28		15798.3	0.4823	3920.09	100.94	5.06	-0.5	3.17		15798.32	0.4872	3920.09
24	98.12	5.16	-0.18	3.3		15798.26	0.4864	3920.09	100.24	5.04	-0.01	3.22		15798.33	0.4815	3920.09
25	98.12	5.25	-0.05	3.34		15798.34	0.4786	3920.09	101.65	5.03	-0.51	3.16		15798.3	0.4891	3920.09
26	100.94	5.15	-0.15	3.27		15798.2	0.4877	3920.09	104.47	4.95	-0.57	3.09		15798.3	0.4701	3920.09
27	97.41	5.17	-0.17	3.3		15798.2	0.4833	3920.09	100.94	5.05	-0.6	3.14		15798.32	0.4835	3920.09
28																
29																
30																
31																
32																
33																
34	93.88	5.62	-0.09	3.41	7.8	15798.14	0.4812	3920.09		5.55	-0.31	3.32	7.69	15798.25	0.4717	3920.09
35	93.18	5.33	-0.16	3.22	7.92	15798.08	0.4831	3920.09	94.59	5.67	-0.04	3.45	7.92	15798.26	0.4807	3920.09
36	92.47	5.66	-0.03	3.46	8.08	15798.1	0.4957	3920.1	95.29	5.7	-0.22	3.45	7.84	15798.26	0.4813	3920.09
37	93.88	5.74	-0.02	3.52	8.04	15798.18	0.4816	3920.09	93.18	5.59	0.22	3.41	7.96	15798.26	0.4811	3920.09
38	91.06	5.39	0.6	3.43	7.57	15798.04	0.487	3920.09	95.29	5.5	0.02	3.41	8.27	15798.29	0.4809	3920.09
39	92.47	5.52	0.12	3.47	8.35	15798.06	0.4894	3920.09	93.17	5.45	-0.02	3.35	8.43	15798.23	0.4808	3920.09
40	92.47	5.53	0.08	3.46	8.43	15798.18	0.4775	3920.09	94.59	5.49	-0.35	3.26	8.28	15798.26	0.4769	3920.09
41	92.47	5.49	0.16	3.46	8.39	15798.15	0.4809	3920.09	93.88	5.68	-0.01	3.45	8.35	15798.28	0.4841	3920.09
42	92.47	5.47	0.18	3.41	8.47	15798.14	0.4822	3920.09	93.88	5.41	-0.17	3.24	8.47	15798.26	0.4729	3920.09
43	93.88	5.59	-0.05	3.44	8.47	15798.14	0.4825	3920.09	93.88	5.37	0.12	3.26	8.43	15798.26	0.4809	3920.09
44	93.18	5.48	0.36	3.44	8.04	15798.11	0.4857	3920.09	92.47	5.24	0.42	3.23	8	15798.26	0.4751	3920.09
45	91.06	5.27	1.12	3.39	7.18	15797.99	0.489	3920.09	93.18	5.17	0.57	3.24	7.57	15798.3	0.4714	3920.09
46	91.06	5.31	0.95	3.42	7.49	15798.24	0.4815	3920.09	93.88	5.35	0.28	3.36	8	15798.29	0.479	3920.09
47	92.47	5.41	0.95	3.49	7.45	15798.19	0.4804	3920.09	94.59	5.39	0.06	3.32	8.28	15798.28	0.4804	3920.09
48	92.47	5.5	0.28	3.47	8	15798.1	0.4822	3920.09	93.88	5.39	0.06	3.34	7.8	15798.27	0.4802	3920.09
49	92.47	5.56	-0.09	3.4	8.2	15798.19	0.4813	3920.09	95.29	5.44	0.06	3.35	8.16	15798.21	0.477	3920.09
50	93.88	5.6	-0.09	3.42	8.16	15798.19	0.4827	3920.09	96	5.61	-0.28	3.39	7.96	15798.22	0.4852	3920.09
51	93.88	5.61	-0.06	3.4	8.16	15798.16	0.4812	3920.09	94.59	5.52	-0.32	3.3	8	15798.24	0.4835	3920.09
52	93.88	5.48	0.47	3.42	7.56	15798.21	0.477	3920.09	93.88	5.53	-0.1	3.36	8.08	15798.25	0.4805	3920.09
53	93.18	5.47	0.57	3.4	7.45	15798.21	0.4781	3920.09	93.88	5.49	-0.08	3.37	8.12	15798.26	0.4786	3920.09
54	93.88	5.41	-0.09	3.31	7.88	15798.21	0.4819	3920.09	96	5.45	-0.23	3.24	7.92	15798.28	0.4804	3920.09
55	93.88	5.27	-0.05	3.18	7.7	15798.12	0.4884	3920.09	95.29	5.38	-0.37	3.16	7.73	15798.26	0.4823	3920.09
56	95.29	5.49	-0.2	3.33	7.88	15798.15	0.4847	3920.09	94.59	5.1	0.34	3.18	7.65	15798.28	0.4862	3920.09
57	93.88	5.37	-0.08	3.2	7.45	15798.2	0.4817	3920.09	95.29	5.26	-0.4	3.07	7.61	15798.28	0.4729	3920.09
58	93.88	5.47	-0.09	3.37	7.57	15798.17	0.4789	3920.09	96	5.23	0.22	3.24	7.33	15798.28	0.479	3920.09
59	94.59	5.47	0.25	3.33	7.41	15798.11	0.4868	3920.09	96	5.2	29	3.24	7.33	15798.29	0.4829	3920.09
60	93.18	5.55	0.23	3.4	7.61	15798.15	0.4862	3920.09	96	5.17	0.17	3.22	7.65	15798.28	0.4773	3920.09
61	93.88	5.3	0.07	3.2	7.53	15798.12	0.4885	3920.09	95.29	5.08	0.24	3.15	7.25	15798.27	0.4879	3920.09
62	94.58	5.54	-0.01	3.35	7.29	15798.16	0.4822	3920.09	96	5.16	0.31	3.25	7.96	15798.29	0.4788	3920.09
63	93.88	5.44	0.23	3.32	7.53	15798.19	0.4752	3920.09	96	5.07	0.18	3.16	7.41	15798.3	0.4822	3920.09
64	94.59	5.34	0.15	3.26	7.65	15798.18	0.4832	3920.09	96	5.08	0.24	3.16	7.41	15798.29	0.4861	3920.09
65	94.59	5.51	0.25	3.36	7.45	15798.19	0.4803	3920.09	96.71	5.07	0.29	3.15	7.02	15798.28	0.4789	3920.09
66	94.59	5.45	-0.02	3.28	7.33	15798.18	0.4776	3920.09	96.71	5.04	0.25	3.14	7.18	15798.34	0.4809	3920.09
67	95.29	5.51	0.01	3.33	7.29	15798.24	0.4798	3920.09	96	5.03	0.33	3.15	7.25	15798.3	0.4794	3920.09
68	93.18	5.32	0	3.28	7.57	15798.22	0.484	3920.09	96.71	5.16	0.32	3.23	6.9	15798.26	0.4773	3920.09
69	93.88	5.39	-0.21	3.23	7.25	15798.22	0.4733	3920.09	94.59	5.07	0.46	3.19	6.98	15798.26	0.48	3920.09
70	93.18	5.39	-0.25	3.22	7.14	15798.21	0.4781	3920.09	96	5.1	0.21	3.18	7.29	15798.3	0.4782	3920.09
71	93.18	5.48	-0.05	3.3	7.14	15798.17	0.488	3920.09	96	5.12	0.34	3.23	7.29	15798.29	0.4813	3920.09
72	94.59	5.52	-0.12	3.34	7.1	15798.18	0.4738	3920.09	96	5.1	0.16	3.17	6.86	15798.28	0.4848	3920.09
73	93.18	5.53	0.01	3.34	7.22	15798.19	0.4729	3920.09	96	5.12	0.23	3.21	7.06	15798.27	0.4819	3920.09
74	93.88	5.55	0.17	3.39	7.18	15798.13	0.4789	3920.09	96	5.08	0.28	3.2	6.98	15798.3	0.4807	3920.09
75	94.59	5.4	-0.2	3.22	7.02	15798.18	0.4806	3920.09	96	4.98	0.15	3.08	7.29	15798.24	0.4861	3920.09
76	93.18	5.44	-0.13	3.27	7.14	15798.18	0.4823	3920.09	95.29	5.07	0.32	3.18	6.98	15798.27	0.4786	3920.09
77	93.18	5.36	-0.22	3.22	7.1	15798.2	0.4849	3920.09	95.29	5.05	0.27	3.17	7.33	15798.26	0.4863	3920.09
78	93.88	5.5	-0.13	3.32	6.98	15798.21	0.4809	3920.09	95.29	5.06	0.32	3.18	7.14	15798.31	0.4835	3920.09
79	93.18	5.29	-0.09	3.24	6.94	15798.15	0.4865	3920.09	96.71	5.02	0.2	3.13	7.02	15798.28	0.4865	3920.09

Appendix F. EEPS Instrument Details

Table F.1 EEPS Channel Diameters Middle of Each Bin (D_p), Lower Bound (D_{pL}) and Upper Bound (D_{pU})

D_p (nm)	D_{pL} (nm)	D_{pU} (nm)
6.04	5.6234	6.4938
6.98	6.4938	7.4989
8.06	7.4989	8.6596
9.31	8.6596	10
10.75	10	11.5478
12.41	11.5478	13.3352
14.33	13.3352	15.3993
16.55	15.3993	17.7828
19.11	17.7828	20.5353
22.07	20.5353	23.7137
25.48	23.7137	27.3842
29.43	27.3842	31.6228
33.98	31.6228	36.5174
39.24	36.5174	42.1697
45.32	42.1697	48.6968
52.33	48.6968	56.2341
60.43	56.2341	64.9382
69.78	64.9382	74.9894
80.58	74.9894	86.5964
93.06	86.5964	100
107.46	100	115.4782
124.09	115.4782	133.3521
143.3	133.3521	153.9927
165.48	153.9927	177.8279
191.1	177.8279	205.3525
220.67	205.3525	237.1374
254.83	237.1374	273.842
294.27	273.842	316.2278
339.82	316.2278	365.1741
392.42	365.1741	421.6965
453.16	421.6965	486.9675
523.3	486.9675	562.3413

Table F.2 Mean Percentage of Non-Detects Across Sampling Runs for the Particle Instruments: EEPS Channels, EEPS Total and CPC Total (with Standard Deviations)

Dp (nm)	Channel No.	Outbound Mean	Outbound Std Dev	Inbound Mean	Inbound Std Dev
6.04	1	59.4%	25.8%	46.7%	27.0%
6.98	2	86.9%	17.0%	78.4%	21.6%
8.06	3	87.5%	15.4%	82.2%	16.6%
9.31	4	79.2%	14.6%	72.9%	12.8%
10.75	5	78.3%	14.1%	72.7%	11.9%
12.41	6	78.8%	14.6%	73.6%	12.8%
14.33	7	81.5%	14.2%	77.8%	12.2%
16.55	8	77.2%	13.9%	73.0%	11.7%
19.11	9	76.3%	14.1%	72.2%	11.7%
22.07	10	71.6%	16.3%	67.1%	13.6%
25.48	11	70.4%	16.7%	65.6%	14.3%
29.43	12	63.4%	17.5%	57.4%	15.0%
33.98	13	62.0%	17.2%	56.2%	14.5%
39.24	14	60.6%	17.9%	55.0%	14.8%
45.32	15	59.6%	18.7%	54.6%	15.6%
52.33	16	61.3%	19.4%	57.5%	16.9%
60.43	17	63.6%	19.7%	60.6%	17.3%
69.78	18	61.5%	22.1%	59.0%	19.5%
80.58	19	62.0%	22.4%	59.6%	19.3%
93.06	20	60.5%	23.7%	57.8%	20.4%
107.46	21	61.5%	24.4%	58.7%	20.9%
124.09	22	59.4%	25.7%	56.9%	21.9%
143.3	23	62.4%	25.1%	60.6%	21.1%
165.48	24	63.1%	24.8%	61.8%	20.4%
191.1	25	67.1%	23.3%	66.0%	18.9%
220.67	26	70.1%	22.2%	68.4%	18.3%
254.83	27	74.0%	21.2%	72.2%	17.7%
294.27	28	73.6%	21.5%	72.2%	18.4%
339.82	29	73.5%	19.1%	70.8%	15.7%
392.42	30	72.8%	17.0%	69.4%	13.6%
453.16	31	74.2%	15.9%	70.6%	12.6%
523.3	32	75.9%	15.7%	72.4%	12.5%
EEPS Total		53.8%	21.7%	42.2%	20.1%
CPC Total		15.9%	31.7%	16.8%	31.5%

Appendix G. Lag Alignment

Tables G.1 to G.5 document the temporal adjustments made to data from various instruments to achieve a time-aligned dataset for analysis. Lag Phase refers to whether the scantool data was collecting data during the outbound or inbound section of the route. Lag Phase 1 was associated with first Scantool initiation during Phase 4 of data collection and Lag Phase 2 was associated with second Scantool initiation during Phase 6 of data collection.

Table G.1 Lag Adjustment of the FTIR (CO_2 concentration) to the Scantool (RPM) by Run

Run No.	Lag Phase	Lag Adjustment (seconds)	Pearson's Correlation Coefficient	N_{FTIR}	N_{RPM}	Run No.	Lag Phase	Lag Adjustment (seconds)	Pearson's Correlation Coefficient	N_{FTIR}	N_{RPM}
5	1	0	0.27664	2473	2469	42	2	-3	0.893885	2079	2199
5	2	-2	0.396402	1624	1962	43	1	-1	0.836545	2509	2702
6	1	-2	0.563225	2240	2431	43	2	-2	0.943124	2154	2337
6	2	-3	0.411394	1679	1832	44	1	2	0.812903	3182	3445
7	1	-2	0.329136	2224	2399	44	2	2	0.884546	2434	2262
7	2	-2	0.443021	1736	1964	45	1	-4	0.859995	2438	1248
8	1	-1	0.490257	2401	2517	45	2	-4	0.916359	1823	2010
8	2	-1	0.436453	1773	1217	46	1	-1	0.848947	2567	2724
9	1	-2	0.616218	2292	1818	46	2	-2	0.921855	1960	2053
9	2	-3	0.424256	1808	1289	47	1	-1	0.60712	2530	2675
10	1	-4	0.614135	1532	2552	47	2	-2	0.907052	1804	2000
10	2	-4	0.41042	688	2082	48	1	-5	0.846734	2611	2777
11	1	-1	0.663228	1473	2725	48	2	0	NaN	2116	0
11	2	-2	0.587666	1175	2076	49	1	-4	0.887758	3152	3081
12	1	-2	0.664938	2423	2482	49	2	0	NaN	2348	0
12	2	-3	0.4492	1833	2013	50	1	0	NaN	2813	0
13	1	-1	0.838135	2197	2295	50	2	-3	0.914415	2875	2002
13	2	-1	0.872499	1431	2039	51	1	5	0.845043	2404	2525
14	1	0	0.80418	2063	2148	51	2	5	0.925985	2034	1924
14	2	-1	0.855443	1744	1919	52	1	12	0.889163	2701	2522
15	1	1	0.826117	2161	2245	52	2	11	0.913078	1913	2073
15	2	0	0.510519	1787	2239	53	1	0	0.805783	2596	2590
16	1	3	0.792724	2071	2170	53	2	-1	0.911595	2018	2129
16	2	3	0.826622	1785	1900	54	1	-2	0.420178	2901	2234
17	1	0	0.625173	2136	2267	54	2	-2	0.452862	1980	934
17	2	-1	0.829808	1633	1751	55	1	-4	0.523255	2637	2754
18	1	-1	0.842263	2470	2579	55	2	-5	0.460908	2125	2261
18	2	-2	0.853173	1736	1896	56	1	2	0.706955	2946	2471
19	1	0	0.715192	479	2660	56	2	2	0.571239	2108	2274
19	2	0	0.907131	1948	2113	57	1	-4	0.801365	2675	2440
20	1	-2	0.857726	2440	2640	57	2	-4	0.508541	1855	2159
20	2	-2	0.909447	2026	2150	58	1	-3	0.7317	2471	2518
21	1	-1	0.853684	2369	2441	58	2	-3	0.489101	2141	2303
21	2	-1	0.886338	1974	2093	59	1	-1	0.420324	2698	2577
22	1	-1	0.865259	2360	2588	59	2	-2	0.3515	1952	2114
22	2	-2	0.86161	1830	2201	60	1	-2	0.351468	2583	2482
23	1	0	0.856854	2618	2675	60	2	-2	0.538196	1921	2009
23	2	0	0.878025	1824	1976	61	1	6	0.637243	2636	2578
24	1	-1	0.863922	2659	2736	61	2	5	0.551521	1888	1992
24	2	-3	0.877854	1746	1978	62	1	0	0.455942	2452	2551
25	1	-2	0.864691	2234	2411	62	2	-1	0.383805	1919	2059
25	2	-2	0.893022	2088	2011	63	1	5	0.675892	2688	1340
26	1	-2	0.871698	2656	2910	63	2	4	0.423028	1876	2120
26	2	-3	0.888399	1924	2018	64	1	-4	0.702697	2443	2663
27	1	-1	0.849635	2586	2824	64	2	-5	0.443162	1819	2043
27	2	-2	0.890168	1870	2043	65	1	-3	0.72365	2826	2940
28	1	0	NaN	0	2583	65	2	-4	0.554369	2027	2155
28	2	0	NaN	0	2008	66	1	8	0.73335	2677	2850
29	1	0	NaN	0	2766	66	2	7	0.463459	1850	1955
29	2	0	NaN	0	1882	67	1	9	0.683749	2252	2389
30	1	0	NaN	0	2535	67	2	9	0.559631	1907	2066
30	2	0	NaN	0	2109	68	1	16	0.890392	2978	3238
31	1	0	NaN	0	2994	68	2	16	0.887382	1836	1966
31	2	0	NaN	0	1944	69	1	-1	0.903375	2921	3051
32	1	0	NaN	0	2997	69	2	-1	0.901106	1919	2140
32	2	0	NaN	0	2088	70	1	0	0.874317	2644	2595
33	1	0	NaN	0	2440	70	2	0	0.906246	2000	2130
33	2	0	NaN	0	2050	71	1	-2	0.889822	3060	3092
34	1	0	NaN	3043	3134	71	2	-2	0.916775	2015	2212
34	2	-9	0.486126	1878	2058	72	1	-1	0.871567	2691	2716
35	1	-3	0.68273	2509	2691	72	2	-1	0.909504	2015	2193
35	2	-4	0.371737	1805	1961	73	1	-2	0.887229	2705	2669
36	1	-4	0.647094	1946	2662	73	2	-2	0.910055	2155	2267
36	2	-5	0.499872	1914	2063	74	1	3	0.887595	2978	3105
37	1	-4	0.548893	2344	2505	74	2	2	0.91156	2020	2266
37	2	-4	0.404162	1791	1946	75	1	0	NaN	3366	0
38	1	9	0.611812	2442	2204	75	2	1	0.879713	1811	2001
38	2	7	0.405342	1945	2123	76	1	2	0.877675	2513	2563
39	1	-3	0.629905	2773	2868	76	2	2	0.903253	1876	1987
39	2	-4	0.676102	1510	800	77	1	-2	0.88744	3056	2868
40	1	-4	0.54034	2324	2469	77	2	-3	0.887528	2461	2269
40	2	-6	0.373434	1878	2026	78	1	-1	0.46162	2568	2529
41	1	-3	0.813079	2478	2586	78	2	-2	0.911545	2069	2184
41	2	-6	0.862217	1993	2098	79	1	6	0.856982	2871	2855
42	1	-3	0.862402	2499	2696	79	2	6	0.898106	2475	2599

Table G.2 Lag Adjustment of CPC to the EEPS by Run

Run No.	CPC Lag Adjustment (seconds)	Pearson's Correlation Coefficient	N_{CPC}	N_{EEPS}		Run No.	CPC Lag Adjustment (seconds)	Pearson's Correlation Coefficient	N_{CPC}	N_{EEPS}
5	3	0.741465	4723	4704		42	-3	0.723777	5055	5066
6	3	0.797514	4387	4364		43	-2	0.890448	5020	5020
7	3	0.920978	4440	4497		44	2	0.210303	5665	5400
8	3	0.869061	73	4641		45	3	0.676349	4695	4693
9	4	0.827139	4536	4525		46	3	0.754119	4877	4866
10	4	0.813395	4657	4682		47	4	0.731065	4727	5274
11	3	0.71031	4879	4907		48	3	0.757548	4868	4866
12	3	0.731335	4556	4597		49	4	0.77783	5647	5399
13	3	0.826768	4376	4392		50	3	0.768218	5751	5765
14	3	0.854351	4082	4135		51	3	0.793741	4799	4843
15	2	0.867909	4511	4529		52	3	0.680072	5092	5025
16	4	0.774218	4101	4140		53	4	0.70516	4951	4833
17	3	0.86378	4094	4117		54	2	0.819626	4980	4998
18	3	0.894635	4516	4518		55	2	0.953562	4988	4970
19	3	0.813954	4732	4732		56	3	0.725207	5251	5400
20	3	0.895865	4819	4814		57	3	0.88508	4995	5013
21	3	0.857533	4677	4675		58	2	0.588674	4731	4836
22	3	0.83193	5015	5028		59	3	0.852033	4914	4762
23	2	0.896184	3893	5361		60	4	0.906191	4658	4696
24	3	0.819203	5553	5400		61	3	0.793877	4919	4937
25	4	0.896659	4560	4560		62	3	0.897996	4826	4821
26	3	0.863834	5400	5400		63	3	0.839707	5006	4950
27	3	0.858965	5225	5166		64	4	0.820227	4334	4740
28	4	0.838272	4897	4901		65	3	0.797507	5248	5198
29	27	0.990885	4791	4813		66	4	0.771259	4933	4964
30	3	0.825499	4676	4691		67	3	0.862171	4530	4542
31	3	0.894307	5504	5282		68	0	NaN	5385	5364
32	4	0.884678	5354	5359		69	3	0.807297	5202	5201
33	-2	0.853861	4637	4656		70	3	0.799542	4778	4671
34	-2	0.837545	5334	5326		71	2	0.205598	5393	5360
35	3	0.817658	4678	4676		72	0	NaN	5048	5044
36	4	0.826102	4798	4814		73	0	NaN	5332	5321
37	2	0.641434	4648	4614		74	3	0.884194	5237	5248
38	3	0.6972	4762	5400		75	0	NaN	5966	5937
39	3	0.66195	3729	3744		76	0	NaN	4855	4740
40	-2	0.796818	4548	4542		77	0	NaN	5918	5880
41	-1	0.822676	4868	4857		78	0	NaN	5123	4983
						79	4	0.366815	6219	5400

Table G.3 Lag Adjustment for EEPS Total Particle Number (and CPC) to the Scantool via RPM (correlation to load also listed)

Run No.	Lag Phase	Lag Adjustment (EEPS to RPM)	Pearson's Correlation Coefficient (for RPM)	Lag Adjustment (EEPS to Load)	Pearson's Correlation Coefficient (for Load)	N_{CPC}	N_{EEPS}	Run No.	Lag Phase	Lag Adjustment (EEPS to RPM)	Pearson's Correlation Coefficient (for RPM)	Lag Adjustment (EEPS to Load)	Pearson's Correlation Coefficient (for Load)	N_{CPC}	N_{EEPS}
5	1	-6	0.174946	-7	0.173541	2661	2469	42	2	-5	0.22057	-4	0.208047	2268	2199
5	2	-6	0.619063	-6	0.558454	2043	1962	43	1	-5	0.161505	-5	0.21478	2705	2702
6	1	-6	0.324534	-6	0.352037	2454	2431	43	2	-5	0.226618	-5	0.235284	2315	2337
6	2	-6	0.591664	-6	0.566013	1910	1832	44	1	-5	0.129589	-4	0.218806	3528	3445
7	1	-6	0.265047	-8	0.246615	2439	2399	44	2	-10	0.219799	-9	0.213996	1872	2262
7	2	-6	0.624275	-7	0.613166	2058	1964	45	1	-6	0.11377	-5	0.185614	2534	1248
8	1	-6	0.349779	-7	0.366594	2590	2517	45	2	-5	0.249535	-4	0.199685	2159	2010
8	2	-6	0.586353	-6	0.556492	2051	1217	46	1	-6	0.152535	-6	0.217773	2725	2724
9	1	-7	0.301814	-8	0.359472	2517	1818	46	2	-6	0.27665	-5	0.240167	2141	2053
9	2	-7	0.60525	-8	0.593778	2008	1289	47	1	-6	0.120019	-6	0.218115	3291	2675
10	1	-6	0.312162	-7	0.318157	2574	2552	47	2	-5	0.2085	-5	0.210835	1967	2000
10	2	-6	0.619313	-7	0.623542	2108	2082	48	1	-5	0.232627	-5	0.275542	2833	2777
11	1	-6	0.235385	-7	0.25561	2764	2725	48	2	0	NaN	0	NaN	2033	0
11	2	-6	0.607544	-7	0.566314	2143	2076	49	1	-6	0.212138	-5	0.26671	3418	3081
12	1	-7	0.19859	-7	0.266306	2527	2482	49	2	0	NaN	0	NaN	1981	0
12	2	-6	0.572294	-7	0.564762	2070	2013	50	1	0	NaN	0	NaN	3024	0
13	1	-4	0.11441	-4	0.151924	1510	2295	50	2	-5	0.214918	-4	0.220404	2226	2002
13	2	-4	0.284432	-4	0.305932	2074	2039	51	1	-4	0.18362	-3	0.245536	2614	2525
14	1	-4	0.140961	-4	0.202679	2198	2148	51	2	-4	0.18754	-3	0.211305	2229	1924
14	2	-4	0.221208	-4	0.271212	1937	1919	52	1	-4	0.237948	-3	0.293132	2894	2522
15	1	-4	0.179822	-3	0.220338	2264	2245	52	2	-4	0.187258	-4	0.199653	2131	2073
15	2	-10	0.157926	-6	0.179168	2265	2239	53	1	-4	0.110934	-3	0.168674	2732	2590
16	1	-5	0.136027	-4	0.167185	2202	2170	53	2	-5	0.222196	-4	0.219995	2101	2129
16	2	-4	0.248536	-4	0.255023	1938	1900	54	1	-5	0.328657	-6	0.300772	2867	2234
17	1	-4	0.126958	-4	0.14648	2303	2267	54	2	-4	0.390543	-5	0.299378	2131	934
17	2	-4	0.180027	-3	0.222717	1814	1751	55	1	-3	0.419093	-4	0.371297	2749	2754
18	1	-3	0.199912	-3	0.255328	2608	2579	55	2	-4	0.422077	-5	0.349656	2221	2261
18	2	-3	0.150331	-3	0.201262	1910	1896	56	1	-5	0.481055	-6	0.419804	3074	2471
19	1	-3	0.188294	-3	0.225695	2580	2660	56	2	-5	0.298276	-6	0.205307	2326	2274
19	2	-4	0.201418	-3	0.254511	2152	2113	57	1	-4	0.365894	-5	0.319319	2740	2440
20	1	-6	0.192062	-6	0.237366	2638	2640	57	2	-5	0.265797	-5	0.148798	2273	2159
20	2	-6	0.177676	-6	0.199546	2176	2150	58	1	-4	0.326603	-6	0.306023	2392	2518
21	1	-4	0.163758	-4	0.236763	2471	2441	58	2	-6	0.221815	12	0.110172	2444	2303
21	2	-5	0.166202	-4	0.20583	2204	2093	59	1	-1	0.405242	-2	0.36765	2678	2577
22	1	-3	0.140617	-3	0.221078	2795	2588	59	2	-1	0.334717	-1	0.277861	2084	2114
22	2	-5	0.170724	-4	0.225986	2233	2201	60	1	-5	0.443962	-7	0.35343	2606	2482
23	1	-3	0.107921	-3	0.192617	2747	2675	60	2	-6	0.407698	-6	0.333895	2090	2009
23	2	-3	0.133492	-2	0.178958	1992	1976	61	1	-5	0.318886	-6	0.254323	2854	2578
24	1	-3	0.149021	-2	0.202367	2866	2736	61	2	-6	0.362729	-6	0.293048	2083	1992
24	2	-5	0.125816	-5	0.204209	2534	1978	62	1	-4	0.427149	-5	0.362522	2708	2551
25	1	-5	0.135578	-4	0.207002	2404	2411	62	2	-4	0.469006	-5	0.393917	2113	2059
25	2	-5	0.168794	-5	0.229177	2156	2011	63	1	-5	0.462122	-6	0.340304	2889	1340
26	1	-4	0.170848	-3	0.239407	2854	2910	63	2	-7	0.329459	-7	0.245568	2061	2120
26	2	-4	0.141492	-4	0.204486	2546	2018	64	1	-5	0.325659	-6	0.295532	2680	2663
27	1	-3	0.140895	-2	0.204168	2766	2824	64	2	-6	0.311547	-6	0.223145	2060	2043
27	2	-4	0.130568	-2	0.195438	2400	2043	65	1	-4	0.232615	-5	0.218145	3005	2940
28	1	-4	0.160448	-4	0.215409	2696	2583	65	2	-5	0.291066	-6	0.156217	2193	2155
28	2	-4	0.144354	-4	0.215159	2205	2008	66	1	-6	0.17092	-6	0.183467	2892	2850
29	1	-5	0.162954	-5	0.231034	2806	2766	66	2	-6	0.332178	-6	0.254799	2072	1955
29	2	-5	0.135023	-5	0.211894	2007	1882	67	1	-6	0.35681	-6	0.322834	2416	2389
30	1	-2	0.145826	-2	0.202363	2575	2535	67	2	-5	0.561904	-6	0.452595	2126	2066
30	2	-4	0.158621	-4	0.206208	2116	2109	68	1	-4	0.20531	-3	0.255336	3248	3238
31	1	5	0.206091	5	0.236955	3166	2994	68	2	-4	0.141596	-3	0.178993	2116	1966
31	2	6	0.419877	5	0.400233	2116	1944	69	1	-4	0.201215	-3	0.240274	3075	3051
32	1	-6	0.296409	-7	0.298624	3047	2997	69	2	-4	0.222858	-3	0.244891	2126	2140
32	2	-6	0.410033	-7	0.356435	2312	2088	70	1	-4	0.18926	-3	0.257812	2653	2595
33	1	-6	0.140044	-7	0.216764	2555	2440	70	2	-4	0.149015	-4	0.205418	2018	2130
33	2	-5	0.484576	-6	0.425944	2101	2050	71	1	-3	0.152166	-2	0.214492	3138	3092
34	1	-7	0.121241	-7	0.150096	3290	3134	71	2	-3	0.186951	-2	0.214342	2222	2212
34	2	-7	0.393954	-7	0.342144	2036	2058	72	1	-3	0.154654	-2	0.235616	2830	2716
35	1	-6	0.241297	-7	0.264546	2652	2691	72	2	-3	0.211105	-3	0.235923	2170	2193
35	2	-6	0.386914	-6	0.350819	2024	1961	73	1	-4	0.220972	-4	0.284894	2906	2669
36	1	-7	0.228525	-7	0.275815	2683	2662	73	2	-5	0.163557	-4	0.212656	2415	2267
36	2	-7	0.46271	-7	0.415813	2131	2063	74	1	-3	0.166707	-2	0.22848	3160	3105
37	1	-6	0.341656	-7	0.230354	2585	2505	74	2	-3	0.169358	-3	0.209593	2088	2266
37	2	-5	0.374732	-5	0.30609	2029	1946	75	1	0	NaN	0	NaN	3613	0
38	1	-7	0.371347	-8	0.265513	2546	2204	75	2	-2	0.177467	-2	0.238385	2197	2001
38	2	-7	0.420446	-8	0.333279	2854	2123	76	1	-4	0.151342	-3	0.208366	2660	2563
39	1	-6	0.203608	-7	0.149423	3002	2868	76	2	-4	0.20765	-3	0.252691	2080	1987
39	2	0	0.204388	-7	0.151485	742	800	77	1	-1	0.204516	0	0.260312	3083	2868
40	1	-49	0.112134	-49	0.101826	2504	2469	77	2	-2	0.123628	-1	0.148056	2177	2269
40	2	-8	0.186028	-8	0.10233	2038	2026	78	1	-4	0.150153	-3	0.215094	2702	2529
41	1	-6	0.126886	-6	0.17044	2654	2586	78	2	-4	0.160995	-4	0.177085	2281	2184
41	2	-8	0.16325	-8	0.15371	2203	2098	79	1	0	0.177985	0	0.220329	3040	2855
42	1	-5	0.196297	-5	0.251336	2798	2696	79	2	-1	0.17271	-1	0.216318	2360	2599

Table G.4 Lag Adjustment of GPS to Scantool via Speed Measured by Each (Flag here indicates whether best matched data was from Garmin (1), Geologger (2), or not available for either (3))

Run No.	Lag Phase	GPS Lag Adjustment (seconds)	Correlation Coefficient (Speed)	Flag	N_{GPS}	Run No.	Lag Phase	GPS Lag Adjustment (seconds)	Correlation Coefficient (Speed)	Flag	N_{GPS}
5	1	0	0.99769	1	4310	43	1	1	0.996973	2	6506
5	2	0	0.997361	1	4310	43	2	1	0.993975	2	6506
6	1	1	0.990424	1	2943	44	1	1	0.999349	1	5104
6	2	-1	0.995723	1	2943	44	2	1	0.997877	2	6984
7	1	-1	0.998886	1	4369	45	1	-1	0.999556	1	4478
7	2	-1	0.99613	1	4369	45	2	-1	0.99852	2	4753
8	1	-4	0.998366	1	4796	46	1	-1	0.999278	1	5186
8	2	-5	0.99175	1	4796	46	2	-2	0.999121	2	4463
9	1	-2	0.996257	1	4875	47	1	2	0.997871	1	4773
9	2	-1	0.993848	1	4875	47	2	1	0.993666	2	6988
10	1	0	0.99792	1	5141	48	1	-45	0.996357	1	2019
10	2	0	0.998365	1	5141	49	1	52	0.997312	2	4195
11	1	0	0.998865	1	5087	50	1	-8	0.99923	1	1877
11	2	-1	0.996619	1	5087	50	2	1	0.990777	1	1877
12	1	-1	0.996583	1	4990	51	1	0	0.99796	1	2025
12	2	-1	0.997198	1	4990	51	2	-59	0.969891	1	2025
13	1	2	0.999219	1	4797	51	3	1	0.87304	2	5674
13	2	1	0.996676	1	4797	52	1	-90	-0.005102	2	2856
14	1	2	0.99851	1	4516	52	2	3	0.991633	1	919
14	2	1	0.997407	1	4516	52	3	2	0.931512	2	2856
15	1	31	0.997487	1	4913	53	1	1	0.998221	1	2032
15	2	17	0.996706	1	4913	53	2	0	0.980043	1	2032
16	1	1	0.999469	2	4957	54	1	9	0.997424	1	2045
16	2	1	0.997667	1	4502	54	2	33	0.951005	1	2045
17	1	2	0.999024	1	4443	55	1	2	0.991626	1	2075
17	2	1	0.99877	1	4443	55	2	2	0.992552	1	2075
18	1	1	0.999411	2	5818	56	1	-1	0.996216	1	2067
18	2	1	0.997766	1	4786	56	2	0	0.981884	2	8722
19	1	1	0.994838	1	3047	57	1	0	NaN	3	NaN
19	2	1	0.986213	2	6570	57	2	1	0.989799	1	2013
20	1	-1	0.997364	1	4363	57	3	1	0.990888	2	5431
20	2	-1	0.994781	1	4363	58	1	1	0.997292	2	7308
21	1	1	0.994164	1	3913	58	2	1	0.979101	2	7308
21	2	0	0.994371	1	3913	59	1	4	0.995473	1	2031
22	1	0	NaN	3	NaN	59	2	4	0.992048	1	2031
22	2	2	0.915714	1	399	60	1	-1	0.993358	2	6999
22	3	0	NaN	3	NaN	60	2	-6	0.987208	1	1902
23	1	1	0.99741	1	4042	61	1	1	0.989647	1	2010
23	2	2	0.994212	1	4042	61	2	1	0.991749	1	2010
24	1	2	0.96275	2	439	62	1	0	NaN	3	NaN
24	2	0	NaN	3	NaN	62	2	-7	0.983248	1	2050
25	1	1	0.994869	1	4697	62	3	-1	0.999122	1	2050
25	2	1	0.995455	1	4697	62	4	0	0.975248	1	2050
26	1	2	0.987262	1	4741	63	1	-1	0.997115	1	1910
26	2	1	0.993544	1	4741	63	2	-4	0.986753	1	1910
27	1	2	0.996711	1	4636	63	3	-9	0.875411	1	1910
27	2	1	0.996438	1	4636	63	4	-1	0.983313	1	1910
28	1	1	0.989642	1	2808	64	1	0	0.995706	1	1932
28	2	1	0.997672	1	2808	64	2	-1	0.976477	1	1932
29	1	0	0.998247	1	4726	65	1	0	0.997561	1	2030
29	2	0	0.996735	1	4726	65	2	0	0.989783	1	2030
30	1	0	0.996083	1	4409	66	1	0	0.997472	1	2016
30	2	1	0.997272	1	4409	66	2	-1	0.990362	1	2016
31	1	0	NaN	3	NaN	67	1	39	0.991594	1	1845
31	2	10	0.997118	1	3799	67	2	24	0.992216	1	1845
31	3	12	0.991089	1	3799	68	1	0	0.998616	1	2031
32	1	35	0.998917	1	4992	68	2	-119	0.994672	1	2031
32	2	15	0.997704	1	4992	69	1	0	0.998647	1	2036
33	1	0	0.99833	1	4432	69	2	0	0.997777	1	2036
33	2	1	0.990294	1	4432	70	1	0	0.99851	1	2048
34	1	0	NaN	3	NaN	70	2	0	0.99805	1	2048
34	2	0	NaN	3	NaN	71	1	1	0.998579	1	2055
34	3	0	0.998299	1	5052	71	2	1	0.991854	1	2055
34	4	0	0.998899	2	6992	72	1	1	0.999338	1	2051
35	1	0	0.998824	1	4768	72	2	1	0.994717	1	2051
35	2	1	0.998104	2	5731	73	1	-6	0.999046	1	1961
36	1	0	0.998511	1	3811	73	2	0	0.997366	1	1961
36	2	0	0.996243	1	3811	74	1	1	0.996768	1	1714
37	1	0	0.998221	1	2987	74	2	-4	0.999537	2	3599
37	2	0	0.993242	2	7288	75	1	1	0.995777	1	1976
38	1	0	0.996573	1	3322	76	1	0	0.992724	1	1843
38	2	0	0.991618	1	3322	76	2	1	0.989576	2	4683
39	1	0	0.997847	1	3911	77	1	-2	0.998987	1	2019
39	2	0	0.996849	1	3911	77	2	3	0.984891	1	2019
40	1	0	0.996382	1	4146	78	1	2	0.998817	1	2078
40	2	0	0.995945	1	4146	78	2	1	0.991375	1	2078
41	1	2	0.992706	1	3864	79	1	0	NaN	3	NaN
41	2	0	0.996393	1	3864	79	2	5	0.993255	1	1718
42	1	1	0.995872	2	7409	79	3	4	0.999694	2	2699
42	2	0	0.992724	1	4223						

Table G.5 Lag Adjustment of the Labview Devices to the Scantool

Run No.	Lag Phase	Lag Adjustment Labview Device 2 (Tailpipe Flow Rate to RPM)	Pearson's Correlation Coefficient (Labview Device 2)	N_{Flow}	N_{RPM}	Lag Adjustment Labview Device 1 (Crossbow to Scantool Acceleration)	Pearson's Correlation Coefficient (Labview Device 1)	$N_{Crossbow}$	$N_{Scantool}$	Run No.	Lag Phase	Lag Adjustment Labview Device 2 (Tailpipe Flow Rate to RPM)	Pearson's Correlation Coefficient (Labview Device 2)	N_{Flow}	N_{RPM}	Lag Adjustment Labview Device 1 (Crossbow to Scantool Acceleration)	Pearson's Correlation Coefficient (Labview Device 1)	$N_{Crossbow}$	$N_{Scantool}$
5	1	1	0.805957	3574	2469	3	0.823555	3961	2454	42	2	2	0.923796	2315	2199	2	0.70621	2332	2193
5	2	1	0.822955	1806	1962	3	0.703134	2006	1951	43	1	2	0.885186	2680	2702	2	0.827016	2676	2689
6	1	1	0.808863	2797	2431	2	0.767924	3127	2417	43	2	1	0.921972	2584	2337	1	0.671585	2646	2332
6	2	0	0.82029	1998	1832	2	0.649057	1959	1815	44	1	2	0.836367	3505	3445	2	0.757765	3482	3433
7	1	3	0.812935	4435	2399	5	0.841872	4518	2385	44	2	1	0.90564	2310	2262	2	0.720496	2347	2258
7	2	3	0.848521	2025	1964	5	0.744562	2007	1952	45	1	1	0.932258	2466	1248	1	0.759849	2517	1247
8	1	1	0.811205	3020	2517	1	0.782641	3082	2470	45	2	1	0.91275	1953	2010	1	0.673317	1965	2009
8	2	1	0.764189	2075	1217	1	0.498967	2071	953	46	1	0	0.870159	2746	2724	1	0.824872	2773	2723
9	1	1	0.750975	3032	1818	1	0.637914	3054	1506	46	2	0	0.918197	2167	2053	1	0.704598	2170	2052
9	2	0	0.778095	1980	1289	1	0.524121	1994	1001	47	1	2	0.901594	3426	2675	2	0.743723	3469	2664
10	1	1	0.783247	3269	2552	2	0.835799	3300	2542	47	2	2	0.925586	1936	2000	2	0.678221	1952	1996
10	2	0	0.803763	2105	2082	2	0.677169	2098	2078	48	1	2	0.885904	2907	2777	3	0.8156	2878	2776
11	1	1	0.782811	3427	2725	2	0.817003	3473	2707	48	2	0	NaN	2022	0	0	NaN	2051	0
11	2	1	0.776024	2130	2076	1	0.691949	2137	2051	49	1	1	0.889485	3251	3081	2	0.778208	3465	3080
12	1	0	0.799609	3199	2482	1	0.828024	3229	2465	49	2	0	NaN	2251	0	0	NaN	2326	0
12	2	0	0.826764	2060	2013	0	0.703255	2067	2000	50	1	0	NaN	2846	0	0	NaN	2957	0
13	1	2	0.916328	2890	2295	3	0.864091	2995	2292	50	2	45	0.1451	2324	2002	0	0.119298	2537	2000
13	2	1	0.934205	2050	2039	2	0.758513	2087	2034	51	1	1	0.835381	1862	2525	2	0.820968	2623	2524
14	1	2	0.908995	2790	2148	2	0.872458	2866	2139	51	2	2	0.924504	2203	1924	2	0.707122	2274	1922
14	2	1	0.925019	1954	1919	2	0.773729	1959	1915	52	1	3	0.894537	2837	2522	3	0.806611	2851	2520
15	1	2	0.91754	2897	2245	2	0.872061	2989	2238	52	2	3	0.9209	2345	2073	3	0.676321	2426	2072
15	2	1	0.93023	2233	2239	1	0.71534	2302	2229	53	1	3	0.876022	2663	2590	3	0.808507	2717	2589
16	1	2	0.902168	2876	2170	1	0.865768	2986	2161	53	2	2	0.925855	2142	2129	2	0.726063	2209	2128
16	2	1	0.917804	1877	1900	1	0.765456	1918	1896	54	1	2	0.674634	2825	2234	2	0.70585	2791	2233
17	1	2	0.919513	3117	2267	3	0.860162	3173	2260	54	2	2	0.618601	2174	934	3	0.637413	2168	933
17	2	2	0.920512	1718	1751	2	0.734745	1808	1743	55	1	3	0.698194	2807	2754	3	0.782876	2819	2753
18	1	2	0.916486	3296	2579	2	0.859063	3338	2565	55	2	2	0.738784	2259	2261	2	0.615619	2250	2260
18	2	2	0.914637	1814	1896	1	0.737755	1929	1888	56	1	1	0.729731	3191	2471	2	0.798637	3178	2470
19	1	0	NaN	3218	2660	1	0.845071	3192	2653	56	2	1	0.694408	2367	2274	2	0.653695	2359	2273
19	2	0	NaN	2134	2113	1	0.735722	2130	2109	57	1	44	0.733355	7984	2440	45	0.78179	8011	2437
20	1	-1	0.915735	2721	2640	0	0.845964	2827	2630	57	2	44	0.758426	2141	2159	45	0.619375	2151	2159
20	2	-1	0.915179	2027	2150	0	0.736951	2195	2145	58	1	1	0.722372	3763	2518	2	0.677689	3758	2517
21	1	1	0.912867	3065	2441	2	0.844103	3164	2429	58	2	1	0.740859	2391	2303	2	0.639733	2474	2302
21	2	1	0.925761	2053	2093	1	0.763475	2191	2087	59	1	19	0.734948	5689	2577	21	0.761691	7579	2575
22	1	2	0.93176	3295	2588	2	0.862613	3567	2579	59	2	19	0.781242	2086	2114	21	0.605802	2079	2114
22	2	1	0.937995	1825	2201	0	0.76994	2282	2193	60	1	9	0.751991	6325	2482	11	0.690701	6540	2481
23	1	2	0.750428	4560	2675	2	0.827471	4635	2666	60	2	9	0.784475	2066	2009	11	0.668465	2079	2008
23	2	2	0.667041	2005	1976	3	0.728852	2021	1968	61	1	1	0.758771	2904	2578	3	0.76943	2912	2577
24	1	3	0.439354	2994	2736	3	0.816728	2982	2726	61	2	1	0.791346	2132	1992	2	0.738102	2149	1991
24	2	0	0.882793	2740	1978	1	0.708131	2739	1970	62	1	2	0.725876	2763	2551	3	0.792355	2786	2548
25	1	2	0.56501	2570	2411	1	0.842165	2642	2403	62	2	1	0.762168	2127	2059	2	0.46318	2127	2058
25	2	2	0.495146	2999	2011	1	0.703929	2999	2004	63	1	1	0.724193	2824	1340	1	0.768208	2842	1339
26	1	4	0.008558	2976	2910	2	0.78635	3001	2902	63	2	0	0.785405	2181	2120	1	0.676025	2194	2117
26	2	3	0.195124	2685	2018	2	0.705832	2686	2009	64	1	1	0.750854	2649	2663	3	0.725054	2638	2661
27	1	4	0.051358	2583	2824	2	0.832019	2605	2814	64	2	0	0.769464	2146	2043	2	0.595673	2164	2043
27	2	3	0.152724	2513	2043	2	0.740719	2469	2037	65	1	2	0.736312	3066	2940	3	0.778384	3076	2939
28	1	2	0.932822	2642	2583	2	0.796673	2728	2562	65	2	1	0.749332	2218	2155	2	0.66932	2225	2154
28	2	2	0.930785	2089	2008	2	0.702284	2279	1998	66	1	29	0.708616	5324	2850	30	0.74339	8049	2849
29	1	1	0.926981	2806	2766	1	0.811986	2851	2747	66	2	28	0.77035	1988	1955	29	0.535254	1996	1954
29	2	1	0.930221	2669	1882	1	0.67401	2897	1865	67	1	4	0.808008	4483	2389	5	0.813226	4310	2387
30	1	2	0.925515	2456	2535	2	0.784672	2539	2513	67	2	4	0.774834	2077	2066	5	0.684071	2072	2066
30	2	1	0.936765	2132	2109	1	0.659421	2412	2093	68	1	2	0.916914	3038	3238	13	0.193747	3225	3236
31	1	0	NaN	0	2994	0	NaN	0	2980	68	2	2	0.928478	1750	1966	-16	0.147313	1990	1965
31	2	12	0.70198	2260	1944	13	0.637975	2330	1935	69	1	1	0.915417	2995	3051	2	0.824545	3099	3050
32	1	2	0.650304	2977	2997	3	0.766513	3088	2978	69	2	1	0.905935	1987	2140	2	0.715697	2139	2139
32	2	1	0.722105	2358	2088	3	0.641481	2397	2079	70	1	1	0.911221	2819	2595	2	0.858252	2963	2593
33	1	1	0.701523	2179	2440	2	0.766936	2313	2348	70	2	2	0.924157	1783	2130	2	0.73349	2081	2130
33	2	1	0.72497	2138	2050	2	0.631594	2130	2038	71	1	2	0.912824	3081	3092	2	0.815735	3155	3090
34	1	0	0.697718	2981	3134	1	0.743661	3070	3125	71	2	3	0.935165	2001	2212	3	0.740686	2197	2212
34	2	0	0.674559	2074	2058	1	0.595489	2122	2052	72	1	2	0.924806	2742	2716	3	0.808174	2898	2715
35	1	1	0.748724	2686	2691	2	0.752576	2701	2684	72	2	2	0.935057	1949	2193	3	0.706796	2251	2192
35	2	1	0.755147	2178	1961	2	0.647562	2162	1958	73	1	1	0.939149	2010	2669	1	0.843178	3005	2667
36	1	1	0.734361	2634	2662	1	0.783159	1935	2655	73	2	1	0.91219	2069	2267	1	0.705772	2285	2267
36	2	0	0.766642	2145	2063	1	0.680317	2158	2059	74	1	0	NaN	21	3105	3	0.809951	3188	3103
37	1	1	0.756259	2675	2505	1	0.756396	2692	2499	74	2	2	0.925763	1849	2266	3	0.721679	2124	2266
37	2	1	0.76147	2089	1946	2	0.672916	2232	1943	75	1	0	NaN	3545	0	0	NaN	3671	0
38	1	0	0.703396	2560	2204	2	0.748358	2639	2199	75	2	3	0.922257	2219	2001	4	0.72196	2379	2000
38	2	0	0.763	2788	2123	2	0.637537	5714	2119	76	1	2	0.919294	2652	2563	2	0.825215	2795	2562
39	1	1	0.750244	2947	2868	2	0.758639	2964	2860	76	2	3	0.921378	1854	1987	2	0.689774	2025	1986
39	2	1	0.840249	794	800	2	0.514004	783	799	77	1	4	0.908175	3188	2868	5	0.804804	3322	2867
40	1	0	0.718323	2529	2469	2	0.766986	2519	2465	77	2	5	0.898696	2455	2269	5	0.711161	2615	2268
40	2	0	0.78927	2153	2026	2	0.650485	2124	2021	78	1	2	0.909122	2656	2529	3	0.802212	2792	2528
41	1	2	0.891193	2625	2586	2	0.807131	2617	2579	78	2	2	0.924015	2035	2184	3	0.69801	2260	2183
41	2	1	0.924343	2292	2098	1	0.700174	2296	2094	79	1	6	0.861762	3045	2855	6	0.855728	2917	2852
42	1	2	0.896773	2694	2696	2	0.834223	2725	2690	79	2	6	0.5624	2574	2599	0	NaN	0	2599

Appendix H. TOTEMS Database Framework

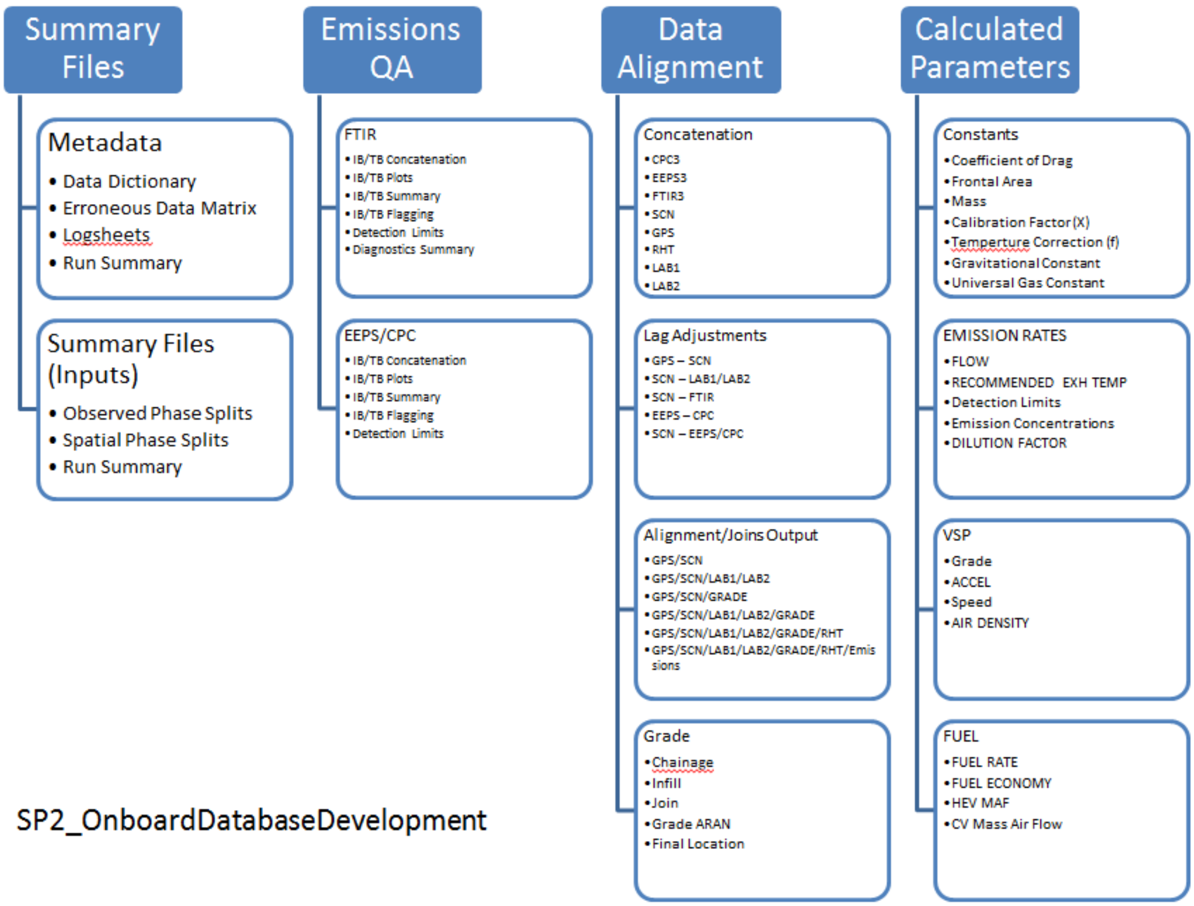

Figure H.1 Overview of Database Framework on HolmenGroup Share Drive

Appendix I. Model Year 2010 Toyota Camry Vehicle Emissions Ratings

Testing Specifics		Exhaust Emissions	CV Certification [g/mi]	CV Standard [g/mi]	HEV Certification [g/mi]	HEV Standard [g/mi]
@ 50,000 miles		NMOG	0.015	0.04		
		CO	0.2	1.7		
		NOx	0.03	0.05		
		HCHO		8		
		PM				
		Hwy NOx	0.01	0.07		
@ Useful Life		NMOG	0.023	0.055	0.008	0.01
		CO	0.3	2.1	0.1	1
		NOx	0.04	0.07	0	0.02
		HCHO		11		4
		PM		0.01		0.01
		Hwy NOx	0.02	0.09	0.01	0.03
SFTP @ 4,000 miles	US06	NMHC+NOx	0.06	0.14	0.01	0.14
		CO	0.1	8	0.5	8
	SC03	NMHC+NOx	0.06	0.2	0	0.2
		CO	0	2.7	0	2.7
@ 20°F & 50,000 miles		CO	1.3	10	0.4	10